2011

# Alternations in the Splenic Marginal Zone with Age

Shirin Z. Birjandi
*Loyola University Chicago*

LOYOLA UNIVERSITY CHICAGO

# ALTERATIONS IN THE SPLENIC MARGINAL ZONE WITH AGE

A DISSERTATION SUBMITTED TO

THE FACULTY OF THE GRADUATE SCHOOL

IN CANDIDACY FOR THE DEGREE OF

DOCTOR OF PHILOSOPHY

PROGRAM IN CELL BIOLOGY, NEUROBIOLOGY AND ANATOMY

BY

SHIRIN Z. BIRJANDI

CHICAGO, ILLINOIS

MAY 2011

## ACKNOWLEDGMENTS

I am grateful to the wisdom, support and guidance of my mentor Dr. Pamela Witte. Dr. Witte allowed me to find my own scientific niche and gave me the freedom to answer my own questions. Under her guidance, I became a more independent thinker and learned that there are multiple ways to interpret any given finding**.** I am also thankful to each member of my dissertation committee: Dr. Richard Schultz, Dr. Phong Le, Dr. John Callaci, and Dr. Dennis Lanning. Their suggestions and expertise added greater depth to the body of my work.

I am thankful to the members of my lab, both past and present, for their friendship and technical guidance. I am particularly grateful to Jill Ippolito and Anand Ramadorai for the many years of support that they have given me. Both Jill and Anand were of tremendous technical help throughout the course of this work.

I would like to thank my parents, fiancé, sister, aunt, and friends for the much love and support that they have given me through the years. Graduate training tests ones confidence and perseverance, and each one of you were there to remind me that I held in me what it takes to be successful within my craft. The many friends I've met through the course of my training have each inspired me and given me much to look up to. My fiancé, a fellow academic, has been a great friend, cheerleader, and colleague these last few years. Lastly, I am most thankful to my parents, both my role models, who have

always seen nothing but genius in me. I hope their dreams of success for their daughter has come true.

To my parents, Nahid Zahedi and Hossein Birjandi

# TABLE OF CONTENTS

# LIST OF TABLES

# LIST OF FIGURES

## LIST OF ABREVATIONS

| | |
|---|---|
| BCR | B cell receptor |
| DC | Dendritic cell |
| FDC | Follicular Dendritic Cell |
| FO B | Follicular B cells |
| MARCO | Macrophage Receptor with Collagenous structure |
| MMM | Metallophilic Macrophages |
| MZ | Marginal Zone |
| MZ B | Marginal Zone B cells |
| MZM | Marginal Zone Macrophages |
| PALS | Periarteriolar lymphoid sheath |
| PC | Phosphorylcholine |
| pHrodo | pHrodo™ S. aureus bioparticles |
| SIGN-R1 | Specific intracellular adhesion molecule-grabbing nonintegrin receptor 1 |
| TD | T-dependent |
| TI | T-independent |

**ABSTRACT**

Splenic marginal zones are architecturally organized to generate a rapid response against blood- borne antigens entering the spleen. The marginal zone is a distinct anatomical micro-environment whose main components include the marginal zone macrophages, the marginal zone B cells, the marginal zone sinus, and the metallophilic macrophages. Marginal zone macrophages, in partnership with marginal zone B cells, are particularly important in host defense against T-independent pathogens and are crucial for the prevention of diseases such as Streptococcus pneumonia. It has been widely reported that with the advancement of age there is a higher rate of mortality as a result of bacterial pneumonia when compared to the young. My objective here was to determine if there are age related changes in the cellular components of the marginal zone in old versus young mice. Gross architectural changes in the marginal zones of old mice when compared to young mice were found and that disruptions were observed among the many components of the marginal zone, including: marginal zone macrophages, marginal zone B cells, the marginal zone sinus lining cells, and the metallophilic macrophages. The reduction in marginal zone macrophages in individual old mice also statistically correlated with reduced frequency of marginal zone B cells. These findings further strengthen a partnership of marginal zone macrophages and marginal zone B cells. Furthermore, the phagocytic properties of marginal zone macrophages were examined live on a per cell basis and no differences in phagocytosis of old marginal zone

macrophages when compared to young were found, demonstrating that it is this reduction in the marginal zone macrophage population that contributes to the decline in the T-independent immune response reported with age. Results obtained from these studies can provide insight for the proper response needed to clear pathogens that have been shown to be detrimental in the old.

# CHAPTER I

## STATEMENT OF THE PROBLEM

More than 12.9 % of the U.S. population is over the age of 65 (1) and life expectancy continues to make rapid gains as a result of advancements in modern healthcare. However, older people suffer greater risks of long-term complications and are still more susceptible to diseases than young and middle-aged individuals because of the effects of a weakened immune system. One of the leading causes of death in persons 65 years and older is invasive pneumococcal disease (2, 3). Vaccines for the prevention of invasive pneumococcal disease show a decline in immune protection in the elderly when compared to the young (4, 5). This is possibly due to the reduced ability of the aged immune system to deal with bacteria load and mount an immune response to the T-independent (TI) antigen components that make up the vaccine. Therefore, understanding how the immune system changes with age is critical for implementing better therapies and vaccines for the prevention of age related disease.

Blood-borne antigens enter the spleen prior to circulating to other immune organs (6). Blood-borne bacteria, viruses, parasites and other antigens enter a compartmentalized area of the spleen, the marginal zone (MZ), where they are sequestered by marginal zone macrophages (MZM) and marginal zone B cells (MZ B) [reviewed in (7, 8)]. MZM are highly phagocytic cells and are responsible for rapid

clearance of blood-borne TI antigens and debris (7-9). MZ B cells are also well known for their ability to respond to TI antigens by rapidly generating an IgM specific antibody response (10)[reviewed in (11, 12)]. It is believed that the pathogen degradation products shed by MZM are taken up by MZ B cells (8). Notably, the antigen components of vaccines important for the prevention of bacterial pneumonia are TI (13). Thus, examining the MZ compartment, especially MZM and MZ B cells, in the old may provide an explanation for the increased susceptibility and decreased efficacy of vaccines for bacterial diseases in the elderly.

MZM are capable of binding TI antigens through specific cell surface receptors. Two important MZM cell surface receptors are: Macrophage Receptor with Collagenous structure (MARCO) and Specific Intracellular adhesion molecule-Grabbing Nonintegrin Receptor 1 (SIGN-R1) [reviewed in (7)]. MARCO binds to *Staphylococcus aureus* (14, 15) and *Escherichia coli* [reviewed in (15)]; SIGN-R1 [homologue of human DC-SIGN (16)] binds the capsular polysaccharide of *Streptococcus pneumoniae* and also to the polysaccharide dextran (17-20). Once MZM bind an antigen, they will introduce it to closely associated MZ B cells (21). MZM and MZ B cells have a direct intercellular interaction via the scavenger receptor, MARCO, expressed on MZM with an undetermined ligand on MZ B cells (22-24). MZM and MZ B cells are positioned around the outer border of the MZ sinus, facing the red pulp of the spleen (7). Positioned around the inner border of the MZ sinus are the metallophilic macrophages (MMM), which face

the white pulp of the spleen (7). The anatomical micro-architecture of the MZ can be seen as critical for the proper binding and clearance of blood-borne pathogens.

Previous studies of the lymphoid architecture of old mice focused on disruption of the white pulp areas, T cell-rich periarteriolar lymphoid sheath (PALS) and B cell follicles, when compared to young mice (25-29). My initial observations of the splenic tissue of most old mice suggested an overall alteration in the micro-architecture of the MZ. Little is known about changes in the structure and cellular components of the MZ with age, **my investigation proposes that there is an alteration in the cellular components that make up the MZ, specifically the MZM and MZ B cells, in old mice when compared to young mice. This cellular alteration may impinge on the functional ability to capture and phagocytize blood-borne antigen.** Results of my studies revealed decreased frequencies of MZM and MZ B cells and disruptions in positioning of the mucosal adhesion cell adhesion molecule (MAdCAM-$1^{+}$) sinus-lining cells and MMM. The consequence of altered MZM in old mice was reflected by reduction in binding of blood-borne dextran particles by the MZM. One explanation for the decreases in MZM and MZ B cells observed with age could be due to alterations in the aged microenvironment. The factors important for MZM and MZ B cell homing to the MZ were examined. In individual animals decreases in MZM in old mice were found to be correlated with decreases in MZ B cells. The chemokine CCL21 and its receptor CCR7, chemotactic factors important for MZM homing were also found to be reduced in old mice when compared to young mice. In cell transfer experiments, mature B cells isolated from young recipient mice had ~50% fewer young donor MZ B cells in old

spleens when compared to young spleens. Lastly, the function of MZM was examined using a novel approach to measure MZM phagocytosis to determine if there were cell-intrinsic alterations in age. On average, the phagocytic function of individual MZM isolated from old mice was found to be unaffected upon administration of S. *aureus* bioparticles, suggesting that a decrease in the MZM compartment rather than cell-intrinsic defects in age is the primary factor for the decreased immune response to TI antigens reported with age.

In this thesis, I will first provide a comprehensive review of the components that make up the MZ. The MZM and MZ B cells will be emphasized as these cells are crucial for the efficient clearance of TI antigens. The origin of MZM and the receptors expressed on its surface will be discussed as well as a general overview of phagocytosis. MZ B cell development in young adults will be reviewed and compared to MZ B cell development in old mice. The MZ sinus as well as the MMM will also briefly be discussed. The reminder of the literature review will discuss a survey of the relevant alterations in immunity with age. The chapter following the literature review will give a complete description of the experimental approaches performed followed by the results (divided into 3 separate chapters). Lastly, I will discuss the significance of my findings and the possible therapies for elderly patients to mount effective immune responses to life-threatening pathogens such as *S. pneumoniae*.

# CHAPTER II

# LITERATURE REVIEW

## Overview of the micro-architecture of the spleen

The spleen houses many of the cells important for an efficient immune response. Histological examination of the spleen reveals a red pulp region and a white pulp region (Fig 1). The red pulp is traditionally known as the region where red blood cells are degraded by the red pulp macrophages that reside in the cords of the red pulp (30). The white pulp is organized into specific zones (Fig. 1): a T cell zone [(periarteriolar lymphoid sheath (PALS)], a B cell zone (follicle), and a marginal zone (MZ). The T cell zone contains T cells that interact with dendritic cells (DC), stromal cells and B cells that pass through. The B cell zone contains the follicular (FO) B cells, follicular dendritic cells (FDC), and stromal cells. FDC and stromal cells secrete the chemokine CXCL13, which is necessary for the FO B cells to home to this zone (31). FO B cells, unlike MZ B cells, require interaction with T cells to mount an effective antibody response. Once activated by T cells, FO B cells undergo immunoglobulin isotype switching, somatic hypermutation, and clonal expansion (11, 32), which can be observed in H&E splenic tissue sections as dark heavily nucleated areas known as germinal centers. The MZ is made up of several components including: the MZM, MZ B cells, MMM, the MZ sinus, natural killer (NK) cells, and DC (7, 8, 30). MZM form the outer ring of the MZ and

interact with the MZ B cells. The DCs are also observed to be localized near the MZM and MZ B cells. MMM form the inner ring of the MZ and are found facing the white pulp of the spleen and are found to be in line with the MZ sinus.

A hallmark feature of the spleen is that it is the site where blood-borne antigens are first detected by cells of the immune system (6). Antigens and recirculating lymphocytes enter the spleen at the MZ. Recirculating lymphocytes enter the MZ from the bloodstream similar to the process by which leukocytes transverse inflamed endothelium (33). Once lymphocytes have re-entered the spleen each cell will position to its corresponding zone as a result of chemotactic signals (31, 34, 35). Antigens will filter through the porous MZ sinus (36) and depending on the nature of the antigens, will initiate an immune response. Traditional FO B cells are activated by thymus-dependent (TD) antigens and MZ B cells are activated by thymus-independent (TI) antigens (37, 38). TD antigens consist of soluble proteins and peptides that associate with MHC molecules on the surface of antigen presenting cells (APC). The APC in the context of MHC class II molecules will then interact with the T cell receptor on the surface of T cells. Activated T cells will recruit and have direct contact with B cells that will produce an immunoglobulin specific antibody response. TI antigens are generally large in molecular weight, have repeating antigenic epitopes, and are able to activate the complement signaling pathway. TI antigens are not able to stimulate MHC molecules on the surface of APC. Therefore, TI antigenic components are able to elicit an antibody response in the absence of MHC class II restricted T cell help.

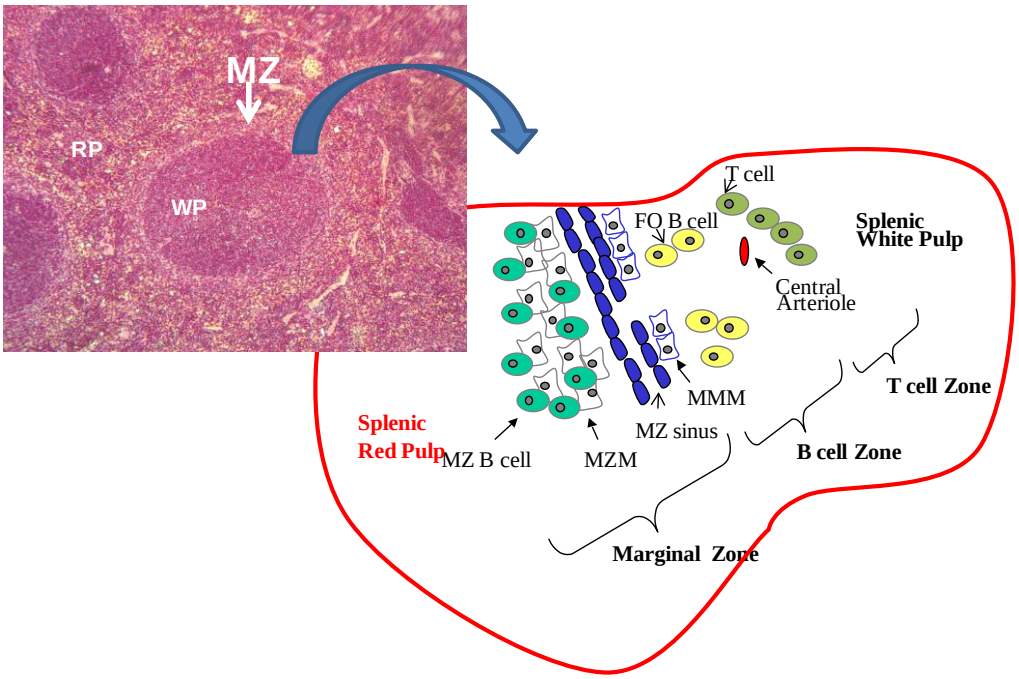


**Figure 1. Schematic representation of the splenic marginal zone**
Top left image is an H&E cross section of a young mouse (10x magnification). The spleen is organized into a red pulp (RP) region and numerous white pulp (WP) areas. The boundary of the MZ is depicted by the white arrow. Bottom left is a cartoon depiction of the spleen narrowing in on the cellular organization of the MZ. The white pulp region is divided into specific zones: marginal zone, B cell zone, and T cell zone. The MZ is comprised of different cell types. The most notable cell types are the MZM and MZ B cells. MZM and MZ B cells are seen interacting throughout the MZ. The MZ sinus-lining cells are capillary extensions of the central arteriole and are the site where blood-borne pathogens first enter the spleen. The MMM are tangentially positioned next to the marginal sinus-lining cells facing the white pulp region.

**MZM and MZ B cell interactions and their functional importance**

In the context of TI antigen responses in the spleen, MZ B cells and MZM are important players in initiating an efficient immune response. At normal basal levels in mice, MZ B cells home to the MZ due to an interaction with MZM (22) (Fig. 2). MZ B cells and MZM interact via the scavenger receptor, MARCO, on MZM with an undetermined cell surface receptor/ligand on MZ B cells (15, 22-24). *In vivo* studies where anti-MARCO antibody was injected intravenously (i.v.) into mice resulted in disruption of MARCO and MZ B cell interactions with displacement of MZ B cells to the white pulp area and MZM retained in the MZ (15). MZM-MZ B cell interactions are important functionally because MHC class II molecules, which are necessary for antigen presentation, are not expressed on MZM. Therefore, it has been postulated that upon binding and phagocytosis of microbes, the pathogen degradation products shed by MZM are taken up by MZ B cells (Fig. 2) (15, 17). This functional interaction between MZM-MZ B cells is another avenue aiding in the clearance of foreign pathogens.

Studies involving depletion of either MZM or MZ B cells in young adult mice report loss of the corresponding cell population as well as morphological disruptions of the MZ (Table I) (21, 39-41). A report by Kraal *et al.* studying MZM kinetics in the spleen observed that depletion of macrophages, including MZM, by *in vivo* liposome treatment lead to a subsequent loss of the B cells in the MZ (39). Recovery of MZM correlated with full restoration of the MZ B cell population of these mice. More recently, studies using SIGN-R1$^{-/-}$ mice, which have reduced MZM, reported decreases in MZ B cell numbers when compared to wild type mice (21). On the other hand, reports in

which MZ B cells were initially depleted in young adult mice by overexpression of CD70 (a TNF family member), which leads to a gradual loss of the splenic B cell pool, reported a subsequent gradual loss of the MZM pool (40). This same study also found that MZM failed to develop in $BCR^{-/-}$ mice lacking B cells. Similar studies have also found that CD19 (determined here to be important for MZ B cell differentiation) deficiency in B cells leads to a loss in MZ B cells by a mechanism believed to inhibit differentiation from precursor B cells to MZ B cells (41). This study reported that absence of MZ B cells corresponded with absence of MZM. Furthermore, adoptive transfer experiments were performed in which mature purified B cells from wild type mice were able to reconstitute the MZM pool after 17 days.

Investigators have also found the functional importance of MZM-MZ B cell interactions. Studies have found that upon infection with *S. pneumoniae*, SIGN-$R1^{-/-}$ mice have a reduced ability to mount an IgM specific antibody response against the phosphorylcholine (PC) epitope of *S. pneumoniae* when compared to wild type mice, which show elevated anti-PC IgM levels upon infection (20, 21). Similar experiments done *in vitro* where B cells derived from SIGN-$R1^{-/-}$ mice showed reduced anti-PC IgM levels upon stimulation when compared to B cells derived from wild type mice (21). It is therefore predicted in age that if either the MZM or MZ B pool is decreased, this will have an impact on the other cell type.

**Table 1. Depletion of MZM or MZ B cells and the effects on the MZ compartment**

| Report | Effect | | | | Reference |
|---|---|---|---|---|---|
| | MZM | MZ B cell | MZ Morphology | MZ B cell Position | |
| Liposome depletion of splenic macrophages | - - | - + | MZM, MMM absent | 80% reduced in MZ | Rooijen *et al.*, 1989 |
| CD70 Tg Mice | - - | - - | MZM, MZ B cells, and MAdCAM1+ cells absent after 8 wks | Completely absent after 8wks | Nolte *et al.*, 2004 |
| BCR $^{-/-}$ | - - | - - | MZM, MZ B cells, & MMM absent | Completely absent | Nolte *et al.*, 2004 |
| *In vivo* blocking of MARCO | + + | + + | MZM Present | White pulp area | Karlsson *et al.*, 2004 |
| CD19 $^{-/-}$ | - - | - - | MZM, MZ B c absent. MMM & MAdCAM1+ cells present | Completely absent | You *et al.*, 2010 |
| CD19 $^{-/-}$ reconstituted with purified B cells | + | + | MZM (17d) & MZ B cells (7d) | MZ | You *et al.*, 2010 |

**Table 1. Depletion of MZM or MZ B cell populations and its effects on the MZ compartment.** Survey of experiments that depleted either MZM or MZ B cell populations in the spleens of mice. Symbols correspond to lack (- -) or presence (+ +) of MZM or MZ B cells in the spleen.

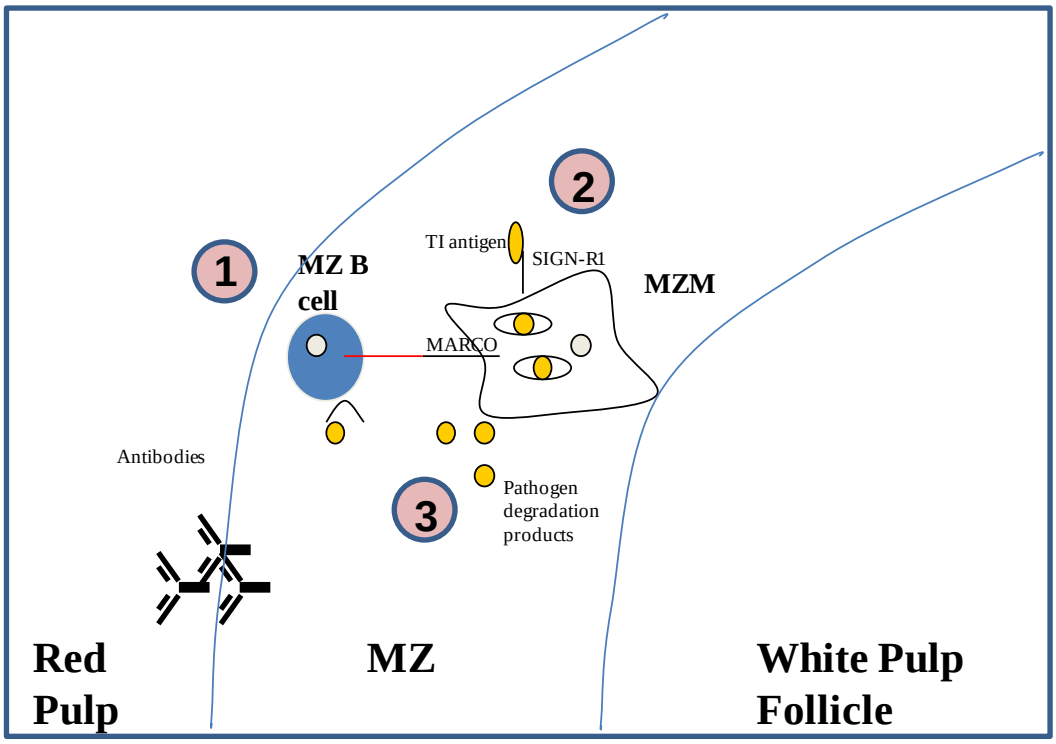


**Figure 2. Functional interaction of MZM and MZ B cells.** MZM and MZ B cells are components of the MZ of the spleen. MZM have a physical interaction with MZ B cells via the scavenger receptor MARCO located on the surface of MZM. **(1)** MZ B cells recognize TI antigens via the BCR and generate a rapid IgM antibody response. **(2)** MZM bind TI antigens predominantly through the cell surface receptors SIGN-R1 (depicted above) and MARCO. The antigen will then be phagocytized by the MZM. **(3)**When antigen has bound MZM it is believed that the pathogen degradation products shed by MZM are taken up by MZ B cells.

**Marginal zone macrophages**

MZM are a type of macrophage population in the MZ that appear as a band of cells forming the outer ring of the MZ. MZM begin to populate the MZ about 10 days post-birth in mice (42). MZM are derived from monocytes that home to the MZ as a result of the chemokines CCL19 and CCL21 that are expressed by $gp38^{+}$ stromal cells known to be important for T cell homing to the PALS (43). The exact origin of MZM has not been determined, but earlier studies examining macrophage kinetics in the spleen found that after liposome-mediated elimination of MZM, MZM did not repopulate the MZ until after 1 month (39). In this study upon liposome treatment, the red pulp macrophages (RPM), MMM, and MZM were eliminated simultaneously 24 hr post treatment. After 1 wk the RPM were found to repopulate, followed by the MMM in 2 wks, and finally MZM after one month (39). This sequence of repopulation suggested to the authors that MZM development may be under the influence of other splenic macrophage subtypes. Interestingly, in this same study an absence of B cells that reside in the MZ was also observed and did not start to re-emerge until after 16 days (39). Although this study shows that MZM can be generated, it is not clear if the MZM established 10 days post birth survives throughout the lifetime of the animal or if MZM are constantly replenished as is the case with other white blood cell populations.

MZM are known for their ability to be highly phagocytic and in fact have been referred to as “real scavenger cells” (8). MZM express on their surfaces a variety of pattern recognition receptors capable of inducing phagocytosis. Three main receptors have been characterized: Scavenger receptor A (SR-A); MARCO, a member of the SR

family of receptors; the C-type lectin SIGN-R1 (the mouse analog of the human dendritic cell-specific intercellular adhesion molecule [ICAM-3 grabbing nonintegrin) ( DC-SIGN)] [reviewed in (8)].

*Function of the MARCO receptor on MZM*

The MARCO receptor is expressed constitutively on MZM and is a member of the scavenger receptors (7). Scavenger receptors are traditionally known for binding a wide range of ligands such as polyribonucleotides, lipopolysaccharides, and silica particles (44). Studies in mice have shown that after ligand binding to MARCO, MZM are observed to traffic to the red pulp and MZ B cells displaced to the white pulp areas (15). To demonstrate this, investigators injected the bacterial pathogen, *S. aureus* (a known ligand for the MARCO receptor) i.v. into mice (14). Within 30 min of injection, *S. aureus* could be visualized exclusively on MZM (15). At 18h after injection *S. aureus* positive MZM were found to migrate into the red pulp, and MZ B cells were found in the white pulp follicles (15). The migratory ability of MZM has been attributed to a downregulation in SH2-containing inosital-5-phosphatase 1 (SHIP) signaling upon binding antigen – as deletion of SHIP leads to displacement of MZM to the red pulp (15).

Structurally, MARCO contains a long collagenous triple helix. The C-terminal region of MARCO has approximately 100 amino acids and has been recognized as the region where bacteria bind (45). Although the downstream signaling pathways of MARCO have currently not been directly determined, over-expression of MARCO by other cell types has been shown to activate Rac1 (46). Furthermore, it has also been

observed that MARCO over-expression results in cell shape changes that result in the formation of what is described as "large lamellipodia-like structures." These cell shape changes have also been shown to be accompanied by rearrangement in actin cytoskelton. It is important to note that while MARCO has been shown to bind antigen, it is believed that this process of antigen internalization occurs as a result of co-receptor involvement by a process not yet identified (47).

*Function of the SIGN-R1 receptor on MZM*

SIGN-R1, another prominent receptor on the surface of MZM was identified as the murine homologue to human DC-SIGN. DC-SIGN is a receptor found on the surface of dendritic cells in humans and is capable of binding the HIV-1 envelope glycoprotein (17). DC-SIGN is a C-type lectin (recognize carbohydrates) (7, 47) that binds to the adhesion molecule ICAM-3/CD50 expressed on resting T cells and ultimately transmits the virus to T cells (17). Notably, more recent studies have shown that DC-SIGN binds the gram-positive bacterium *S. pneumoniae* (16). SIGN-R1 on MZM has also been shown to bind the capsular polysaccharide of *S. pneumoniae* (19, 20) as well as the gram-negative bacteria such as *Escherichia coli* (48) and the polysaccharide dextran (18). Upon dextran binding, the SIGN-R1 receptor and antigen will internalize and this antigen receptor complex has been shown to localize to lysosomes (17). Briefly, K562 cells were transfected with monoclonal SIGN-R1 and administered dextran-FITC for 45 min at 37$^{o}$ C. Immunofluorescence microscopy revealed dextran-FITC internalized to the lysosomes. It has also been shown that the SIGN-R1 receptor on MZM is capable of

interacting with the toll-like receptor 4 (TLR4), initiating the production of proinflammatory cytokines (48). Transfection of SIGN-R1 into macrophage-like RAW264.7 cells resulted in enhanced TLR4 oligomerization. Immunoprecipitation experiments also revealed a physical association between SIGN-R1 and TLR4 (48). TLR4 is important for the production of a wide range of proinflammatory cytokines (49-51), which are important for proper immune function by inducing costimulatory molecules and other inflammatory mediators at the site of invasion (52).

**The binding of *S. pneumoniae* to murine SIGN-R1**

In humans, *S. pneumoniae* is transmitted from an infected individual through direct contact with their respiratory secretions (53). An estimated 10% of healthy adults are carriers of some serotype of *S. pneumoniae,* which are non-invasive and stay within the nasopharynx. When *S. pneumoniae* enters lung tissue through passage from the nasopharynx, it is referred to as invasive, leading to the development of pneumococcal disease. How does *S. pneumoniae*, a bacterium known to infect lung tissue, enter the MZ to bind the SIGN-R1 receptor? *S. pneumoniae* crosses lung tissue and enters the blood using the host's receptor for platelet-activating factor (PAF) (53). This receptor is known for the recognition of the phosphorylcholine (PC) determinant of the ligand PAF and is expressed on a wide variety of cells including but not limited to platelets, monocytes, and neutrophils found in the blood [reviewed in(54)]. *S. pneumoniae* express PC in their bacterial cell wall and therefore are recognized by the host's receptor. Once in the bloodstream, *S. pneumoniae* will filter to the spleen and bind to SIGN-R1$^{+}$ MZM. Mice

that are SIGN-R1-deficient are more susceptible to pneumococcal infection (20, 21). Once *S. pneumoniae* has bound SIGN-R1$^+$ MZM, antigen is then believed to be presented to the MZ B cells, which produce anti-PC IgM antibodies (21). Recently, studies done on the human DC-SIGN have shown that this receptor also binds to *S. pneumoniae.* DC-SIGN, a receptor expressed on DC that reside in mucosal tissue, was shown to specifically bind to *S. pneumoniae* serotypes 3 and 14 *in vitro* (16). Yet, DC were not observed to have any immunomodulatory effects. Therefore, further investigation needs to target human DC-SIGN and determine the mechanism involved in initiating an immune response after binding *S. pneumoniae.* Examining the murine homologue SIGN-R1 can lead to a better understanding of the immunomodulatory role of human DC-SIGN.

**Phagocytosis**

After binding antigen such as *S. pneumonia* MZM, will begin the process of phagocytosis. Phagocytosis is a form of endocytosis (the process by which cells engulf particles, molecules, and/or fluids) [reviewed in(55)]. Phagocytosis occurs when particles are greater than 0.5 μm in diameter. Phagocytosis of microbes is a complex process that involves multiple receptors, signaling molecules, and signaling pathways to effectively internalize the microbe. The receptors and endosomal compartments involved in the engulfment and clearance of microbes are discussed below.

*Receptor-mediated phagocytosis*

Multiple receptors have been shown to bind microbes simultaneously [reviewed in (47)]. Briefly, immunoglobulin Fc receptors, complement receptors, integrins, lectins, and scavenger receptors are believed to directly bind the microbe or bind opsonins on the surface of the microbe. Receptor binding induces many signaling pathways that use numerous molecules to undergo proper signaling that lead to a plethora of responses like microbial killing and the production of inflammatory cytokines and chemokines. Fc receptors bind immunoglobulin-opsonized pathogens and complement receptors bind complement-opsonized pathogens. Integrins are both adhesion and phagocytic receptors and have been seen to mediate both (55). For example, the fibronectin receptor ($\alpha_M\beta_1$ integrin) has been shown to bind ligand at the substrate-adherent surface of monocytes. This binding of ligand to receptor promotes the activation of the complement receptor CR3 ($\alpha_M\beta_2$ integrin), which mediates phagocytosis. Lectins, such as SIGN-R1, recognize self and non-self carbohydrates often seen on the cell wall of microbes (7, 47). Studies with the lectin for receptor mannose have shown that ligation of receptor leads to particle internalization (47). Scavenger receptors are well-known for their ability to bind and internalize modified lipoproteins. The MARCO receptor is a member of the scavenger receptors. Scavenger receptors are divided into two groups: SR-A and MARCO. They bind diverse ligands such as polyribonucleotides, lipopolysaccharides, and silica particles (44). It has been suggested that while scavenger receptors bind microbes, they do not contribute to the internalization; co-receptors are required for internalization (47).

*Phagocytic compartments*

Once a receptor has bound and internalized a microbe, the formation of a phagolysosome is initiated. The phagolysosome will fuse with compartments of the endocytic pathway and will be degraded [reviewed in (56)]. The main compartments of the endocytic pathway are the early endosome, late endosome, and the lysosome (56-58). Each compartment of the endocytic pathway has been characterized based on the intracompartmental pH, luminal composition and morphology.

The early endosome is often referred to as the major sorting station. Here, organelle materials may get recycled to the plasma membrane, proceed to late endosome, or be targeted to secretory vesicles (58). Using ratiometric measurements, the pH of the early endosome has been reported to be ~ 6 [reviewed in (58)]. The structure of the early endosome is described as multivesicular, consisting of cisternal regions with thin tubules (57). The late endosome and lysosome are regarded by some authors as one compartment; however there are differences between late endosomes and lysosomes. Both contain acid hydrolases, lysosome-associated membrane proteins (LAMPS), and lysobisphosphatidic acid (a phospholipid that plays a role in glycolipid degradation and the transport of lipids and membrane proteins) [reviewed in (56)]. Differences between late endosomes and lysosomes include their function and morphology. The late endosome functions as the main site for proteolysis and the lysosome functions as the main site for hydrolase by acid hydrolases. At the ultrastructural level, late endosomes are observed to have a complex morphology with a multivesicular appearance containing

cisternal, tubular and vesicular regions similar to the early endosome (59, 60), whereas, lysosomes are observed to be spherical in shape and said to resemble vesicles (60). The pH of the late endosome has been reported to be approximately 5.5 and the pH of the lysosome close to 4 (56). The pH varies from cell to cell and is controlled by a complex system controlled by the luminal environment of each compartment. A system of vacuolar ATPases (V-ATPases) and redox chains pump protons into the luminal compartments, which are regulated by $Na^+/H^+$ exchangers (early endosome) and $Cl^-$ ion channels (late endosome and lysosome) (56).

**The marginal zone B cell**

The B cell population is comprised of several functional and phenotypically distinct subpopulations, including newly-formed immature (transitional and preMZ B cells), mature FO, B1 B cells, regulatory B cells, and MZ B cells (Table II). These subpopulations have been suggested to be a result of evolutionary pressures that allowed the host to defend against invading pathogens with and without help from T-cells (61, 62).

Recent attention has been given to MZ B cells because of their ability to provide a rapid defense against TI bacterial antigens – an attribute lacking in TD FO B cells, which can take up to 7 days to produce antibodies. MZ B cells in normal adults make up ~5% of the total B cell pool in the spleen, and FO B cells comprise ~90%. Upon stimulation by TI antigens, MZ B cells differentiate rapidly into short-lived plasma cells and secrete IgM antibodies (10). In addition, MZ B cells have been shown to mediate TD responses *in vitro* [reviewed in Allman et al (11)]. In humans, MZ B cells are found in the MZ of

the spleen, and B cells with the MZ B phenotype are also seen in lymph nodes in the outer extra-follicular rim (11). Yet in rodents, MZ B cells have only been demonstrated to reside in the MZ of the spleen.

Once thought to be sessile, recent work has shown that MZ B cells shuttle between the MZ and follicles of the spleen, resulting from the balance of two main factors. The first is downregulation of the sphingosine 1-phosphate receptor ($S1P_1$) that is present on MZ B cells (15, 63, 64). $S1P_1$, like MARCO, is also required for MZ B cells to remain lodged in the MZ, because in the absence of $S1P_1$, MZ B cells are found displaced to the white pulp follicle (64, 65). The chemokine CXCL13 and its receptor CXCR5 that is present on MZ B cells are the second major factor important for MZ B cell shuttling. The white pulp follicle has high levels of CXCL13 and it is believed that MZ B cells naturally move toward this chemokine gradient (64, 65). This shuttling occurs during homeostatic conditions (64) and in response to antigen (15, 63, 64). Antigen that has entered by way of the MZ sinus is believed to be phagocytized by MZM and the pathogen degradation products are then taken up by MZ B cells (15, 17). On the other hand, some believe MZ B cells are able to bind the antigen directly and transport it to the white pulp follicles (63). Upon exposure to TI antigens, MZ B cells will bind the antigen via the BCR thereby initiating the BCR-mediated signaling pathway. BCR aggregation results from antigen binding leading to phosphorylation of tyrosine residues on immunoreceptor tyrosine activation motifs (ITAMS) located on the cytoplasmic tails of the BCR co-receptors. Once phosphorylated, the tyrosine kinase Syk will facilitate the initiation of downstream signaling pathways that lead to the activation of phospholipase

C-γ (PLC-γ). In parallel to BCR aggregation, the complement receptor CD21/35 binds complement-coated antigens and enhances BCR signaling. Activation of CD21/35 leads to Bruton's tyrosine kinase (Btk) signaling that causes further activation of PLC-γ and also causes activation of NFκB, which are both components necessary for proliferation and clonal expansion of B cells [reviewed in (32)].

**Table 2.** Splenic B-lineage subpopulations and phenotypes

| B cell subset | Phenotype | Location | Function | Frequency |
|---|---|---|---|---|
| Transitional T1 | $B220^{+a}$ $CD23^{-b}CD21/35^{c}_{low}$ $IgM_{high}$[d] $IgD_{low}$[e] | MZ | Immature B cell | 3-5% |
| Transitional T2/T3 | $B220^{+}CD23^{+}CD21/35_{low}$ $IgM_{high}$ $IgD_{high}$ | MZ/Follicle? | Immature B cell | < 3% |
| preMZ B cells | $B220^{+}$ $CD23^{+}CD21/35_{high}$ $IgM_{int/high}$ $IgD_{high}$ | Follicle | Immature B cell | <3% |
| Follicular B cells | $B220^{+}CD23^{+}CD21/35_{int}$ $IgM_{int/high}$ $IgD_{high}$ | Follicle | Mature B cell important in TD response | >90% |
| Marginal Zone B cells | $B220^{+}CD23^{-}$ $CD21/35_{high}$ $IgM_{high}$ $IgD_{low}$ | MZ | Mature B cell important in TI response | 3-5% |
| B1 B cells | $B220_{+}$ $IgM_{high}$ $IgD_{low}$ CD9[f] | MZ? | Mature B cell important in TI response | <3% |
| Regulatory B cells | $CD1d^{hi}CD5^{+}$ | ? | Produce IL-10 | 1-2% |

[a] B220/CD45 is belongs in the protein tyrosine phosphate family and is a major cell surface glycoprotein. It primarily recognizes the proB cell stage through mature B cells.

[b] CD23 is a type II transmembrane glycoprotein present on resting follicular B cells. CD23 is also a low affinity receptor for IgE.

[c] CD21/35 are expressed by mature B cells and CD21 is a receptor for complement component C3d and Epstein-Barr virus.

[d] IgM a class of immunoglobulin expressed on the surface of immature and mature B cells.

[e] IgD a class of immunoglobulin expressed on the surface of mature B cells.

[f] CD9 is a cell surface glycoprotein important for cell adhesion and migration.

**Marginal zone B cell production in young and old mice**

In normal young adults, B cell development starts in the bone marrow. B cells arise from common lymphoid progenitors (CLP) and through a series of gene rearrangements (V(D)J regions) develop into a pro-B cell, pre-B cell, and an immature B cell phenotype (Fig. 3). An immature B cell will leave the bone marrow and enter the spleen. In the spleen, immature B cells will transition into T1, T2/T3 transitional B cells, and pre-MZ B cell before taking on the mature MZ B or FO B cell phenotype. Production of MZ B cells is influenced by several factors including but not limited to: interleukin-7 (IL-7) cytokine and receptor levels, B cell receptor (BCR) signal strength, the helix-loop-helix protein E2A, and more recently the adapter molecule SHEP1 (SH2 domain-containing Eph receptor-binding protein 1) [reviewed in (11, 32, 66-68)]. For proper MZ B cell development, Notch 2 levels need to be high, and E2A protein activity and BCR signal strength need to be low. An interesting observation is that in age decreases in IL-7 (69, 70), BCR signal strength (71-74), and E2A protein levels (75-77) have been observed (Fig. 4). Since these conditions favor MZ B cell development over FO B cell development, a shift towards MZ B cell differentiation at the expense of FO B cell production may be predicted. However, increases in MZ B cell numbers in age have only been reported by the Cambier group using a BCR transgenic mouse model (78). Furthermore, results in this dissertation and the work by Frasca *et al.* (79) show a decrease in MZ B cells with age.

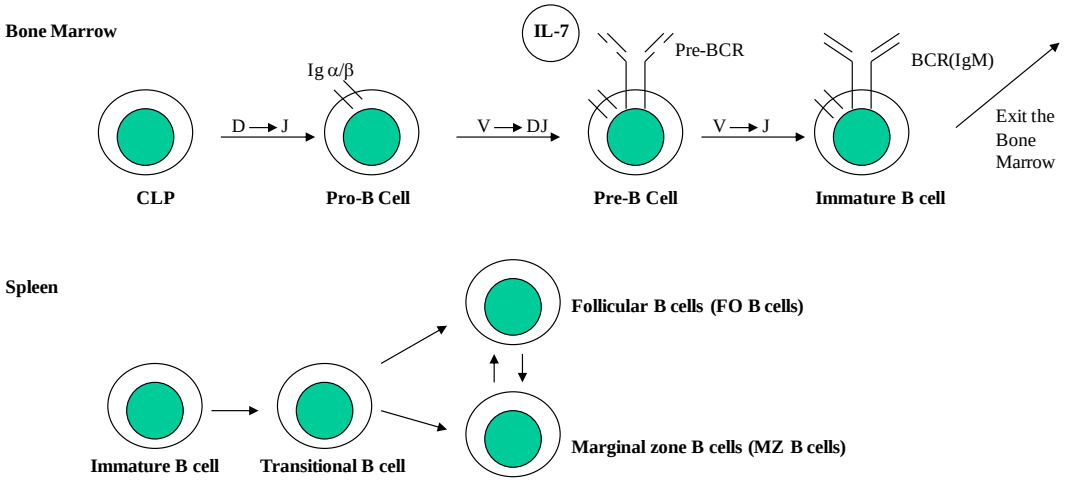


**Figure 3. MZ B and FO B cell production in young mice.** Figure depicts normal B cell development which arises in the bone marrow. B cells arise from common lymphoid progenitors (CLP) and through gene rearrangement (V(D)J regions) will progress through a pro-B cell, pre-B cell, and an immature B cell phenotype. An immature B cell will leave the bone marrow and enter the spleen. In the spleen, immature B cells will transition into Transitional B cells before taking on the mature MZ B or FO B cell phenotype. It has been suggested that MZ B and FO B cells also possess the ability to interchange, taking on the other's phenotype depending on the environmental conditions.

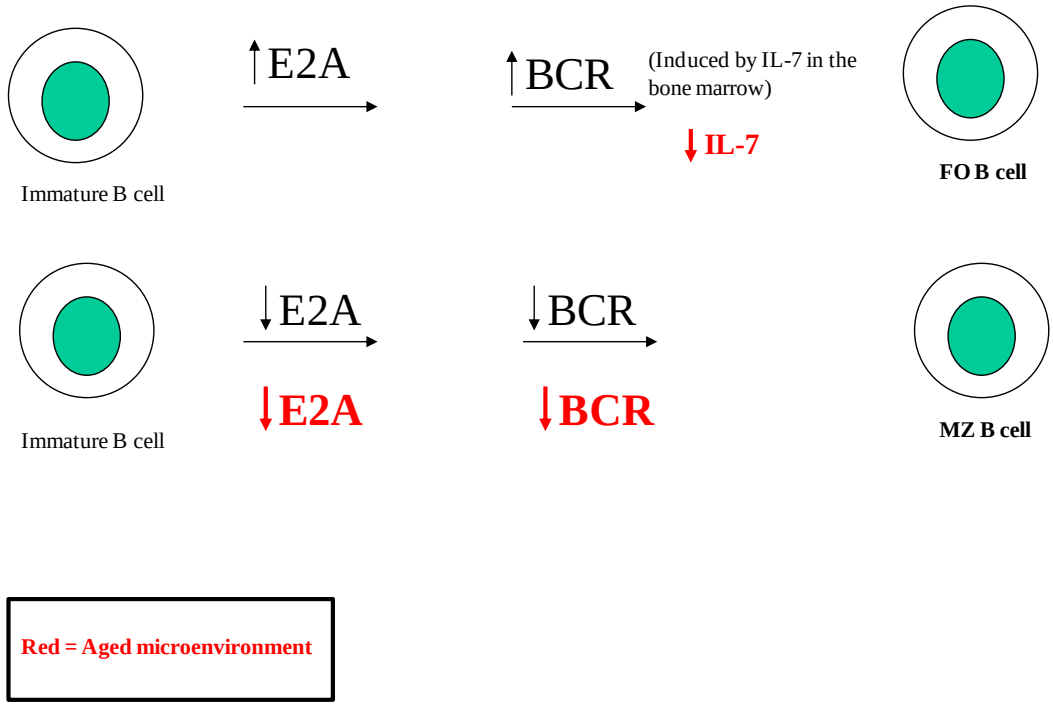


**Figure 4. Factors important for the production of MZ B and FO B cells in young and old mice.** Immature B cells will develop into FO B cells as a result of the availability of high amounts of the transcription factor E2A and increased BCR signal strength induced by IL-7 secreted by bone marrow stromal cells. MZ B cells will arise when there is less E2A available and the BCR signal strength is low. Red text corresponds to the factors that are present in the aged microenvironment.

**MAdCAM1$^+$ marginal zone sinus and metallophilic macrophages**

The MZ compartment is also comprised of non-immune cells including the MAdCAM1$^+$ sinus-lining endothelial cells, which line the site where pathogens and recirculating lymphocytes enter into the MZ (30). MAdCAM1 is a homing receptor on the high endothelial venules (HEV) of gut-associated lymphoid tissue (80, 81). MAdCAM1 expressed on HEV has been shown to be responsible for lymphocyte traffic into these mucosal sites. However, similar roles for the MAdCAM1 expressed on the endothelial cells that form the MZ sinus could not be demonstrated (82). Recent studies have implicated the role of MAdCAM1 in the homing of bone marrow- derived hematopoietic stem cells into the spleen (83). The MZ sinus is a capillary extension of the central artery. Ultrastructurally, the MZ sinus of rats was found to have a basement membrane with discontinuous walls wider on the MZ side than the follicle side (36). Lymphocytes, macrophages, plasma cells, and occasionally polymorphonuclear leucocytes were found adjacent to these discontinuities; presumably these discontinuities are wide enough for the passage of cells as large as macrophages.

The positioning of the MAdCAM1$^+$ sinus-lining cells is thought to be under the influence of sphingosine-1-phosphate receptor 3 ($S1P_3$). $S1P_3$ is a G-protein-coupled receptor belonging to a family of five different isotypes, $S1P_{1-5,}$ found ubiquitously on most cells including lymphocytes [reviewed in (7)]. The known ligand for the $S1P_{1-5}$ receptors is sphingosine-1-phosphate (S1P), which is a lysophospholipid found predominantly in peripheral blood and produced by many cells including macrophages

(7). In a study by Girkontaite *et al.*, $S1P_3$- deficient mice showed morphological disruptions in the $MAdCAM1^+$ sinus-lining cells that resembled multiple layers of $MAdCAM1^+$ cells (84). Disruptions in the MZ sinus most likely would lead to a hindrance in passage of cells and antigens through the discontinuities of the sinus. Studies presented in this dissertation will examine the $MAdCAM1^+$ MZ sinus in old mice to determine if there are any gross morphology alterations, such as disruptions in cell positioning.

Situated along the inner border of the MZ sinus facing the white pulp area, MMM form a tight ring around the MZ sinus. As seen with the $MAdCAM1^+$ sinus, $S1P_3$ has also been found to be necessary for the positioning of MMM (84). MMM express the cell surface adhesion molecule Siglec-1 (sialoahesin) that can bind sialic acid containing molecules on the surface of pathogens and immune cells [reviewed in (7, 30)]. Siglec-1, however, is not involved in the internalization of antigen and requires other receptors for phagocytosis (7). MMM produce the cytokines interferon-α and interferon-β after challenge with virus (30). MMM have a high content of nonspecific esterase (85). This enzyme is involved in the cleavage of fatty acids and removal of apoptotic cells. In sum an alteration in MMM may impinge on the ability to remove dead cells that accumulate due to natural cellular turnover. Furthermore, MMM positioning is continuous with the MZ sinus. Therefore, it is also conceivable that disruptions in the sinus can indirectly cause damage to this pool of macrophages.

**Survey of relevant age-associated declines in immune function**

The elderly population 65 years and older has a greater susceptibility to infections than young adults. Histological examination of splenic tissues with age have found reduced germinal centers (29) and disrupted T cell zone (PALS) of the spleen with visual changes in the MZ (26). It has been well documented that aging is associated with a decline in cell-mediated and humoral immunity. The thymus involutes and the naïve T cell pools decline with age while the memory T cell pool increases (86, 87). In terms of the humoral immune response, the mature B cell pool (FO B cell phenotype) in the spleen has been reported to be similar in young and old mice (88); however, the pre B cell pool in the bone marrow has been reported to decrease when compared to young mice (88). The maintenance of the mature B cell pool in the spleen is thought to be due to an accumulation of long-lived mature B cells in the old and not a result of turnover with newly formed B cells (27). Recent studies determined if B cells in old mice developed at similar rates when compared to B cells of young mice (89, 90). BrdU labeling showed that the production rate of immature B cells is similar in young and old mice, yet newly made immature B cells of old mice were less frequent in the spleens of old mice when compared to young mice (89). More recently, the migration of immature B cells to the spleens of old mice was examined by transferring immature B cells from young mice into old and young mice (27). Results found that the number of donor immature B cells in old mice was significantly reduced when compared to the amount of donor cells recovered in young mice. Together these data suggest that the reduced frequency of newly made

mature B cells observed in old mice is the result of alterations in the splenic microenvironment hindering newly formed B cells from populating the spleen.

B cells are ultimately important for the production of antibodies against invading pathogens. In age, levels of serum antibody against tetanus toxoid, plant mitogens and allogenic lymphocytes of older humans are reduced compared to young adults and are maintained for shorter periods (91-93). Moreover, the antibodies produced by aged individuals have been reported to have reduced affinity and avidity when compared to antibodies of young adults (94-96). Reports using mice have shown antibodies generated in old mice against PC, found in the cell wall of *S. pneumoniae*, are less protective when compared to the antibodies generated in young mice (73, 74). PC-specific hybridomas were generated from young and old mice and isolated RNA was used to determine which immunoglobulin $V_H$ and $V_L$ gene families (important for the variable region of the immunoglobulin) were utilized. Results revealed that 12/13 of the hybridomas tested from young mice expressed restricted $V_H$ and $V_L$ gene families, whereas only 2/13 of the hybridomas from old mice expressed the same $V_H$ genes and none expressed the $V_L$ gene family seen in young. Thus, the repertoire of immunoglobulin gene usage appears to change with age. Furthermore, the antibodies generated against PC in old mice were able to cross react with a number of unrelated antigens (74). In humans, the IgM antibody titers of elderly individuals vaccinated against *S. pneumoniae* or pneumococcal polysaccharides has also been reported to be reduced when compared to young adults (97). Given that *S. pneumoniae* infection can

elicit a TI immune response these data suggest a breakdown in the TI immune response in the old. As mentioned previously, MZM are key in the response to TI antigens.

Although there are no reports on the immune response of MZM in age, whole splenic macrophages (13), peritoneal macrophages (98, 99), and alveolar macrophages (100) of aged rodents have been reported to decrease in function when compared to young rodents. Studies by Chelvarajan *et al.* measured the cytokine profiles of whole splenic macrophages *in vitro* after treatment with the TI antigens trinitrophenol (TNP)-LPS and TNP-Ficoll. Results showed that aged macrophages secreted reduced amounts of the proinflamatory cytokines IL-6, TNF-α, IL-1β, and IL-12 and elevated amounts of the anti-inflammatory cytokine IL-10 when compared to young mice (13). Similarly, studies with peritoneal macrophages isolated from young and old mice found that after LPS stimulation, cultured macrophages from old mice produced less IL-6 and TNF-α when compared to young mice (98). It was further determined by Boehmer *et al*. that this decrease was due to decreases in p38 and c-jun NH2-terminal(JNK) mitogen-activated protein kinase (MAPK), which are transcription factors important for the production of IL-6 and TNF-α. Notably, this same study found no differences in the surface expression of TLR4 (recently shown to interact with SIGN-R1) between age groups.

There is also a wide body of literature that has found heightened levels of proinflammatory cytokines with increasing age (101, 102). This heightened proinflammatory state is termed "Inflam-aging" and is described as the underlying factor attributing to the immunosenescence observed in aging. It has been suggested that

phagocytic cells such as macrophages and neutrophils are responsible for increased production of proinflammatory cytokines in age. It is argued that this hyper-proinflammatory state result in damage to neighboring immune cells and thereby contributes to immunosuppressive effects. Whether a hyper-proinflammatory state can lead to a hindrance in normal cell frequencies still, however, remains to be elucidated.

## Goals of my experiments

The MZ of young mice is a highly organized region comprised of MZM, MZ B cells, the MZ sinus and MMM. Since little is known about changes in the cellular components of the MZ with age, **the goal of this dissertation is to compare the MZ compartment in old and young mice and to assess the age-associated alterations of the MZ.** Results presented in this dissertation first show that there is a morphological disruption of the MZ with age and decreases in MZM and MZ B cell frequencies are seen in old mice. Results have also determined the possible micro-environmental factors contributing to this loss of MZM and MZ B cells with age. Lastly, the functional differences of MZM of young and old mice were investigated. These results determined that the decline in the TI immune response reported in age is a result of loss in cell frequency/number and not a cell intrinsic defect.

# CHAPTER III

# MATERIALS AND METHODS

## Animals

Female BALB/c mice were purchased from Harlan Laboratories (Indianapolis, IN) or Charles River (Wilmington, MA) through contract with the National Institute of Aging at 17-18 mo of age and from Harlan Laboratories at 6-8 wks of age. Upon receipt, the animals were housed at the Animal Research Facility (Loyola University Medical Center, Maywood, IL) under specific pathogen-free conditions until sacrificed. Old animals with any visual abnormalities such as enlarged spleens and presence of tumors were not used in these studies.

## Tissue histology

Spleens were fixed in 10% buffered formalin and processed using an automatic tissue processor, dehydrated through graded alcohols, cleared in xylene and infiltrated with paraffin. Paraffin sections were cryosectioned on a microtome (4 μm) and applied on Superfrost®/ Plus microscope slides (Fisher Scientific, Pittsburg, PA). Sections were then treated with xylene to deparaffinize the tissue and rehydrated in successive decreasing grades of alcohol. The splenic sections were stained with hematoxylin and eosin (H&E).

Sections were cleared and mounted. Slides were viewed and photographed with a Leitz Diaplan microscope (W. Nuhsbaum, Inc., McHenry, IL).

**Tissue specific scoring of MZ architecture**

H&E stained slides were blinded and four well-oriented white pulp areas were chosen for each animal and scored independently by two investigators. In consultation with a pathologist, criteria were established to evaluate the morphology of the MZ. The interface between the white pulp and MZ was evaluated subjectively for the percent of distortion around each white pulp area and given a score ranging from 0-4. A score of 0 corresponded to ≥ 75% distortion, 1 was ≥ 50% but ≤ 75%, 2 corresponded to ≥ 12.5% and ≤ 50% distortion, 3 corresponded to ≤ 12.5% distortion, and finally a score of 4 corresponded to no evidence of interface distortion. For each white pulp area, the extent of interface distortion was also evaluated by determining the percent of radius involvement. This was defined by taking the area that was distorted and evaluating the amount of distortion that protruded toward the center of the white pulp. As before, for each white pulp area, a score ranging from 0-4 was given. A score of 0 was ≤ 20%, 1 corresponded to ≤ 15%, 2 corresponded to ≤ 10%, 3 corresponded to ≤ 5%, and finally 4 corresponded to no distortion protruding inwards. The summation of the interface distortion and percent of radius involvement per white pulp area was determined and given a total score ranging from 0-8. The final distortion was characterized either as severe (0-2), moderate (3-4), mild (5-6), or minimal (7-8). Finally, the average score of all four white pulp areas per animal was determined and reported for each mouse.

**Tissue specific scoring of MAdCAM-1$^+$ MZ sinus lining cells**

MZ sinus lining cells were revealed by immunofluorescence staining of spleen frozen sections from the middle 1/3 of the spleen. A tiled image (25x) of a complete cross section of spleen (6-8μm) from each animal was compiled using a Zeiss LSM 510 confocal microscope (Carl Zeiss, Inc., Jena, Germany). Using LSM image browser software (Carl Zeiss, Inc), the lines of MAdCAM-1$^+$ cells were outlined using the polyline drawing and measurement tools. Measurements of the length of MAdCAM-1$^+$ cells enveloping all white pulp areas in a single section were recorded. Disrupted lengths were then discriminated and measured by identifying dispersed, non-compact MAdCAM-1$^+$ staining. Relative proportion of the disrupted areas verses total length of the lines covered by MAdCAM-1$^+$ cells was calculated.

**Immunocytochemistry**

One-third of each spleen was frozen in Tissue-Tek® O.C.T. freezing medium (Sakura, Torrance, CA) and stored at -70$^o$C. Frozen spleens were cryosectioned (6-8 μm) onto Superfrost®/ Plus microscope slides. Splenic sections were fixed in acetone for 10 min, blocked in 5% normal mouse serum (NMS) (The Jackson Laboratory, Bar Harbor, Maine) and then incubated for 1 hr with an unconjugated rat anti-mouse IgG2a anti-MAdCAM-1 mAbs (MECA-367; BD Pharmingen, San Diego, CA) followed by a 30 min incubation with alkaline phosphatase conjugated mouse anti-rat IgG2a (2A 8F4; Southern Biotech, Birmingham, AL) to detect the MZ sinus lining cells. Positive cells were

revealed using Alkaline Phosphatase Substrate Kit III (Vector Laboratories, Burlingame, CA). For double immunocytochemistry, sections were then blocked with 5% NMS for 20 min and subsequently incubated for 30 min with either unconjugated rat anti-mouse IgG1 anti-MARCO mAbs (ED31; BMA Biomedicals, Switzerland) or unconjugated armenian hamster anti-mouse SIGN-R1 (ebio22D1; eBioscience, San Diego, Ca) followed by a 20 min incubation with horseradish peroxidase (HRP) conjugated mouse anti-rat IgG1 (G1 1C5; Southern Biotech) or rabbit anti-armenian hamster IgG HRP (Abcam Inc., Cambridge, MA), respectively, to detect MZM. Positive cells were revealed using DAB Substrate Kit for Peroxidase (Vector Laboratories). All antibody incubations were at room temperature. Slides were counterstained with Nuclear Fast Red (Vector Laboratories) for 30-60 seconds, mounted with VectaMount (Vector Laboratories) and viewed and photographed with a Leitz Diaplan microscope.

**Tissue specific scoring of MZM**

MARCO was revealed by immunocytochemical staining of spleen frozen sections. Slides were blinded and four well oriented white pulp areas were chosen per animal and scored independently by two investigators. Each area was given a score of 1, 2, or 3 for the abundance of $MARCO^+$ MZM and the percent of the continuity of MZM encircling each white pulp area. A score of 3 equated to a high abundance of MZM present that tightly encircled the MZ sinus. A score of 2 equated to a moderate abundance of $MARCO^+$ MZM that partially encircled the MZ sinus. Finally, a score of 1 equated to low or virtual absence of $MARCO^+$ MZM that, if present, were found in patches along the MZ sinus.

An average score of the four white pulp areas graded was determined and reported for each individual animal.

**Immunofluorescence and confocal microscopy**

Cryosections of spleen were fixed in acetone for 5 min and incubated with Super Block (ScyTek Laboratories, Inc., Cache, UT) for 5 min according to manufacturer's protocol. Sections were incubated at room temperature with primary antibodies for 1 hr followed by respective secondary antibodies for approximately 30-45 min. To identify MZ sinus lining cells, sections were stained with unconjugated rat anti-mouse MAdCAM-1 followed by goat anti-rat Alexa Fluor® 633 (Invitrogen, Carlsbad, Ca). For isotype control, rat IgG2a unlabeled with goat anti-rat Alexa Fluor® 633. To reveal MMM, sections were incubated with fluorescein isothiocyanate (FITC) conjugated rat anti-mouse CD169 (MOMA-1; AbD Serotec, UK). For isotype control, rat IgG2a FITC. To reveal MZM, sections were stained with unconjugated armenian hamster anti-mouse SIGN-R1, goat anti-armenian hamster IgG biotin (The Jackson Laboratory) and Streptavidin (SA)-Dylight™ 549 (The Jackson Laboratory). For isotype control, Armenian hamster IgG. Sections were blocked with 5% normal armenian hamster serum for 20 min and stained for co-localization of MARCO using unconjugated rat anti-mouse MARCO followed by donkey anti-rat Dylight™ 488 (The Jackson Laboratory). Isotype control used, rat IgG1. To reveal CCL21, sections were stained with goat anti-mouse CCL21 (R&D Systems) and donkey anti-goat Alexa 555 (Invitrogen). For isotype control, goat IgG (Jackson Laboratory). Sections were blocked with 5% normal rat

serum for 20 and stained for MZ sinus lining cells as a landmark using unconjugated rat anti-mouse MAdCAM1 followed by donkey anti-rat Alexa 488 (Invitrogen). For isotype control, rat IgG2a (AbD Serotec). Slides were mounted with fluorescent mounting medium (Dako, Carpinteria, CA) and viewed using a Zeiss LSM 510 confocal microscope (Carl Zeiss, Inc., Jena, Germany).

***In vivo* uptake of dextran by MZM**

Using a protocol previously described by Ato *et al.* (43), mice were injected i.v. in the tail vein with 200 µl of dextran-FITC (500,000 MW, Invitrogen) at 100µg/ml in sterile PBS. After 45 min, the mice were sacrificed and spleens harvested. One third of the spleen was placed in Tissue-Tek® O.C.T. freezing medium for immunofluorescence analysis and the remaining 2/3 was used for flow cytometry analysis (as described below). For co-localization of MARCO with dextran-FITC positive cells, cryosections were incubated with unconjugated rat anti-mouse MARCO followed by donkey anti-rat Dylight™ 488 (as described above). Slides were mounted with fluorescent mounting medium and viewed using a Zeiss LSM 510 confocal microscope.

**Flow cytometry – revisited**

Flow cytometry is a highly sophisticated instrument that can be used to gather a plethora of information about a cell population such as the cell size, cells frequency/number, and amount of protein expressed on the cells surface (103). A cell can be identified via flow cytometry analysis through the use of fluorescently labeled

antibodies that recognize the cells antigens. Current flow cytometry methods utilize the use of a multiple fluorescently labeled antibodies for the precise identification of cell populations. After cells are stained with the appropriate antibodies they are run through the flow cytometer. Cell samples are suspended in saline solution, and 1000 cells/second are passed through the flow cytometer like a stream. At the integration point of the instrument each cell is hit with a laser beam and information about how the cell scatters light and the fluorescence of the conjugated antibodies bound to the cell is recorded.

Light scattered in the forward direction is called the cells forward scatter (FSC). The FSC gives information about the size of the cell – small cells have low FSC and large cells have high FSC. Light scattered in angular directions is called the side scatter (SSC). The SSC gives information about the cells granularity. Cells such as neutrophils have high SSC because they are highly granular due to high levels of lytic enzymes within the cell compared to lymphocytes that have virtually no lytic enzymes.

The fluorophores conjugated to the antibodies each have a unique excitation and emission spectrum. The simultaneous measurement of multiple fluorescently labeled antibodies on a cell will result in spectral overlap in the emission spectrums. Special filters will correct for this overlap, however, compensation also needs to be utilized. Compensation is the process by which the spectral overlap of the interfering fluorophore is subtracted as a percentage of the signal. For this subtraction to be achieved single fluorescently stained beads/cells for each fluorophore used to mark the cell need to be run

on the cytometer before the cell sample is run. Once compensations are set the experimental samples are ready to be run through the flow cytometer.

Lasers are used to excite the fluorophores and optical filters are used to separate emission of varying wavelengths. Optical filters can be either high pass (for one fluorophore detection; allows light of high wavelengths to pass while attenuating low wavelengths), short pass (allows light of short wavelengths to pass while attenuating light of high wavelength), or band pass (for multiple fluorophore detection; a combination of low and high pass filters). A blue 488 nm, red 633 nm (HeNe), and a violet 405 nm laser are in the FACSCanto™II cytometry used at the Loyola University Medical Center Core Facility.

*Analyzing data gathered*

For years the isotype antibody of the antibody used to target antigen was used as the control to determine where the positive cell populations of interest separated from the negative cell populations. In the last decade the use of fluorescence minus one (FMO) has become the standard for flow cytometry controls (104). FMO employs all the fluorophores used to target a population except the one of interest to determine the positives and negatives of that particular population. Once the gates are determined populations of cells can be revealed through recognition of protein determinants known to be associated with the cell. Analysis of the data collected by the flow cytometer is

done using Tree Star FlowJo software version 7.5.5 (Becton Dickinson, Mountain view, CA).

**Flow cytometric staining for identification of MZ B cells, FO B cells, MZM, CCR7$^+$ MZM, dextran$^+$ MZM, pHrodo$^+$ MZM, and CD4$^+$ T cells**

Splenocytes, from approximately 1/2 - 2/3 of each spleen, were obtained by gently pressing the splenic tissue between two frosted glass slides. The dispersed cells were collected in RPMI 1640 supplemented with 10% FBS, 1% L-glutamine, 1% penicillin/streptomycin, and 500 µl M β2-ME (referred to as media here on end), and small clumps were allowed to settle in a conical tube and discarded. Erythrocytes were lysed with 0.8% ammonium chloride solution and incubated on ice for 4 min. For four-color analysis of MZ B and FO B cells, 1 x $10^6$ cells per sample were incubated with rat anti-mouse CD23-PE-CY7 (B3B4; eBioscience), rat anti-mouse B220-FITC (RA3-6B2; Southern Biotech), rat anti-mouse CD21/35-PE, and rat anti-mouse IgM-PE-Cy5.5 (II/41; eBioscience) for 20 min on ice, protocol modified from Won *et al.* (105). Cells were then fixed in 1% paraformaldehyde and the samples were analyzed using FACS Canto II with Tree Star FlowJo software version 7.5.5. MZ B cells were identified as CD23$^-$ B220$^+$ CD21/35$_{high}$ IgM$_{high}$. FO B cells were identified as CD23$^+$ B220$^+$ CD21/35$_{int}$ IgM$_{int/high}$.

For MZM characterization, approximately 1/2 - 2/3 of each spleen was treated with Collagenase D (Roche Diagnostics, Indianapolis, IN) or without (as described above) for 1.5 hr at 37$^o$C, and the single cell suspension was recovered after gentle

filtration of the minced tissue through a fine nylon mesh. The erythrocytes were lysed by 0.8% ammonium chloride and the cells were washed and resuspended media. For two-color analysis to identify MZM, 1 x $10^6$ cells per sample were pretreated on ice with rat anti-mouse CD16/32 FcR-block (FCR4G8; AbD Serotec) and subsequently incubated with either allophycocyanin (APC)-Cy7 labeled rat anti-mouse CD11b (M1/70; eBioscience) or biotinylated CD11b (M1/70; eBioscience) with armenian hamster anti-mouse SIGN-R1-Alexa Fluor® 647 (22D1; eBioscience) for 20 min on ice. Streptavidin-peridinin chlorophyll protein (SA-PerCP; 16904; BD Pharmingen) was used as a second-step reagent. For isotype control to SIGN-R1, armenian hamster anti-mouse IgG-Alexa Fluor® 647 (22D1; eBioscience) was incubated for 20 min on ice. Cells were fixed in 1% paraformaldehyde, except in experiments using dextran; cells were resuspended in PBS and analyzed using flow cytometry.

For characterization of $CCR7^+$ MZM, 1 x $10^6$ cells per sample of dispersed splenocytes were incubated with anti-mouse CCR7-PE (eBioscience) for 30 min in 37° C followed by pretreated on ice with rat anti-mouse CD16/32 FcR-block and subsequently incubated with antibodies to identify MZM (described above). For isotype control to CCR7, Rat IgG2a (eBioscience) for 30 min in 37° C. For characterization of CD4+ T cells, thymus was removed and single cell suspensions were made and resuspended in media. For one color identification of $CD4^+$ T cells, 1 x $10^6$ cells per sample were stained with anti-mouse CD4-PE (eBioscience). Cells were fixed in 1% paraformaldehyde and resuspended in PBS and analyzed using flow cytometry.

For characterization of pHrodo$^{+}$ MZM splenocytes obtained from both young and old cells were harvested and allowed to adhere onto 35 mm culture plates for 1 hr in media. Non-adherent cells were removed and 125 µl of 125µg/ml pHrodo were added and allowed to incubate in 37 C for 2 hrs. Cells were collected using a policeman scraper, stained for to identify MZM, and analyzed using FACScanto, which records fluorescence of the phagocytized pHrodo in the PE channel.

**Adoptive transfer of mature B cells to young and old recipient mice**

Spleen was prepared from young (IgM$^{b}$) C.B17 mice and transferred into young and old (IgM$^{a}$) BALB/c mice. C.B17 mice differ from BALB/c mice in expression of the IgM allotype, allowing for donor cells to be identified from recipient cells. Donor spleen cells were dispersed as described above, and then donor mature B cells were purified using a magnetic antibody cell sorting (MACS) B cell isolation kit (Miltenyi Biotech) according to the manufacturer's protocol. Each recipient mouse received an intravenous injection of 20 x $10^{6}$ donor purified mature B cells in 200 µl PBS. Spleens from recipient mice were harvested 6 hr post-transfer. Donor MZ B and FO B cells were analyzed by flow cytometry stained with antibodies previously mentioned for the identification of MZ B and FO B cells (note: anti-allotype IgM biotin was used in place of rat anti-mouse IgM PE-Cy5.5 for identification of donor cells).

For detection of MZ B cells in bone marrow, lymph node and blood cell preparation was performed as follows: Bone marrow was harvested by flushing the tibias

and femurs from one leg of each mouse using a 27-gauge needle and a 10 ml syringe filled with media. Aggregated cells were separated by pipetting up and down with a 5 ml pipette. Cells were centrifuged and the cell pellets were resuspended in 5 ml media. Inguinal, axial, and cervical lymph nodes were removed from each mouse and single cell suspensions were made by rubbing the nodes between two frosted glass slides. Cells were pelleted and resuspended in 3ml media. Blood was collected by cardiac puncture after mice were $CO_2$ asphyxiated. To prevent blood coagulation blood is drawn from the cardiac chamber using a 10 ml syringe containing 1 ml citrate to yield a total volume of 1.5-2 ml blood + citrate. Blood suspensions were diluted with 2 ml of PBS and 3 ml lymphocyte separation medium was added. The preparation was centrifuged for 30 min at room temperature at a speed of 1500 rpm. Lymphocytes were recovered by gentle pipetting. Media was then added to the cell suspension and centrifuged for 7 min at 4°C. Cells were pelleted and resuspended in 1 ml media.

**Quantitative RT-PCR analysis of expression of the chemokine CCL21**

Quantitative RT-PCR analysis was performed on spleen from young and old mice. Spleens were frozen in liquid nitrogen for homogenization at a later date. Homogenization was done using a rotor-stator homogenizer. Total RNA was isolated from whole homogenized spleen using the Qiagen RNeasy Kit (Valencia, CA) according to the manufacturer's suggested protocol. Complementary DNA (cDNA) was synthesized using the Amersham First Strand cDNA synthesis kit (Buckinghamshire, UK) and real-time PCR analysis was performed using a GeneAmp 2400 thermal cycler

(PerkinElmer, Wellesley, MA). Primers were as follows: CCL21: forward 5' – AAAGAAAGGAAAGGGCTCCAA-3' and reverse 5'TGCGCTCATCTTAGGCTTTGT-3'. The real-time PCR thermal cycler profile was run as follows: one cycle at 50°C for 2 min, one cycle at 95°C for 10 min, 40 cycles of denaturing at 95°C for 15 seconds, and annealing and elongation at 60°C for 1 min, followed by a dissociation protocol run to test the melting temperature of the product. The data were analyzed using GeneAmp 5700 SDS software (Applied Biosystems). The relative expression levels for each sample were calculated by determining the ratio of the number of copies/µl for CCL21 to the number of copies/µl of HPRT.

**pHrodo treatment and analysis via microplate reader**

Splenocytes were harvested as described above from young and old mice and allowed to adhere onto a 96 well plate at 1 x $10^6$ cells/well. Non-adherent cells were washed after 1 hr and 100µl of 100µg/ml pHrodo were added per well and allowed to incubate in 37 C for 2 hrs. After 2 hrs, the 96 well plate was placed in a microplate reader and cells were excited using a 550 nm laser and the emission was recorded at 600 nm. The percent net effect was determined by using the manufacture suggested formula.

***Ex vivo* treatment of pHrodo**

Young and old mice were injected with dextran-FITC (as described above). Splenocytes were harvested and 4 x $10^6$ splenocytes were allowed to adhere onto 1 ml chamber slides (Nunc Labtek) for 1 hr at 37°C incubator. After 1 hr non-adherent cells were removed

and pHrodo™ S. *aureus* BioParticles® (pHrodo) (Molecular Probes™ Invitrogen) were given at 100 µg/ml in Hank's balanced salt solution HBSS (GIBCO® Invitrogen) containing 20 mM Hepes (GIBCO® Invitrogen) for 1.0-1.5 hr. After 1.0-1.5 hr cells were viewed using a Leica TCS SP5 confocal microscope (Leica) remaining incubated at 37°C. Each chamber containing cells from one animal was examined for 15 min. The following exceptions were made with time lapse experiments: pHrodo was administered and 10 min after administration, MZM were imaged once every min (for total of 60 min) or once every 2 min (for total of 120 min). For each animal sample dextran$^{+}$ pHrodo$^{+}$ MZM were located and approximately 10-15 MZM were imaged/animal live at 5000x magnification. Three criteria were needed to qualify as an MZM: first, cells needed to be dextran$^{+}$; second, cells needed to be pHrodo$^{+}$; and lastly, cells needed to have macrophage morphology.

Phagocytosis of pHrodo by MZM was measured using ImageJ version 1.43u. For each animal sample, single images of dextran$^{+}$ pHrodo$^{+}$ MZM were evaluated for the mean fluorescence intensity (MFI) of pHrodo and dextran within MZM, and the number of phagocytic compartments/MZM. For young mice approximately 7-10 MZM images were analyzed and for old mice 4-5 MZM images were analyzed. The average value was reported for each measurement assessed.

**Statistical analysis**

Statistics were calculated using Graphpad Prism software (version 5.01). To compare compared differences in cells populations between young and old mice Mann-Whitney test or Unpaired t-test was used. To determine if there was a direct correlation between changes in one cell type to another Pearson Correlation was applied where appropriate.

# CHAPTER IV

## THE ANATOMICAL AND CELLULAR CHANGES IN THE MARGINAL ZONE OF YOUNG AND OLD MICE

This chapter provides a survey of the morphological and cellular alterations of the MZ with age. Initial observations revealed visual disruptions of the MZ with age. These disruptions were first observed on H&E cross sections of mice spleens, which could not identify specific cell population involved in the alterations. By examining the various cell components that make up the MZ in young and old mice, the populations responsible for these morphological disruptions were determined. Given that the cells that comprise the MZ are vital for the proper immune response to TI antigens, establishing which cells are altered with age would provide insight into the reported age associated declines in immunity.

Previously established methods, as well as novel methods using flow cytometry and tissue histology, were used to identify and properly assess MZ cells and to determine if alterations were present in old mice. Results showed gross alterations in the structure of the MZ with age are attributed to decreases in the MZM and MZ B cells pools and disruption in the positioning of the MAdCAM-$1^{+}$ lining cells and MMM. Results also showed that in ~20% of old mice, a "young-like" phenotype persist within the MZM and

MZ B cell compartment. Therefore, unless animals fall into this 20th percentile of having young-like cell frequencies, a consequence of a reduction in cells of the MZ with age can have an impact on an efficient immune response.

**Morphological disruption of the splenic MZ areas in old mice**

The morphological organization of the MZ region in young animals is well defined (7, 8, 106). In consultation with a pathologist, two morphological criteria were selected to discriminate the degree of morphological disruption in the MZ areas of aged spleens. Sections of H&E stained spleens from young and old mice were scored independently by two investigators, "blinded" to the identity of the specimens. The criteria used were (1) the interface distortion (defined as the boundary between the white pulp area and the inner edge of the MZ) and (2) the percent radius involvement (defined as the percentage of interface distortion protruding towards the center of the white pulp (Fig.5). Each criterion was given a score ranging from 0-4 (severe to minimal). Four MZ areas were scored for each spleen. A sum of scores for both criteria was calculated for each MZ area, and this sum was averaged to yield a value for each individual spleen (Fig.5B) (detailed in material and methods). The MZ from young mice (2-6 months, Fig., top panels) uniformly encircled the white pulp areas. However, the MZ of old mice (18-23 months, Fig.5A, bottom panels) showed a great deal of variability and many had a high degree of distortion around the white pulp compared to spleens from young mice. In many old mice, the splenic MZ areas were diffuse and some were even difficult to discern. Figure 5B shows that on average, the morphology of splenic MZ from old mice

could be histologically discriminated from those of young mice. Of note, the splenic MZ from some old mice retained a "young-like" morphology, in which the MZ areas appear to have intact organization by the criteria assessed (Fig. 6).

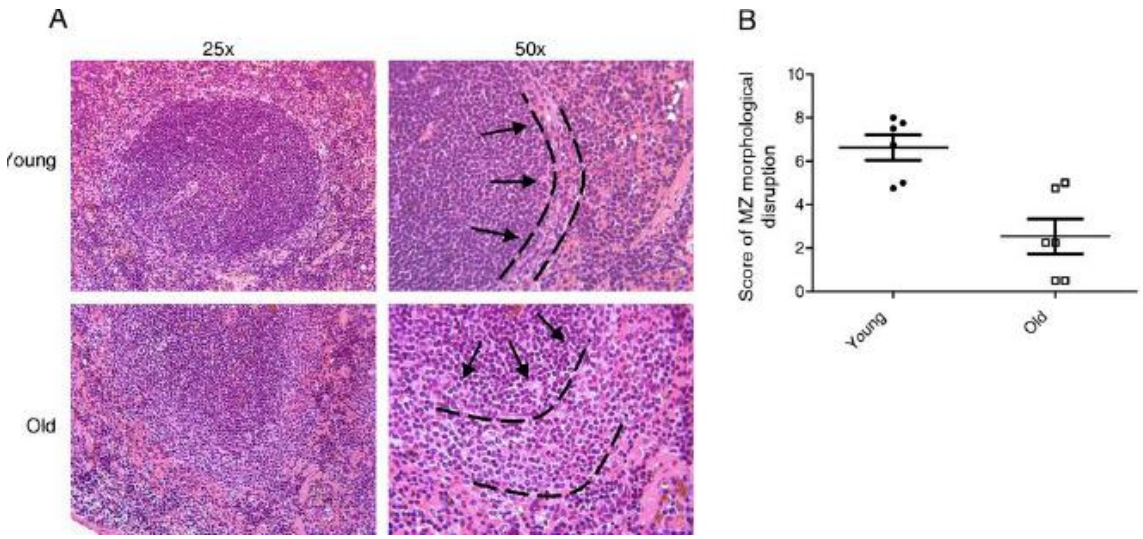


**Figure 5. Morphological comparison of the MZ architecture of young and old mice.** (A) Fixed, paraffin-embedded cross-sections of spleens stained with H&E demonstrating the range of disruption in the MZ of young and old mice. The top panels are a 25x and 50x magnification of a white pulp area from one representative young mouse. At 50x magnification the interface distortion (depicted by the inner line) is uniform and the percent radius involvement (arrows point to minimal protrusion of cells inward) is ≤ 5%. The lower panels are a 25x and 50x magnification of a white pulp area from one representative old mouse. At both low and high power magnification the interface distortion is severe and the percent radius involvement is ≥ 20% (arrows point at cells protruding into the white pulp area). (B) Qualitative scoring of MZ histology as detailed in Materials & Methods. The average score for four white pulp areas from each of six young (2-6 mo), filled circles and six old (18-23 mo), open squares is shown. The horizontal bars indicate the average and SEM for each group. $p = 0.0021$ determined by Unpaired t-test .

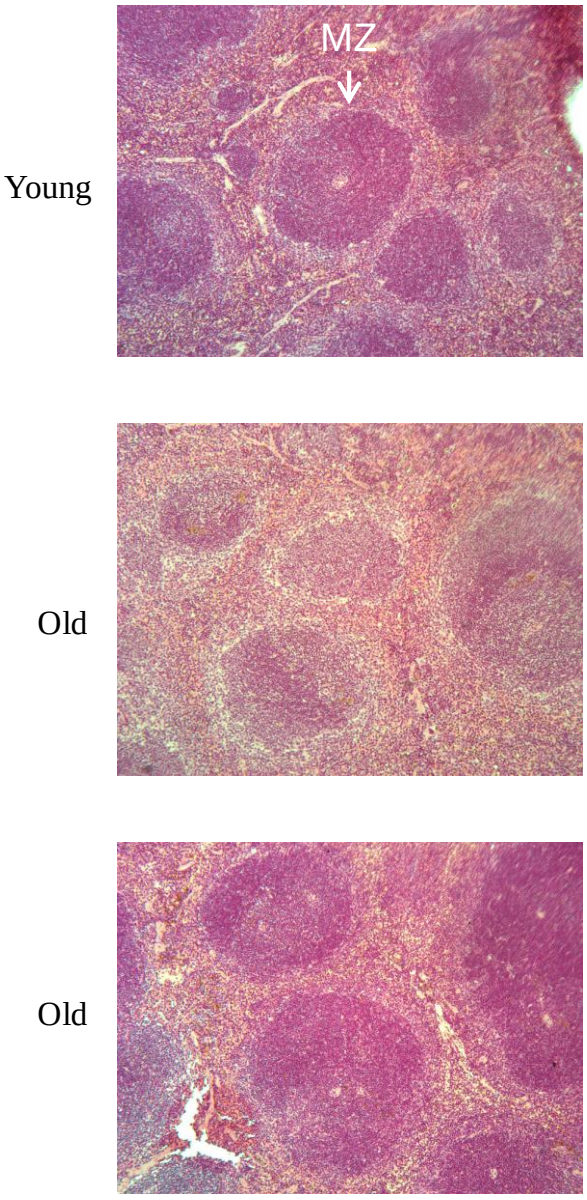


**Figure 6. Representative images of H&E stained splenic sections from young and "young-like" old mice.** The top panel is a 50x magnification of a white pulp area from one representative young mouse. The boundary of the MZ is visible and the interface distortion is uniform and the percent radius involvement is ≤ 5%. The bottom two panels are 50x magnification of white pulp areas of old mice that exhibit "young-like" MZ. The interface distortion and percent radius involvement are similar to that of which is observed in young mice.

**Alterations in the cells of the MZ region in spleens of old mice revealed by immunofluorescence staining**

The MZ is a compartment composed of different types of macrophages and B cells that are highly organized for the function of detecting and clearing antigens from the blood. Therefore, any changes in these cells or their position within the MZ of old mice could account for the decreases in clearance of TI antigens with age. Staining was included for MAdCAM-$1^+$ MZ sinus lining cells to provide a landmark, since both MZM and MMM relate in position to the MZ sinus. Similar to numerous reports of spleens from young mice, MAdCAM-$1^+$ MZ sinus lining cells (red or purple) showed continuous, thin rings surrounding white pulp areas (Fig. 7A top panel). In contrast, the MAdCAM-$1^+$ cells from old mice exhibited a less even, more diffuse distribution and often appeared as multiple layers of cells oriented toward the white pulp (Fig. 7A bottom panel). Figure 6A shows an assessment of MAdCAM-$1^+$ disruptions in young and old mice. In spleens from young mice, MMM (green) were closely aligned with the MAdCAM-$1^+$ cells and formed a continuous line of cells on the follicular side of the MZ sinus (Fig. 8A top panel), similar to published examples (7). In the spleens from old mice, the MMM were aligned along the MZ sinus but were highly diffused into the white pulp/follicle area (Fig. 8A bottom panel). The diffused distribution of MAdCAM-$1^+$ cells and MMM was consistently observed in old mice.

The most pronounced difference between old and young spleens was in the distribution of the MZM (marked by expression of either MARCO or SIGN-R1). MZM in young spleens formed continuous rings on the outer edge of the MZ sinus (Fig. 8B top

panel), similar to numerous published reports (18-21, 40). However, in many old spleens, MZM appeared to be reduced in abundance and aligned in discontinuous patches along the MZ sinus (Fig. 8B lower panel). In summary, with age there are several disruptions in the positioning of cells specific to the MZ region, including the MAdCAM-$1^+$ sinus lining cells, MMM, and MZM. It appeared that with age the variability in MZM was greater than that seen in the MAdCAM-$1^+$ cells and MMM. The degree of alteration in the MZM population within individual old animals was next assessed. MZM bind and phagocytize blood-borne bacteria (7, 20), thus changes in the number of MZM with age can affect the clearance of blood-borne bacteria as less MZM are available to phagocytize.

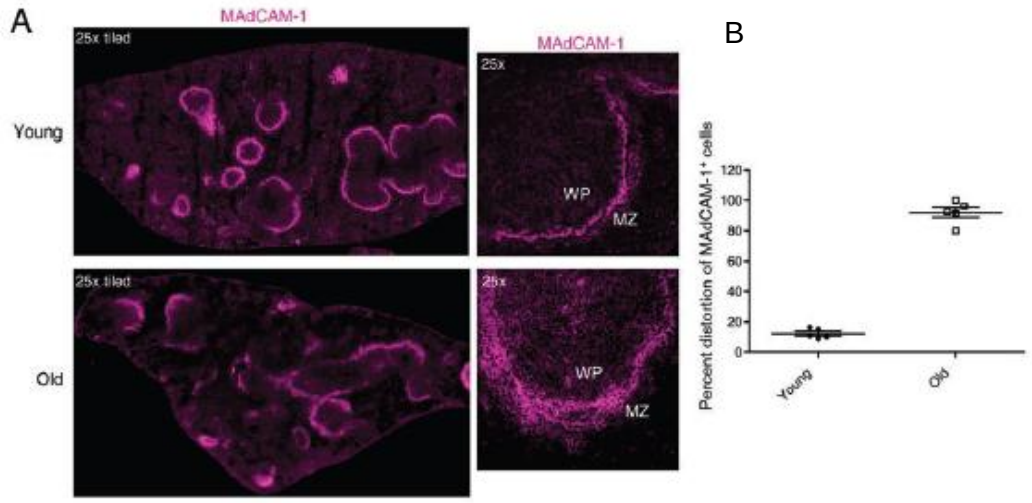


**Figure 7. Morphological comparison of disrupted MAdCAM-1$^+$ MZ sinus lining cells in young and old mice.** Representative photos are shown of frozen sections (6-8µm) stained for MAdCAM-1$^+$ MZ sinus lining cells. **(A)** Left are representative images (25x tiled magnification) taken from cross sections of whole mouse spleens with the MAdCAM-1$^+$ MZ sinus lining cells (purple) observed encircling numerous white pulp areas. Images to the right (50x magnification) are the MAdCAM-1$^+$ MZ sinus lining cells of one white pulp area from a representative young (top) and old (bottom) mouse spleen.. **(B)** Relative linear proportion of disrupted MAdCAM-1$^+$ cells in five young mice (2-3 mo, filled circles) and five old mice (18-23 mo, open squares). Each symbol indicates an individual animal. The horizontal bars indicate the average and the SEM for each group. p = 0.0001 determined by unpaired t-test

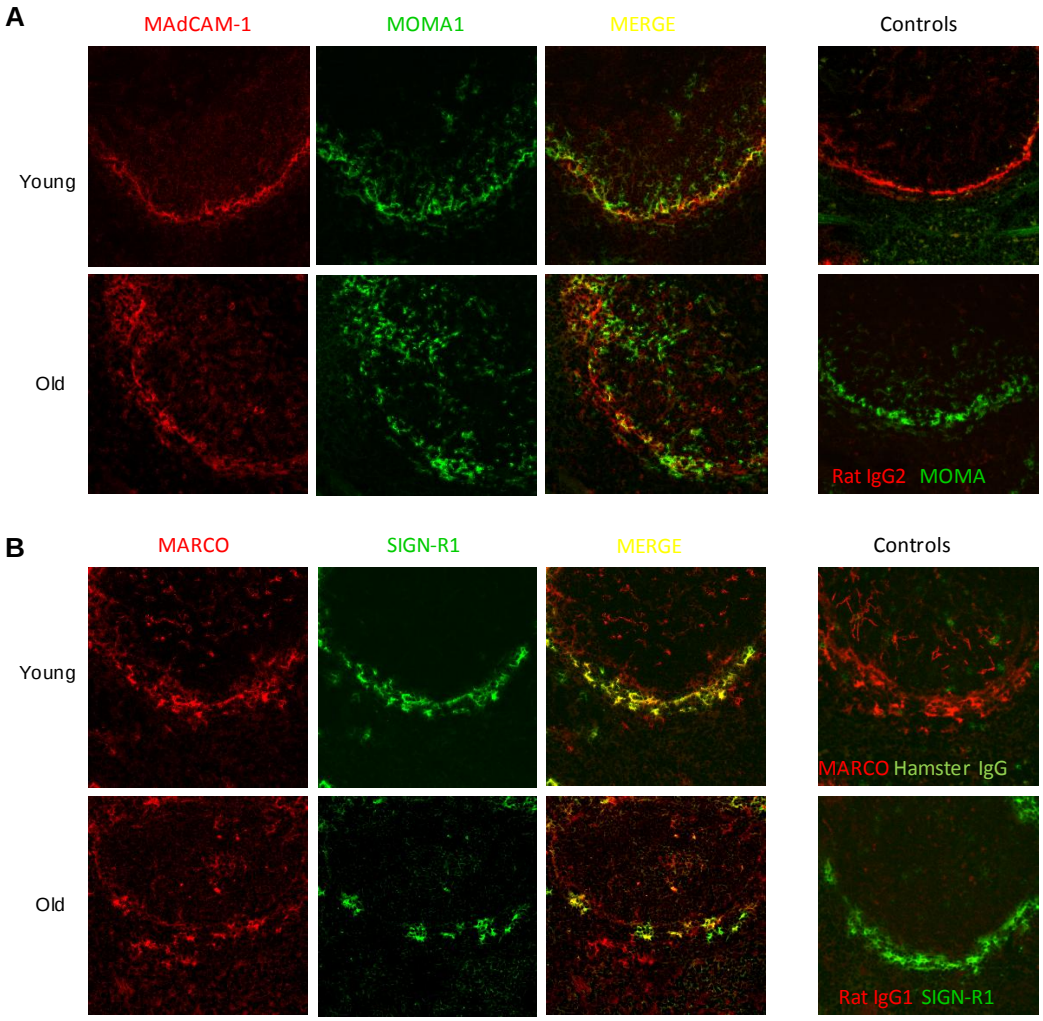


**Figure 8. Immunofluorescence of cellular compartments of the MZ region of young and old mice.** Representative photos are shown of frozen sections (6-8 microns) stained for cells within various compartments of the MZ and analyzed by confocal microscopy (all images taken at 50x magnification). **(A)** The continuous, tight ring of MAdCAM-1$^{+}$ MZ sinus lining cells (red) typical of young and the diffused distribution observed in old mice (examples from 2 mice of each age). Young MOMA$^{+}$ macrophages MMM (green) contrast with aged MMM which appear diffuse and infiltrated into the white pulp in old tissue. Right panels show representative photos of isotype controls. **(B)** Shows a representative example of the changes in distribution of MZM (indicated by staining for MARCO (red) and SIGN-R1 (green)) found in spleens of many old mice. MZM showed a continuous line encircling the white pulp in young animals in contrast to a patchy, discontinuous distribution in many old mice. Right panels show representative photos of isotype controls.

**A reduction in MZM in the spleens of old mice revealed by immunocytochemical staining**

Sections of young and old spleens were stained using antibody to MARCO (brown) to mark MZM and antibody to MAdCAM-1 (blue) to mark the MZ sinus lining cells. Figure 9 top panel shows the typical, consistent pattern observed in young spleens: the MZM population was present in a continuous line of cells adjacent to the sinus lining cells. However, the distribution of MZM in spleens of old mice was highly variable, ranging from a young-like distribution of MZM to negligible stain for MZM. Many spleens from old mice had notably decreased staining for MARCO (Fig. 9A middle panel, representative of intermediate reduction). In these spleens, the expression of MARCO was localized in patches rather than in a continuous line of cells around the MZ sinus. A semi-quantitative scoring was devised in order to compare the MZM distribution in young vs. old spleens. For each spleen, four well oriented white pulp areas were graded "blind" for (1) the relative abundance of $MARCO^+$ MZM present and (2) the continuity of $MARCO^+$ MZM positioning around the MZ sinus (detailed in Materials and Methods). Scores ranging from 1-3 were given for each criterion graded (worst to best; Fig. 9A shows representative tissue sections for each score). An average of scores was calculated and shown for individual animals (Fig. 9B). Expression of $MARCO^+$ MZM showed a statistically significant decrease in old tissue compared to young ($n = 13$ young and $n = 15$ old, $p = 0.0012$). Using serial sections, immunocytochemical staining for SIGN-R1, although less intense than for MARCO, also reflected reduced abundance and patchy pattern (representative examples in Fig. 8B middle panel and data not shown)

confirming that reduction of MARCO expression reflected a decreased presence of MZM.

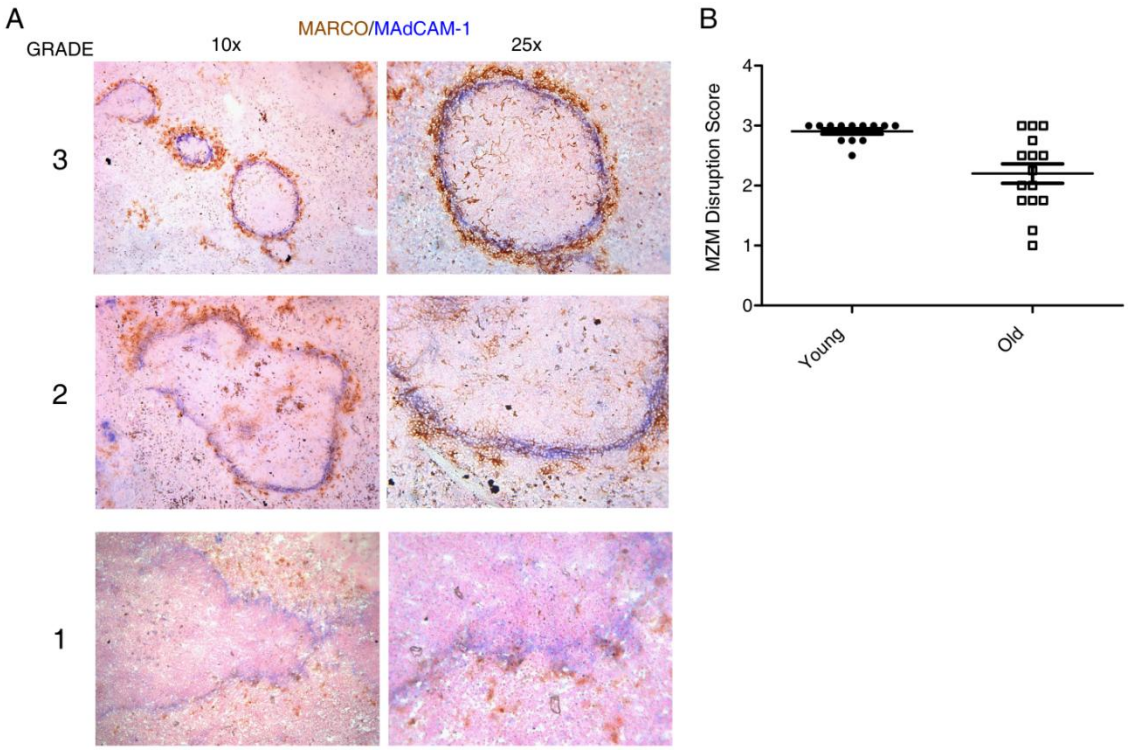


**Figure 9. Semi-quantitative assessment of MZM disruption in spleens from old mice. (A)** Immunocytochemistry of frozen sections (6-8 microns) stained to reveal MAdCAM-1$^+$ MZ sinus lining cells (blue) and MARCO$^+$ MZM (brown). Left panels are images taken at 10x and right panels are images taken at 50x magnification. MZM were semi-quantified for the (1) abundance of MARCO$^+$ stain present and (2) the continuity of MARCO$^+$ MZM positioning around the MZ sinus. Four separate white pulp areas were graded "blind" per animal and given a score from 1-3 (worst to best). Shown are representatives from each grade. Top panel represents a grade of 3 showing the typical abundant and continuous stain for MARCO$^+$ MZM surrounding the MZ sinuses. The middle panel corresponds to a grade of 2 showing moderate abundance of MARCO$^+$ MZM that moderately encircled the MZ sinus with patches. The lower panel corresponds to a score of 1, which equates to low or virtual absence of MARCO$^+$ MZM that, if present, were found in patches along the MZ sinus. **(B)** Semi-quantitative scoring of MZM for the criteria above. Each symbol represents an average of the summation of the four scores for each animal. Horizontal bars indicate the average and SEM for each group. $p = 0.0012$ as determined Mann-Whitney test (n = 13 young mice (2-3 mo), filled circles; n = 15 old mice (18-23 mo), open squares).

**A reduction in MZM in the spleens of old mice revealed by flow cytometry**

To further explore the interpretation that MZM appeared reduced in many aged mice, MZM were quantified using flow cytometry analysis. Many reports agree that MZM express MARCO and SIGN-R1 (7). Although anti-MARCO antibody worked well in immunocytochemistry, anti-SIGN-R1 antibody more clearly distinguished a subpopulation in flow cytometry. MZM comprise a minor subset of dispersed spleen cells; therefore, another marker was used to aid in gating the population. Published reports indicate that MZM lack expression of the typical macrophage marker F4/80 (18) and express negligible CD11b (107). By flow cytometry, the SIGN-R1$^{+}$ population were consistently identified within a population of large cells that expressed very low levels of CD11b (Fig. 10A). Based on previous reports that dextran particles bind to SIGN-R1 and are rapidly cleared from the blood by MZM (17, 18), FITC-labeled dextran administered i.v. was used to verify the identity of the SIGN-R1$^{+}$, CD11b low subset as MZM. Figure 10B shows that the SIGN-R1$^{+}$, CD11b low cells bound dextran within a short time, confirming that these cells were MZM. To confirm that the MZM are within the CD11b low population FACS was used to isolate the CD11b high, CD11b low, CD11b negative subsets (Fig. 11), which were then H&E stained for morphological examination. The CD11b low subset contained cells that were large and macrophage like in morphology, while the cells in the CD11b high subset appeared to be largely neutrophils and cells in the CD11b negative subset were lymphocytes. Attempts to enrich for MZM via column isolation were unsuccessful, as the column enrichment population had the same

frequency of MZM as the unenriched population. Therefore, the frequency and number of MZM of total splenocytes was determined and reported for individual young versus old animals. Figure 10C shows that there was a significant decrease in the average frequency of MZM in old mice when compared to young mice ($n = 30$ young and $n = 22$ old, $p = 0.0001$). Table III shows that the number of MZM in old mice also declines when compared to young mice. The frequency of MZM in some old mice was equivalent to the frequency of MZM in young mice. Overall, the results indicate a decline in frequency and positioning of MZM in the marginal zones of aged splenic tissue. It is possible that the decrease in MZM frequency with age is due to a decrease in the levels of the SIGN-R1 receptor; however, there was a significant increase in SIGN-R1 expression on MZM from old mice compared to young ($p = 0.0088$) (Fig. 10D). To determine if this increase in SIGN-R1 is attributed to an increase in MZM size with age, flow cytometry was used to examine the FSC of MZM in young and old mice. MZM from old mice had a higher FSC value when compared to young MZM, suggesting that MZM from old mice are larger in comparison to MZM from young mice, a possible explanation for the increase in SIGN-R1 expression on MZM from old mice ($p = 0.0006$) (Fig. 10E).

A

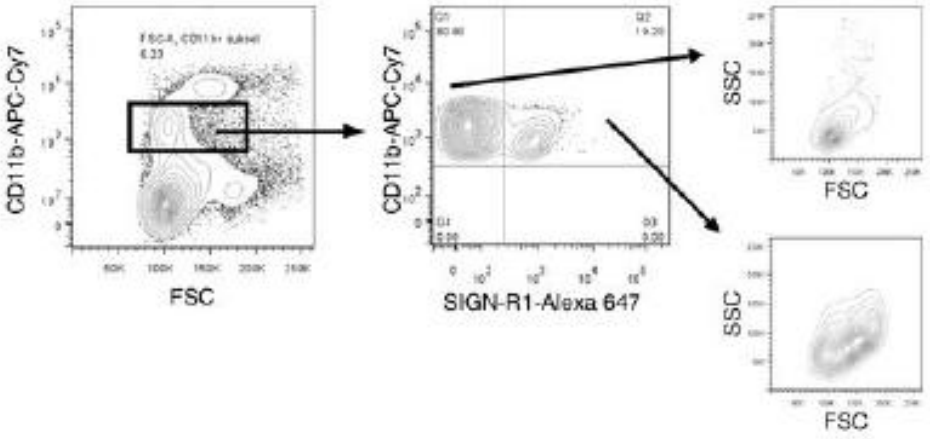
CD11b-APC-Cy7
FSC
CD11b-APC-Cy7
SIGN-R1-Alexa 647
SSC
FSC
SSC
FSC

B

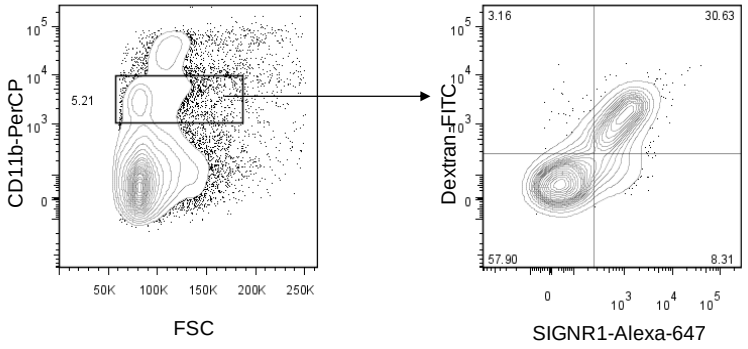
CD11b-PerCP
5.21
50K
100K
150K
200K
250K
FSC
Dextran-FITC
3.16
30.63
57.90
8.31
SIGNR1-Alexa-647

C

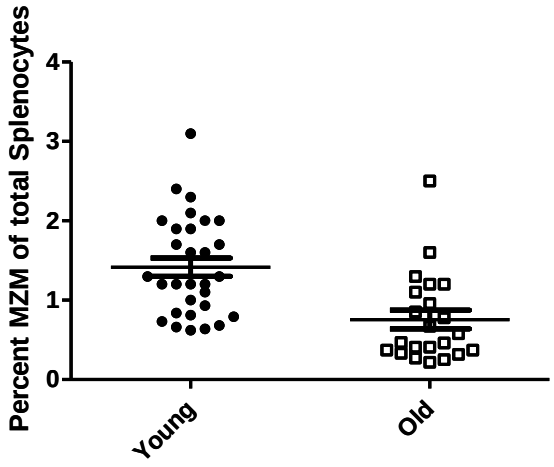
Percent MZM of total Splenocytes
4
3
2
1
0
Young
Old

D

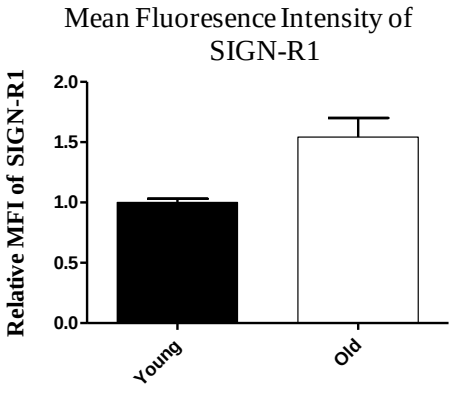
Mean Fluoresence Intensity of SIGN-R1
Relative MFI of SIGN-R1
2.0
1.5
1.0
0.5
0.0
Young
Old

E

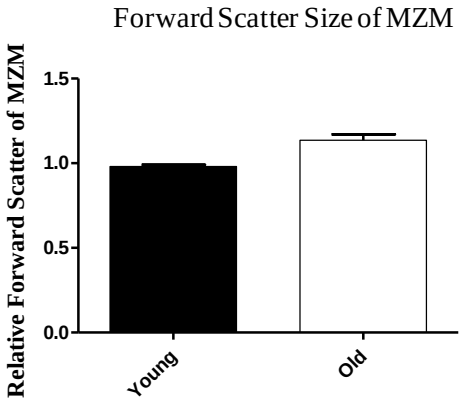
Forward Scatter Size of MZM
Relative Forward Scatter of MZM
1.5
1.0
0.5
0.0
Young
Old

**Figure 10. Quantitative assessment of the frequencies of MZM in spleens from old and young mice by flow cytometry. (A)** Identification of SIGN-R1$^+$ cells (MZM) in the CD11b low splenic fraction. Contours shown are representative of young spleen cells. **(B)** Contour plots from a separate experiment demonstrating that a majority of the CD11b low/SIGN-R1$^+$ cells took up FITC-labeled dextran within 45min after i.v. delivery, as expected of MZM (43). **(C)** Comparison of the frequencies of MZM present in spleens from young and old mice. Each symbol represents an individual animal. Horizontal bars indicate the average and SEM for each age group. Old mice have approximately on average a 45 percent reduction in MZM when compared to young mice. $p = 0.0001$ determined by Mann-Whitney test (n = 30 young mice (2-3 mo), filled circles; n = 22 old mice (18-23 mo), open squares). **(D)** Comparison of the MFI of SIGN-R1 of MZM from young and old mice ($p = 0.0088$). **(E)** Comparison of the forward scatter of MZM from young and old mice ($p = 0.0006$). Data presented in (D) and (E) are represented using the ratio of sample value over the average value of all young mice taken within each experimental group. Data is expressed as mean ± SEM and are representative of four separate experiments (n = 10 young mice (2-3 mo); n = 10 old mice (19-23 mo).

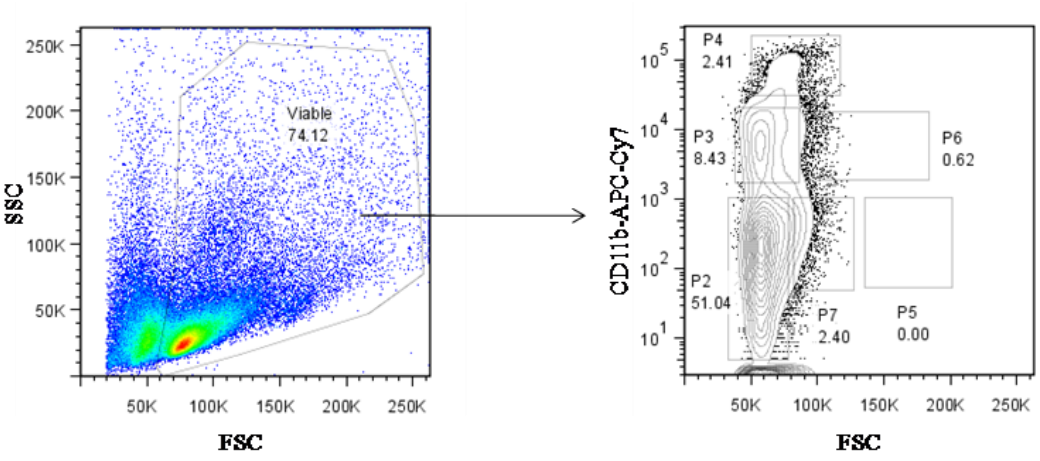


**Figure 11. FACS cell sort of CD11b positive and negative populations.** FACS was utilized to separate the CD11b high, low, and negative populations (represented in the left image as P2-P7; P2 = lymphocyte fraction, P3 = the CD11b low fraction, P4 = CD11b high fraction, P5 & P = 7 cell doublets, P6 = large macrophages) for visualization of cell morphology. The cells were cytospun onto microscope slides and H&E stained.

**Decrease in the frequency of MZ B cells in old mice**

Knowing that MZM have a direct interaction with MZ B cells I next determined if there were differences in the MZ B cell compartment with age. For flow cytometry, gating on MZ B cells was adapted from Won *et al.* (105). Spleen cells were initially gated on the $B220^{+}$, $CD23^{-}$ population followed by gating on the $CD21/35_{high}$ and $IgM_{high}$ fraction (Fig. 12). The frequency (Fig 13A) and number (Table III) of MZ B cells of the total $B220^{+}$ cells was then determined and reported for individual young versus old animals. Figure 13A shows that there was a significant decrease in the average frequency of MZ B cells in old mice when compared to young mice (n = 30 young and n = 41 old, p = 0.0001). Furthermore, as seen with MZM, MZ B cells also have a decline in total cell numbers in old mice when compared to young mice (Table III). As observed with the MZM population, the frequency of MZ B cells in some old mice overlapped with the MZ B cell frequency in young animals. Initially, an increase in MZ B cells was anticipated with age based on the factors present in age that favor MZ B cell development (69, 70) (71-74) (75-77), however, results showed that there was a significant decrease in the MZ B cell pool with age.

Given that the MZ B cell population declines with age I next determined if there were any alterations to the FO B cell population with age. Using flow cytometry, the frequency (Fig.13B) of FO B cells of young and old mice was determined. Spleen cells were gated on the $B220^{+}$, $CD23^{+}$ population followed by gating on the $CD21/35_{int}$ and $IgM_{int/high}$ fraction (Fig. 11). The frequency of FO B cells was determined from the total

$B220^+$ cells. The data show no differences in the FO B cell pool in young and old mice ($n = 14$ young and $n = 16$ old mice, $p = 0.3277$) These results support published reports that the mature B cell (FO B cell phenotype) pool in old mice is similar to that of young mice (88). The distributions of FO B cells in old mice were also similar to that of young mice. It has previously been reported that there is a decline in the pre B cell pool in the bone marrow of old mice; however, no differences were present in the mature B cell pool in the spleens of young and old mice (89). Using BrdU labeling Johnson *et al.* later reported that the production of newly formed immature B cells in old mice is similar to that of young mice. However, this same study also reported that newly formed immature B cells of old mice were less frequent in spleens of old mice when compared to young mice, suggesting that the microenvironment of the aged spleen does not allow for the homing of newly formed B cells. It has been suggested that the mature B cell pool of old mice are long lived and newly formed immature B cells of old mice are unable to home to the spleen because the niche is over crowed and does not require more cells (27). The frequency of FO B cells determined here in old mice may be a reflection of the long lived mature B cell population and not a result of newly formed FO B cells as previously discussed by Johnson *et al* (89). Therefore, decreases in MZ B cells could also be a reflection of alterations present in the microenvironment of the MZ region of old mice.

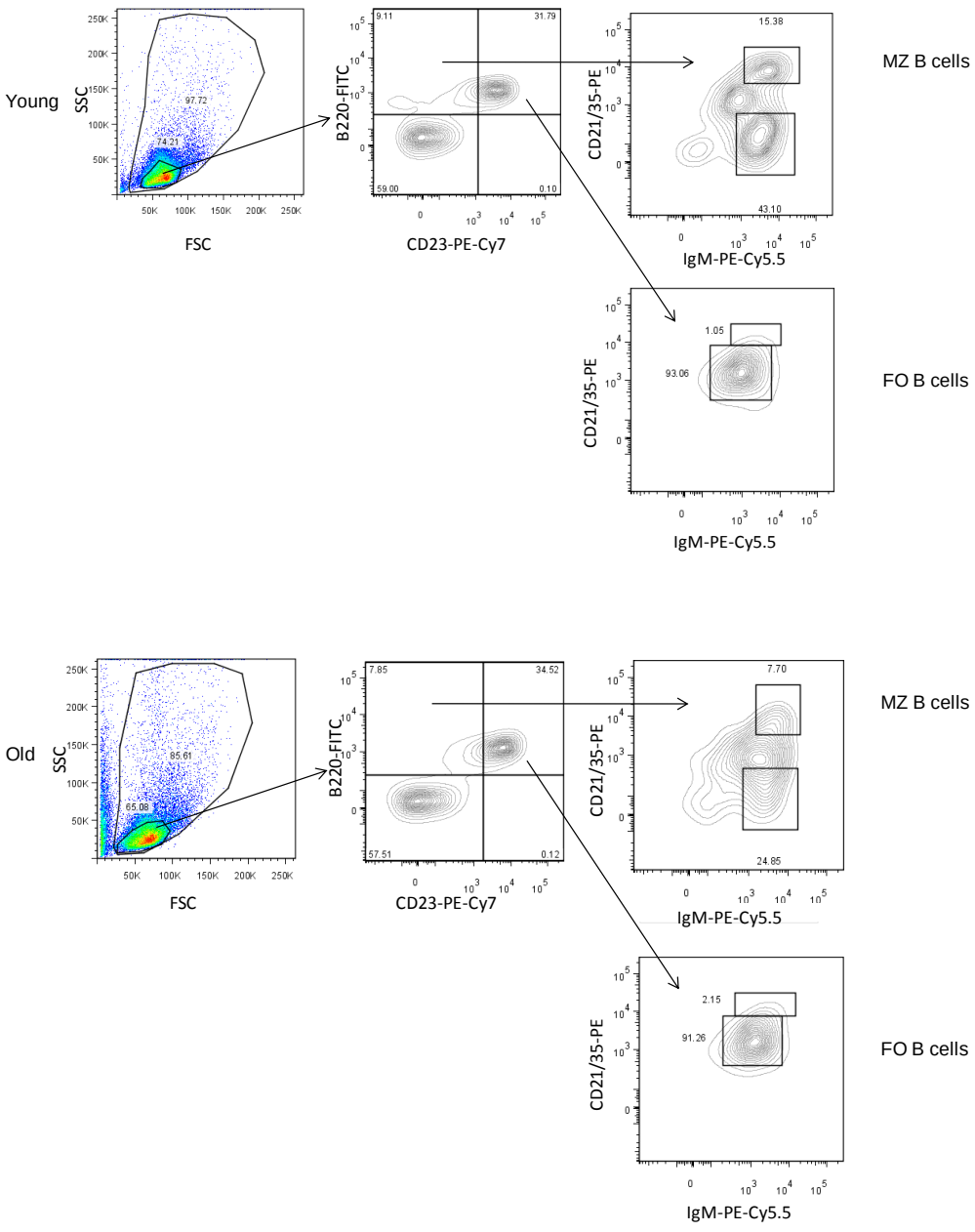


**Figure 12. Representative profiles of MZ B and FO B cells from young and old mice.** Flow cytometry was used to determine MZ B and FO B cell frequencies. The MZ B cell population was determined by gating on the $B220^{+}/CD23^{-}$ fraction followed by gating on the CD21/35 $^{high}$/ IgM $^{high}$ fraction. The FO B cell population was determined by gating on the $B220^{+}/CD23^{+}$ fraction followed by gating on the CD21/35 $^{int}$/ IgM $^{high}$ fraction.

**Table 3. Number of MZM and MZ B cells in the spleens of young and old mice**

| Cell | Average number of total nucleated splenocytes ($\times 10^6$) | | Average number of cells/spleen ($\times 10^6$) | | Fold difference in Y & O |
|---|---|---|---|---|---|
| | Young | Old | Young | Old | |
| MZM | 84.0 ± 4.20 | 76.0 ± 13.0 | 0.81 ± 0.10 | 0.29 ± 0.01** | 2.8-fold |
| MZ B | 85.0 ± 2.90 | 84.0 ± 5.10 | 1.20 ± 0.14 | 0.52 ± 0.12* | 2.2-fold |

**Table 3. Representative absolute numbers of MZ B cells and MZM of young and old mice.** Flow cytometry was used to determine MZM and MZ B cell absolute numbers. Absolute numbers of MZM determined within all viable splenocytes and absolute numbers of MZ B cells within the $B220^+$ population. **p = 0.0070 ; *p = 0.0081 determined by Unpaired t-test. Data is expressed as mean ± SEM and are representative of two separate experiments (n = 8 young mice (2-3 mo); n = 4 old mice (19-23 mo).

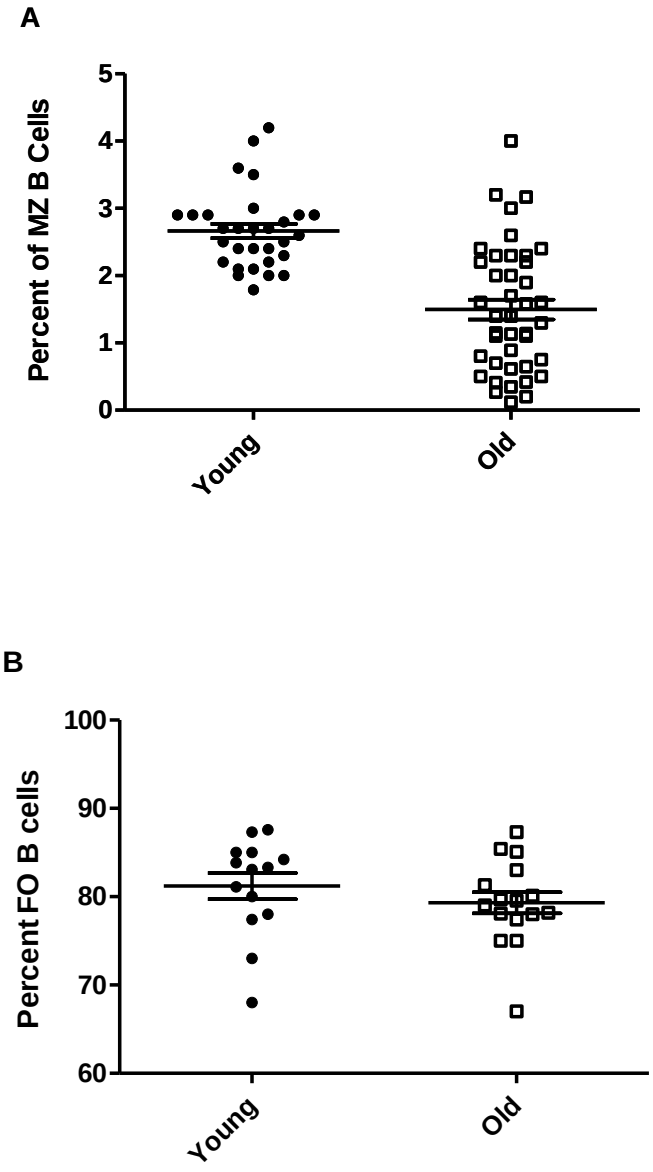


**Figure 13. Comparison of frequencies of MZ B and FO B cells in young and old mice. (A)** Frequency of MZ B cells within the $B220^+$ population. $p = 0.0001$ determined by Mann-Whitney ($n = 30$ young; $n = 41$ old mice). **(B)** Frequency of FO B cells within the $B220^+$ population. $p = 0.3277$ determined by Unpaired-t test ($n = 14$ young; $n = 16$ old mice).

# CHAPTER V

## THE MICRO-ANATOMICAL FACTORS THAT MAY CONTRIBUTE TO DECREASES IN MZM AND MZ B CELLS IN OLD MICE

Chapter IV showed that there is a decrease in MZM and MZ B cell frequencies and numbers with age. However, what causes the decrease in these two important immune cell type is currently not known. This chapter will explore possible factors that may contribute to the decline in MZM and MZ B cells with age.

MZM and MZ B cells have a direct physical interaction that when disrupted leads to their displacement within the spleen (15). Therefore, determining if there is a direct correlation between the reduction in MZM and MZ B cells observed in old mice could provide insight for the decreases in both immune cells. Reduction in cell frequency/number can also be attributed to cell intrinsic or extrinsic factors. The cell extrinsic factors important for MZM and MZ B cells were examined by looking at the microenvironmental factors important for the maintenance of these cells as components of the MZ of the spleen.

The chemokine CCL21 and its receptor CCR7 are important for the localization of MZM within the MZ (43). Therefore it is possible that changes in either chemokine and/or receptor with age could account for the decline in the MZM frequency found in old spleens. The decrease in MZ B cells with age could be due to the inability of MZ B

cells in old mice to be retained in the spleen. The microenvironment of old mice was examined by determining if it can attract young transferred MZ B cells. Can young transferred MZ B cells home to the spleens of old mice that have reduced MZM, or do they aberrantly home to other lymphoid organs, such as the lymph nodes and bone marrow?

**Decrease in the frequency of MZ B cells in old mice correlates with the decrease in MZM**

It is well established that MZM directly interact with MZ B cells via the scavenger receptor MARCO located on the surface of MZM and an undetermined cell surface ligand on MZ B cells (22-24). Furthermore Nolte *et al.* found that in young adult mice, loss of the B cell population corresponded with loss of MZM (40). Therefore, it is possible that the decrease in MZM in old mice could correlate with the decline in MZ B cells also seen with age. The spleens were removed from young and old mice, and 2/3 of each spleen was prepared for flow cytometry analysis in which both MZM and MZ B cell frequencies were determined. The remaining 1/3 of the spleen was frozen for immunocytochemistry staining to assess the MZM qualities described in Figure 9. For flow cytometry, MZ B cells were gated as shown in Fig 12 (Chapter IV) and MZM were gated as shown in Figure 10 (Chapter IV). Figure 14A shows a significant reduction in average frequency of MZ B cells in old vs. young mice ($n = 17$ old, $n = 15$ young; $p = 0.0002$). Although the average reduction was statistically significant, a wide variation was again apparent in individual old mice. Some spleens had extremely

reduced MZ B cells; whereas in other spleens, the MZ B cell frequencies were equivalent to the mid-range of the young group. Furthermore, the reduction in MZ B cell frequencies appeared to correlate with reductions in MZM assessed by the semi-quantitative tissue scoring method (Fig. 14B, $r = 0.6429$ and $p = 0.0003$) or by frequency determined in flow cytometry analysis (Fig. 14C, $r = 0.4930$ and $p = 0.0320$). This correlation remained present within the correlation pairs of each individual old animal when the correlation pairs of young animals were removed (Fig. 14B, $r = 0.5237$ and $p = 0.0451$; Fig. 14C, $r = 0.7076$ and $p = 0.0330$).

Although there is a significant correlation present between levels of MZM and MZ B cells in both young and old mice, the individual values in Figures 14 B and C can further be divided into 3 separate groups: Poor, moderate, and good. The poor group corresponds to low MZM and MZ B cell populations in individual animals, the moderate corresponds to animals with moderate levels of MZM and MZ B cells, and the good corresponds to animals with frequencies of MZM and MZ B cells that are at levels normally observed in young mice. It is possible that at some point all the animals will fall into the poor group and that the moderate group is a type of biomarker showing the beginning of the collapse in MZM and MZ B cell populations. We are limited in the data interpretation because one cannot assess decreases in MZM and MZ B cells in an individual animal over time, therefore highlighting the importance of this analysis.

The correlation present between MZM and MZ B cells frequencies suggests that the spleens of old mice with decreased MZM may also show a decline of the MZ B cell population as less MZM are available to physically interact with the MZ B cells (or vice

versa). It is possible that MZM do not home to the MZ of old mice because of the decline in the MZ B cell pool present with age. On the contrary, it is also possible that MZ B cells do not home to the MZ as a result of the decline in the MZM pool with age. Therefore, data here suggests that extrinsic microenvironmental factors important for both MZM and MZ B cells appear to be altered in old mice.

A

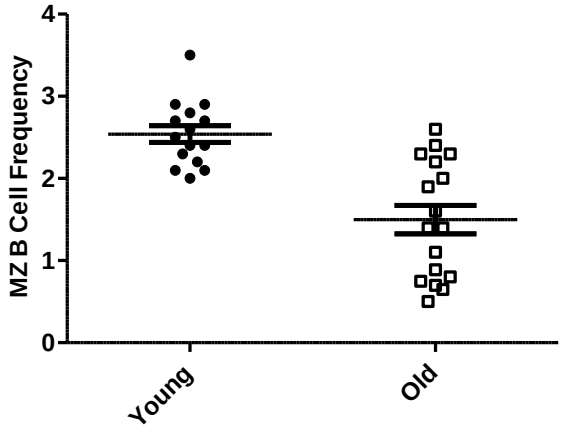
MZ B Cell Frequency
0
1
2
3
4
Young
Old

B

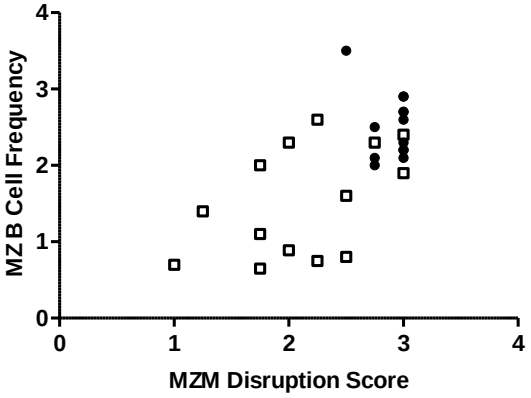
MZ B Cell Frequency
0
1
2
3
4
MZM Disruption Score

C

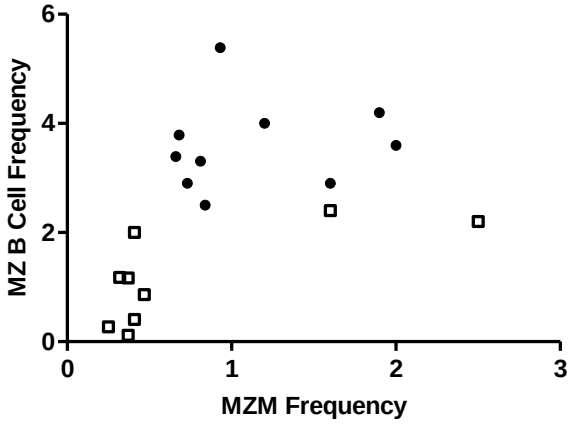
MZ B Cell Frequency
0
2
4
6
0
1
2
3
MZM Frequency

**Figure 14. Comparison of frequencies of MZ B cells in young and old mice and correlation with abundance of MZM. (A)** Frequency of MZ B cells within the $B220^{+}$ population. The MZ B cell population was determined by gating on the $B220^{+}/CD23^{-}$ fraction followed by gating on the CD21/35 $^{high}$/ IgM $^{high}$ fraction. Symbols represent individual mice and the horizontal bars indicate the average and SEM for each age group; p=0.0002 determined by Mann-Whitney test (n = 15 young; n = 17 old mice). **(B)** Pearson correlation analysis was performed on 27 spleens from both age groups shown in panel A that were also sectioned, stained with anti-MARCO, and scored for MZM criteria; r = 0.6429 and p=0.0003. **(C)** Pearson correlation analysis was performed in a separate experiment to compare frequency of MZ B cells versus frequency of MZM assessed by flow cytometry; r = 0.4930 and p = 0.0320 on 19 spleens from both age groups. Symbols in A, B, and C represent young mice (2-3 mo), filled circles; old mice (18-23 mo), open squares.

**Adoptive transfer of MZ B cells to evaluate extrinsic factors in age for the maintenance of MZ B cells to the MZ**

Decreases in MZ B cells with age can be due to failure of MZ B cells to be retained in the spleens of old mice. Studies in aged animals have shown that the there is a gross morphological alteration in lymphoid tissues, including smaller germinal centers (29), and changes in the T cell rich PALS and MZ (26). Studies discussed earlier have also reported immature B cells of young mice have a reduced ability to home to the spleens of old mice when compared to young mice but old donor immature B cells had no homing defect (27). On the other hand, mature follicular B cells (FOB) homed appropriately in either young or old recipients. Cells enter the spleen at the MZ; the difference is that the FOB cells move quickly into the white pulp follicles but the immature B cells linger in the MZ for a period of further maturation. It has been suggested that the aged defect is a result of alterations in the MZ microenvironment of old mice. Therefore, I tested the efficiency of the aged microenvironment to allow homing of young transferred MZ B cells can home to the spleens of old mice or if they were found in other lymphoid compartments such as the lymph nodes or bone marrow.

MZ B cell homing to the spleen was examined by injecting total enriched splenic B cells isolated from young mice (of which MZ B cells were approximately 5%) into young or old mice (Fig. 15). Mice were sacrificed 6 hrs post injection and the spleens were harvested for staining of donor cells via flow cytometry. The 6 hr time point was based on experiments done by Cyster and colleagues for homing of FO B cells to follicles

(108). Results show a reduced frequency of donor MZ B cells in the spleens of old hosts compared to young, indicating old mice have reduced MZ B cell homing to the spleen when compared to young mice (Fig 16A, $p = 0.0308$) (27). This type of experiment may suggest that some environmental factor such as a chemokine or its ligand is altered with age. This analysis was performed in concert with experiments by others in the lab to assess homing of FO B cells to follicles. Independently, I also examined the FO B cell population using the antibody staining paradigm adapted from Won *et al.* (105). My results showed no statistical differences in FO B cell homing between age groups (Fig 16B), which confirmed the now published work of Minges-Wols *et al.* from our group (27).

As previously discussed in the background section of this dissertation, skewing toward MZ B cell output in old animals might be predicted based on the environmental conditions that favor MZ B cell development over FO B cell development (69-77). Yet, data presented in Chapter IV show decreases in MZ B cells in most old mice when compared to young mice (Fig. 13A). Furthermore, results demonstrate that there is a direct correlation between the decreases in MZ B cells with the decreases in MZM in individual old mice. Therefore, it may be possible that MZ B cells are being developed at normal or increased frequency in advanced age, yet the splenic microenvironment in old mice does not allow for effective homing to the MZ (in this case because absence of MZM). Results obtained from adoptive transfer experiments found fewer donor MZ B cells in spleens of old host mice compared to young host mice. To determine if MZ B cells in normal, unmanipulated mice could be displaced to other lymphoid organs in age,

lymph nodes, bone marrow and blood of old mice were examined for MZ B cells and compared to young mice. Results showed that small populations in 2 of 7 old mice examined had an MZ B cell phenotype present in the bone marrow (Fig. 18) and lymph nodes (Fig. 19) (Table IV) that was similar to the MZ B cell phenotype observed in the spleen (Fig. 17). Young mice had no MZ B cell phenotype present in any of these lymphoid compartments (Table IV). Donor MZ B cells from young mice into old mice were also examined in the lymph node of the old and results show that 3 of the 6 old mice examined had characteristic MZ B cell profiles present in the lymph nodes of recipient mice (Table V). Furthermore, based on previous reports that dextran particles bind to MZ B cells and MZM (17, 18), FITC-labeled dextran administered i.v. was used to verify the identity the MZ B cells (similar to the prior study done in Chapter IV, Fig 9B) . Figure 18 (lower left panel) shows that the MZ B cells bound dextran within a short time, confirming that these cells were MZ B cells.

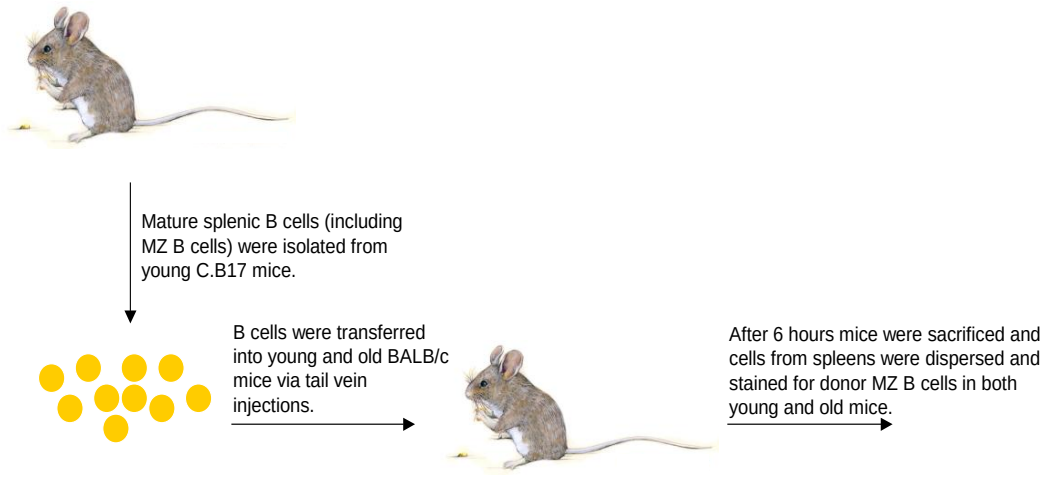


**Figure 15. Adoptive Transfer of B cells**
Mature B cells isolated from the spleens of young C.B17 mice (2-3 mo) were injected into the tail vein of either young (2-3 mo) or old (19-21 mo) BALB/c recipient mice. 6 hours post injection, spleens were removed and antibody staining with an antibody to the $IgM^b$ allotype was performed for donor MZ B cells. C.B17 mice express the $IgM^b$ allotype on the BALB/c background. BALB/c mice are $IgM^a$ allotype, so donor B cells can be distinguished from host B cells.

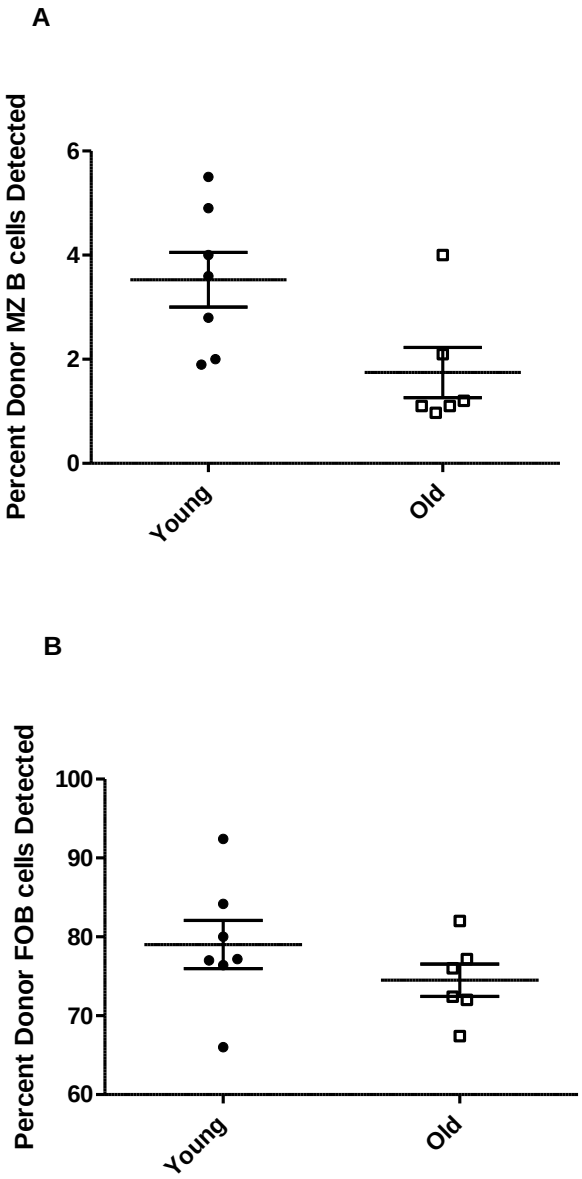


**Figure 16. Adoptive transfer of B cells from young C.B17 mice into young and old BALB/c mice.** Total splenic B cells, including MZ B cells, were isolated from young C.B17 mice (that have an IgM/D$^{b}$ allotype) and injected into young and old BALB/c mice (that have an IgM/D$^{a}$ allotype). Transferred cells were analyzed by flow cytometry using an antibody to the IgM$^{b}$ allotype that is strain specific and stained for **(A)** donor MZ B cells; Unpaired t-test, p = 0.0308 **(B)** and donor FO B cells; Unpaired t-test, p = 0.2603. Data represent 7 young into young and 6 young into old transfer pairs. Statistical analysis was performed on the mean of 7 young host and 6 old host ± SEM.

Table 4. Presence of MZ B cells in secondary lymphoid organs of wild type BALB/c mice

| Animal | Spleen | Lymph Node | Bone Marrow | Blood |
|---|---|---|---|---|
| Young | ++++<br>++ | - - - -<br>- - | - - - | - - |
| Old | ++++<br>+++ | + + - -<br>- - - | + + - -<br>- - - | - - |

Table 5. Presence of MZ B cells in secondary lymphoid organs following adoptive transfer of mature B cells isolated from BALB/c mice into C.B17 mice

| Animal | Spleen | Lymph Node |
|---|---|---|
| Young | ++++<br>+++ | - - - -<br>- - - |
| Old | ++++<br>++ | +++ -<br>- - |

**Table 4 and 5. Evaluation for MZ B cells in secondary lymphoid organs of young and old mice.** In Table IV the spleen, lymph nodes, bone marrow, and blood of 6 young and 7 old BALB/c mice were evaluated for MZ B cells. Each plus and minus sign corresponds to an individual mouse. The plus signs indicate presence of the MZ B cell phenotype and a minus sign indicates an absence. Table V evaluates the presence of the MZ B cell phenotype in the spleens and lymph nodes of 7 young and 6 old C.B17 mice after transfer of B cells isolated from young BALB/c mice.

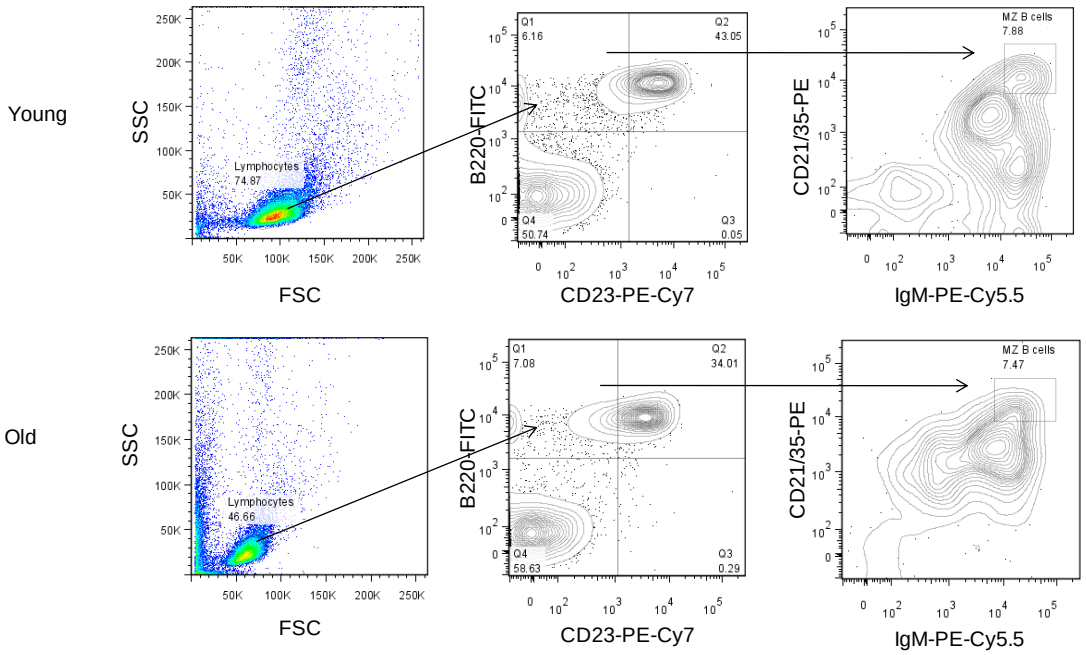


**Figure 17. Representative profile of MZ B population in the spleen of young and old mice.** Shown are contours representative of young or old splenocytes. Top panel is representative of splenocytes of young mice (4 mo). Lower panel is representative of splenocytes from an old mice (21 mo). MZ B cell phenotype present in the CD21/35 $^{high}$/ IgM $^{high}$ fraction of B220$^{+}$ CD23$^{-}$ splenocytes.

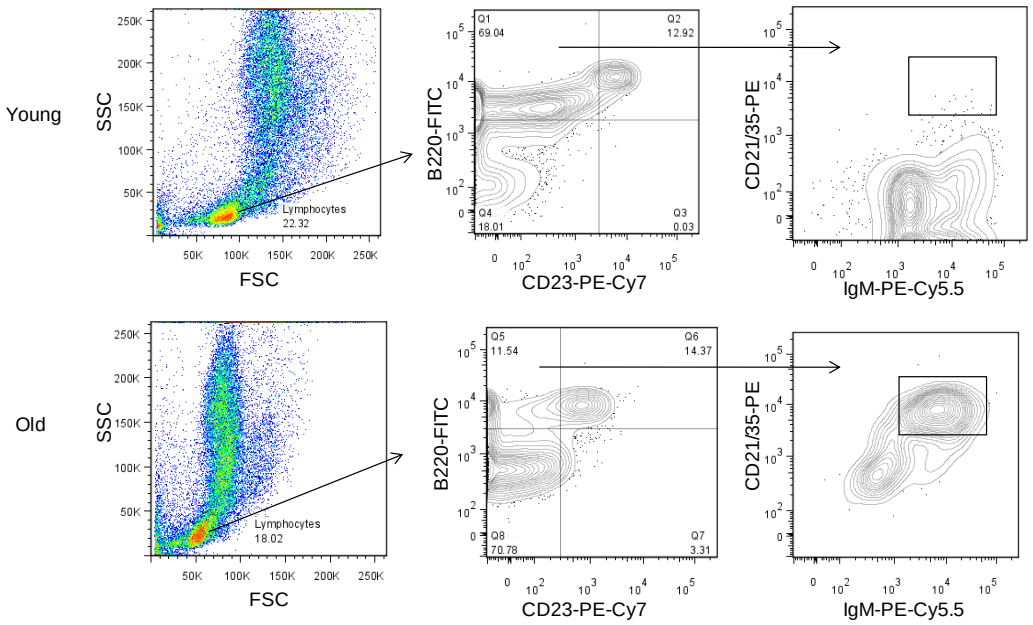


**Figure 18. Representative profile of MZ B population in the bone marrow of young and old mice.** Shown are contours representative of young or old bone marrow cells. Top panel is representative of bone marrow cells of young mice (4 mo). No MZ B cell phenotype was present in the CD21/35 $^{high}$/ IgM $^{high}$ fraction. Lower panel is representative of bone marrow cells from an old mice (20 mo) that reveals a MZ B cell like phenotype in the CD21/35 $^{high}$/ IgM $^{high}$ fraction. Normal MZ B cell flow profiles of same mouse (young and old) in Fig. 17.

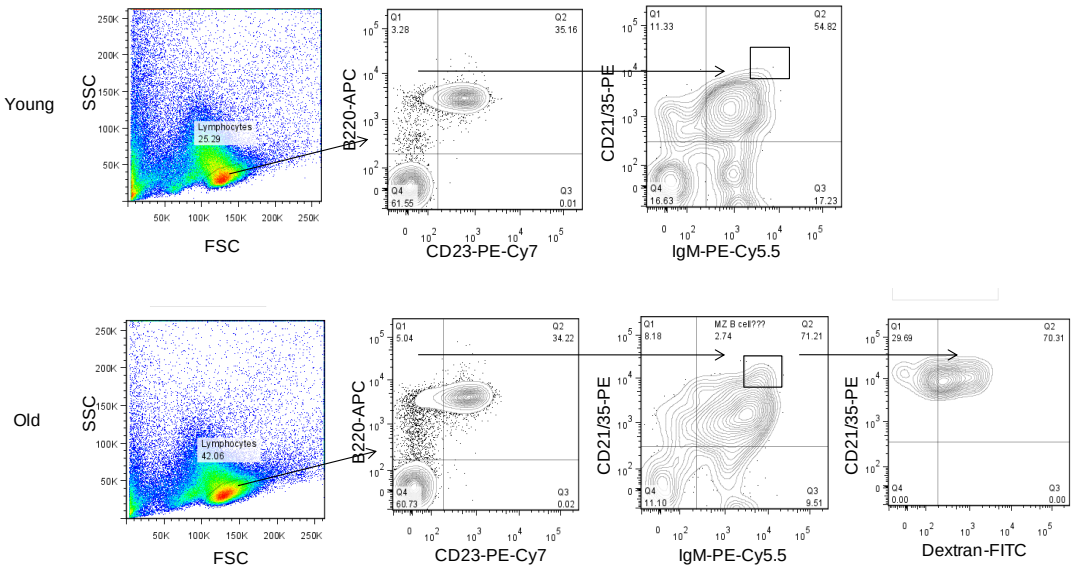


**Figure 19. Representative profile of MZ B population in the lymph node of young and old mice.** Shown are contours representative of young or old lymph node cells. Frequency of MZ B cells was determined within the $B220^{+}$ population. The MZ B cell population was determined by gating on the $B220^{+}/CD23^{-}$ fraction followed by gating on the CD21/35 $^{high}$/ IgM $^{high}$ fraction. Top panel is representative of lymph node cells of young mice (4 mo). No MZ B cell phenotype was present in the CD21/35 $^{high}$/ IgM $^{high}$ fraction. Lower panel is representative of lymph node cells from an old mice (21 mo) that reveals a MZ B cell phenotype in the CD21/35 $^{high}$/ IgM $^{high}$ fraction, which took up FITC-labeled dextran within 45min after i.v. delivery, as expected of MZ B cells.

**Evaluation of the chemokine CCL21 and its importance for MZM homing to the MZ**

The cell populations that home to the MZ do so as a result of chemotactic factors that are secreted by neighboring stromal cells (31, 34, 35, 43). I have shown that the distribution and frequency of MZM appears altered in many old mice. Furthermore, fewer young MZ B cells appeared to home to the spleens of old mice compared to those of young mice, suggesting an extrinsic defect that could be related to the reduction of MZM. One study suggests that MZM home to the MZ in response to the chemokine CCL21 and to a lesser extent the chemokine CCL19. Ato *et al*. observed a decrease in MZM in plt/plt mice, which lack functional CCL21 and CCL19, (43); furthermore, *in vitro* migration assays of enriched MZM demonstrated that CCL21 resulted in migration of MZM(43). Examination of CCL21 at the protein level using anti-CCL21 antibody was revealed on splenic tissue sections (Fig. 20A). CCL21 is secreted by the stromal cells important for T cell homing to the PALS of the spleen (43). Results from young (n = 7) tissue sections revealed an abundance of CCL21 present in the PALS (T cell regions of the white pulp areas) (Fig. 20A, top and middle panels). CCL21 was detected in 85% of the PALS regions examined in the tissues from 7 young mice (Table). However, in splenic tissue sections of old mice (n = 7) (Fig 20A, bottom panels) CCL21 appeared to be absent in 55% of the PALS regions examined (Table). CCL21 was also present in the bridging channels of splenic tissue of both young and old mice (Fig. 20A, top right panels).

CCL21 was also evaluated in the MZ areas of splenic tissue from young and old mice to determine if present near MZM. $CCL21^{+}$ protein was observed to localize in

clusters adjacent to the outer edge, but not encompassing the MZ in 3/7 young mice examined. CCL21was also observed in clusters adjacent to the outer edge of the MZ in 3/7 old mice examined. To determine co-localization of CCL21 on MZM, anti-MARCO antibody was used to reveal the MZM (Fig. 20B). Results revealed that there was no co-localization of CCL21 on MZM in splenic sections from young and old mice. Results also showed that animals with poor $MARCO^{+}$ MZM (2 old mice) appeared to have a heightened CCL21protein in the spleen (Fig.20 C); however, in this figure it was difficult to determine the amount of $CCL21^{+}$ PALS/total PALS, $CCL21^{+}$ protein adjacent to the outer edge of the MZ, and $CCL21^{+}$ bridging channels/total bridging channels in these splenic tissue sections.

To determine if there were differences in mRNA levels of CCL21 in the spleens of young and old mice, spleens were isolated and homogenized and quantitative RT-PCR was performed. Results showed no significant differences in CCL21 mRNA between young and old spleens ($p = 0.4234$ as determined by Mann-Whitney test; $n = 9$ young; $n = 8$ old) (Fig.21). For some individual animals stained for CCL21 at the protein level, the level of mRNA was also determined. Results show no definitive correlations.

**A**

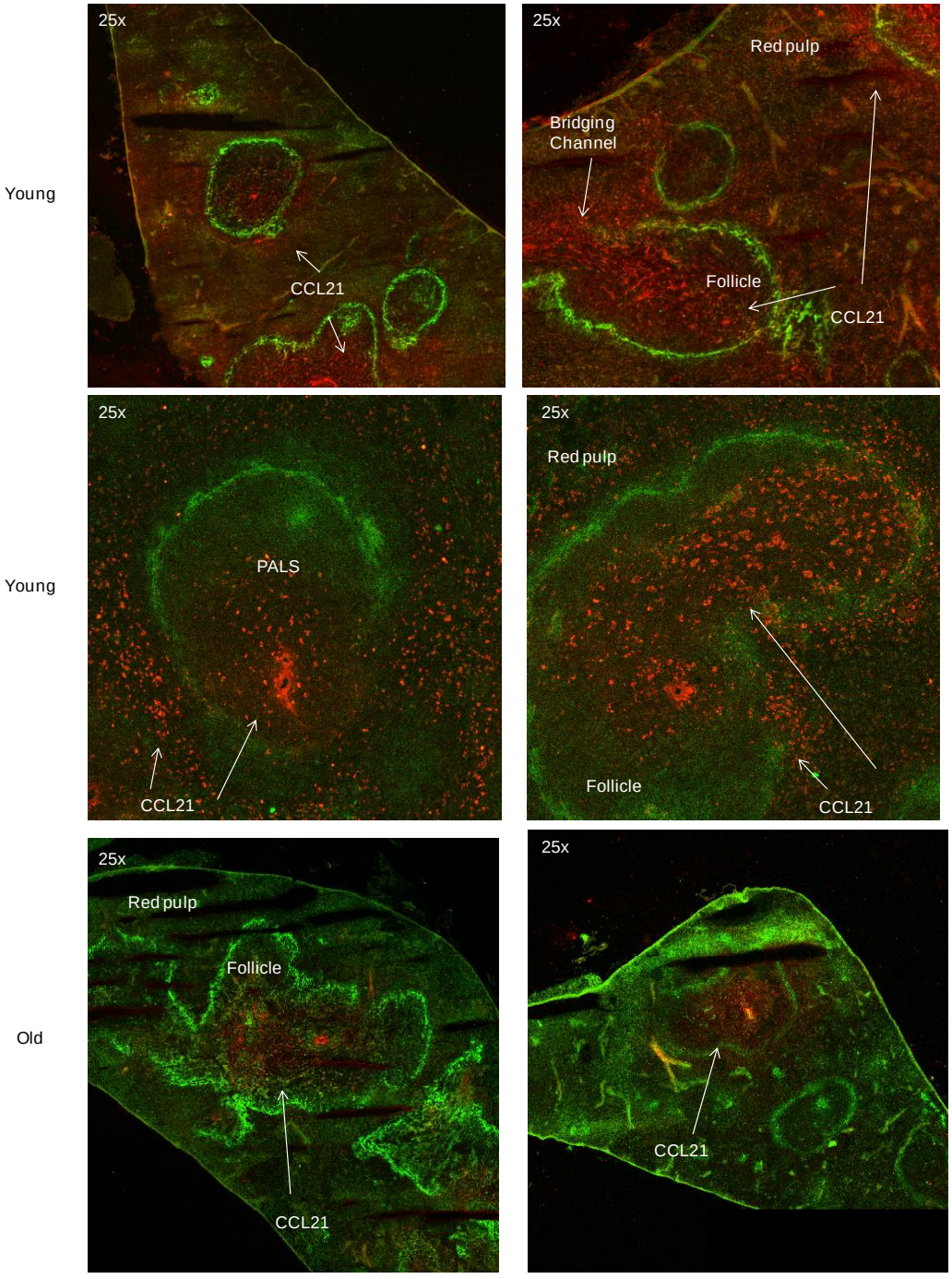
Young
25x
CCL21
25x
Red pulp
Bridging
Channel
Follicle
CCL21
Young
25x
PALS
CCL21
25x
Red pulp
Follicle
CCL21
Old
25x
Red pulp
Follicle
CCL21
25x
CCL21

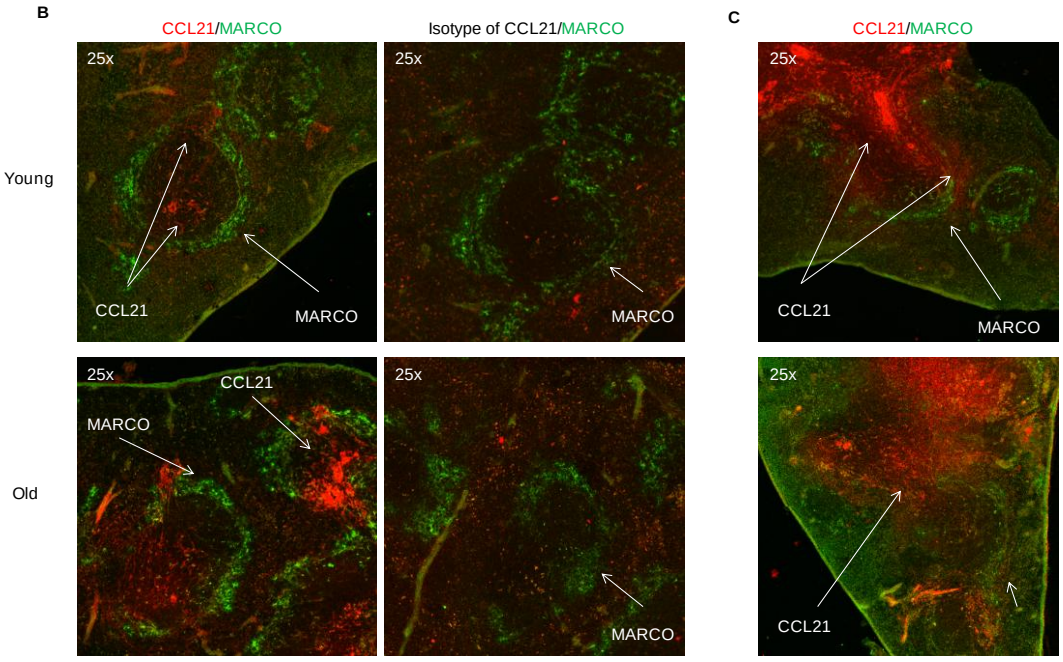


**Figure 20. CCL21 distribution in spleens from young and old mice. (A)** Sections are stained with antibodies specific for MAdCAM1$^{+}$ MZ sinus lining cells (green) and the chemokine CCL21 (red). Confocal microscopy was used to reveal localization of CCL21, which is found in the T cell rich PALS region of the white pulp follicle, bridging channels, and around the outer edge of the MZ. Top panel shows the distribution of CCL21 in young splenic sections from 2 separate animals (top right and left) 25x tile 6x6. Middle panel shows 2 separate MZ and white pulp follicles from 1 representative young mouse (25x). Bottom panel shows the distribution of CCL21 in old splenic sections from 2 separate animals (lower right and left) 25x tile 6x6. **(B)** Sections are stained with antibodies specific for MARCO (green) and the chemokine CCL21 (red). Top panel shows the distribution of CCL21 in one young splenic section (top left, isotype control top right) 25x tile 6x6. Bottom left panel shows the distribution of CCL21 in one old splenic section 25x tile 6x6 (bottom left, isotype control bottom right). **(C)** Top and bottom panels are representatives of 2 separate splenic sections from old mice. MARCO$^{+}$ MZM in both mice have a poor distribution and CCL21 appears to be abundant.

Table 6. Presence of CCL21 in Splenic Sections from Young and Old mice

| Animal Number | CCL21+ PALS/Total PALS | CCL21+ Protein Adjacent to Outer Edge of MZ | CCL21+ Bridging Channels/ Total Bridging Channels | Degree of MARCO |
|---|---|---|---|---|
| Y-330 | 3/3 | No | 0/0 | |
| Y-331 | 4/5 | Yes | 0/0 | |
| Y-334 | 3/3 | Yes | 2/2 | |
| Y-335 | 5/5 | No | 2/3 | |
| Y-462 | 3/4 | Yes | 4/4 | |
| * Y-469 | 1/2 | No | 1/1 | Good MARCO |
| * Y-470 | 3/4 | No | 1/1 | Good MARCO |
| O-332 | 1/3 | Yes | 2/2 | |
| O-333 | 1/4 | No | 0/0 | |
| O-336 | 1/3 | No | 0/1 | |
| O-450 | 1/4 | Yes | 0/0 | |
| * O-471 | 3/3 | No | 3/3 | Good MARCO |
| * O-472 | ? | Yes | 0/0 | Poor MARCO |
| * O-473 | 2/3 | ? | ? | Poor MARCO |

**Table 6. Distribution of CCL21 protein in splenic sections of young and old mice.** The spleens of 7 young and 7 old BALB/c mice were evaluated to determine differences in CCL21 protein throughout the spleens. The number of $CCL21^+$ PALS/Total PALS, the presence of $CCL21^+$ protein adjacent to the outer edge of the MZ, the number of $CCL21^+$ bridging channels/ total bridging channels, and the amount of MARCO (where appropriate) was evaluated between age groups. Splenic tissue sections were stained to reveal either CCL21 and MAdCAM-$1^+$ MZ sinus lining cells or CCL21 and $MARCO^+$ MZM (*).

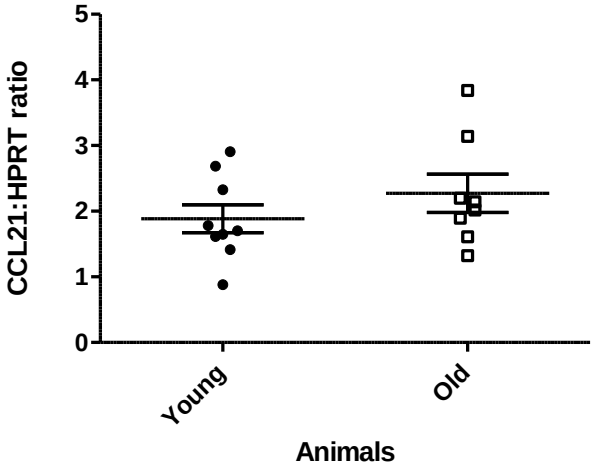


**Figure 21. Expression of CCL21 protein and mRNA** Quantitative RT-PCR on spleens from young (2-4 mo) and old (18-23 mo) mice showed no statistical differences between age groups. p = 0.4234 as determined by Mann-Whitney test (n = 9 young mice; n = 8 old mice).

**CCR7 levels in young and old MZM**

The receptor for CCL21 is CCR7, which is expressed on MZM (43). In order to determine if CCR7 receptor levels on MZM are altered with age, the flow cytometry staining paradigm developed for MZM identification was implemented (Fig. 22). The percentage of MZM that were $CCR7^+$ was determined for both young and old mice, and results showed that there was a decrease in the percentage of $CCR7^+$ MZM in old mice when compared to young mice (Fig. 24). Yet, it is of interest to note that although there is a decrease in the percentage of $CCR7^+$ MZM in old, the overall expression of $CCR7^+$ MZM of both young and old mice was low compared to what is normally observed with T cells (Fig. 23). Work by Ato *et al.* first revealed that MZM express CCR7 weakly compared to naïve T cells and DCs (43). This was determined by staining splenocytes isolated from dextran-FITC injected mice (used to identify MZM) with a recombinant CCR7 ligand, CCL19-Ig chimeric protein, which was generated by Manjunath *et al.* (109). CCL19 like CCL21 is a chemokine for the CCR7 receptor (43). MZM were identified as $FITC^+$ SIGN-$R1^+$ by flow cytometry and the level of CCR7 was determined from this pool and observed to be low (43).

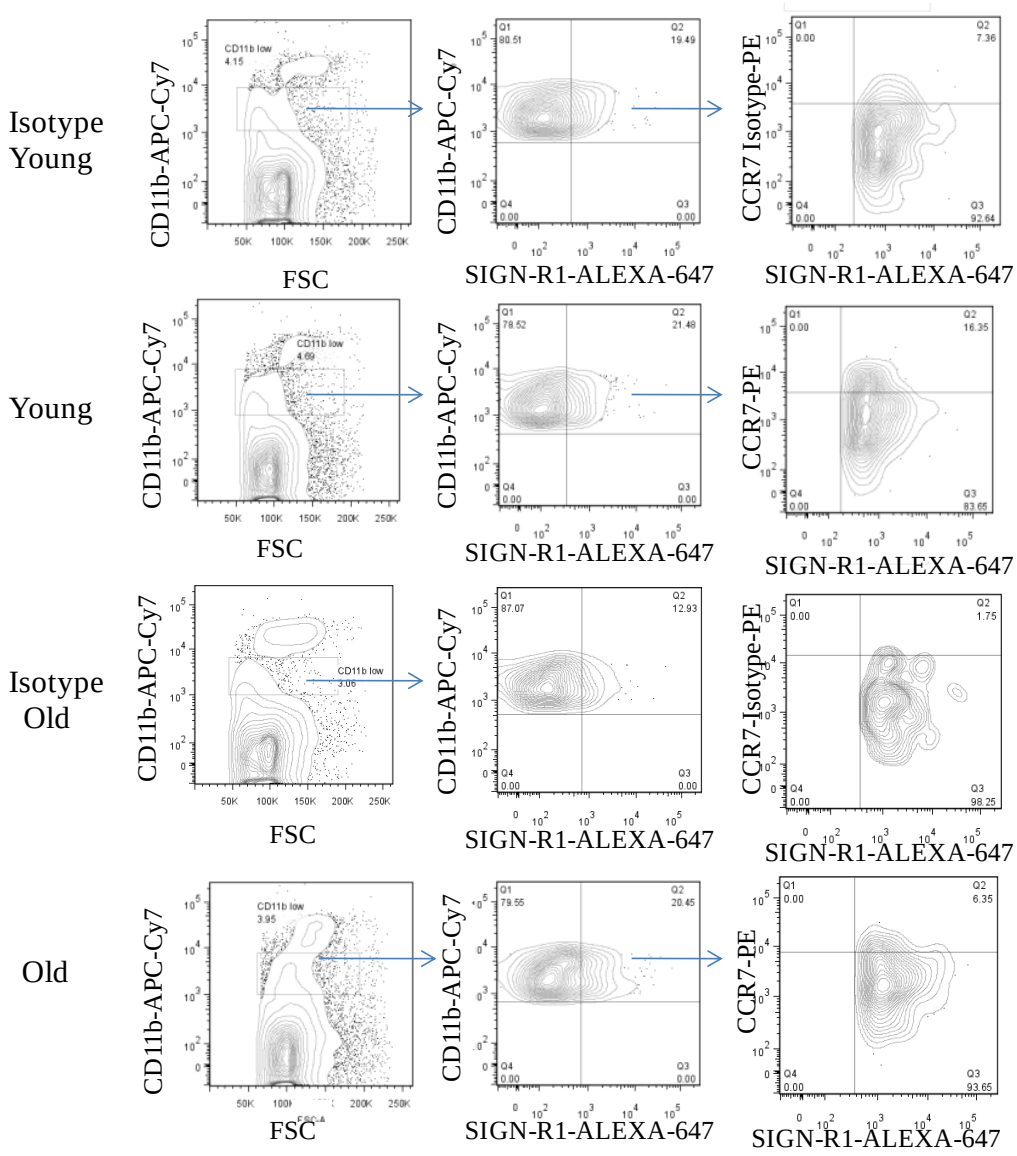


**Figure 22. Flow cytometry profiles reveal the percentage of CCR7$^{+}$ MZM of young and old mice.** The MZM population is determined from the CD11b low SIGN-R1$^{+}$ fraction and the percentage of CCR7 is revealed in the PE channel. Top panels are the isotype control for CCR7 and representative profile from young mouse depicting the CCR7 positive MZM. The lower panels are the isotype control for CCR7 representative MZM profile and representative profile from an old mouse depicting the CCR7 positive MZM.

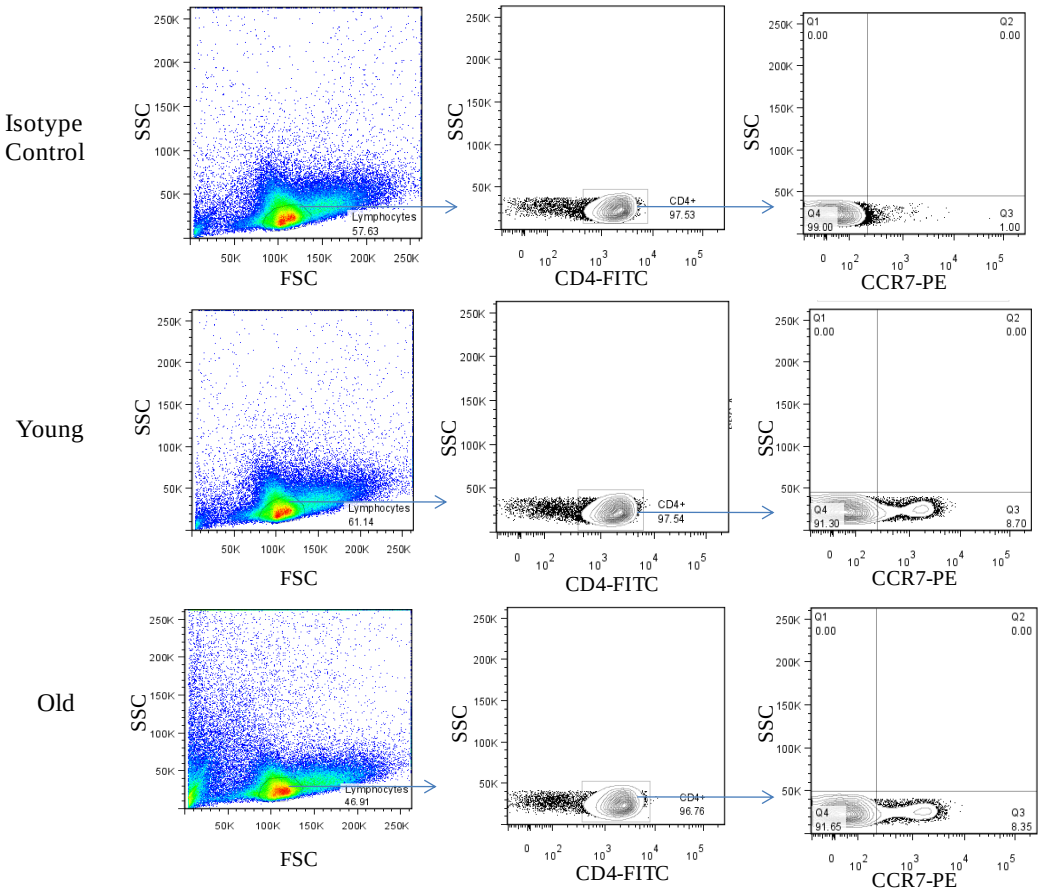


**Figure 23. Flow cytometry profiles reveal the percentage of CCR7$^{+}$ CD4+ T cells of young and old mice.** The CD4+ population is determined from viable lymphocyte fraction and the percentage of CCR7 is revealed in the PE channel. Top panel is a representative profile of the isotype control for CCR7. Middle panel is a representative of young profile and the lower panel is representative of old profile.

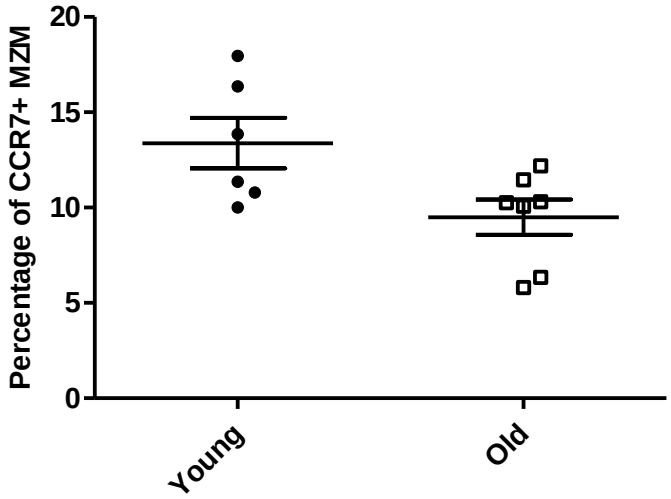


**Figure 24. Percentage of CCR7$^+$ MZM of young and old mice.** The percentage of CCR7$^+$ MZM in young and old mice was determined by flow cytometry. Data show that old mice have significantly lower percentages of CCR7 expressed on MZM when compared to young mice. $p = 0.0314$ as determined by Unpaired t test ($n = 6$ young mice; $n = 7$ old mic

# CHAPTER VI

## EVALUATION OF THE FUNCTIONAL DIFFERENCES BETWEEN MZM OF OLD AND YOUNG MICE

Data presented in Chapter IV revealed that there are decreases in the MZM pool with age. I next wanted to determine if loss in cell number alone or a combination of loss of number and decrease in cell function may contribute to the age related decline in the TI immune response. The MZM from old mice were evaluated to determine if they are functionally different compared to MZM of young mice by measuring differences in phagocytosis by MZM.

In order to measure the phagocytic ability of MZM in young and old mice a number of experimental approaches were examined. The first experiment aimed to examine the functional differences of MZM *in vivo* through intravenous delivery of dextran. Analysis was done via confocal microscopy and flow cytometry. The second series of experiments aimed to measure the phagocytic function of MZM *in vitro* after treatment with pHrodo ™ *S. aureus* bioparticles (pHrodo); analysis was done via flow cytometry. Techniques established from the first two series of experiments helped build the next series of studies. In these last experiments, MZM were successfully targeted for measurement of phagocytosis and live visualization of phagocytosis by MZM was revealed using a Leica TC5 SP5 confocal microscope.

**Functional differences in capture of blood-borne dextran particles by MZM in old mice**

Since an important function of MZM is the clearance of blood-borne antigens, I asked whether reduced capture of blood-borne antigen would be a consequence of the changes in MZM with age. MZM have been shown to decrease in age; however, whether this decrease in cell frequency/number implied reduced cell function needed to be clarified. SIGN-R1 [homologue of human DC-SIGN (16)] binds the capsular polysaccharide of *Streptococcus pneumoniae* and also to the polysaccharide dextran (17-20). For these experiments the rapid, *in vivo* binding of FITC-labeled dextran to SIGN-R1 was used to mimic antigen (18, 43). Dextran-FITC was administered i.v. into tail veins of young and old mice (Fig. 25). It has been previously shown that dextran binds MZM in tissue in as early as 45 min and at later time points dextran is no longer visualized on MZM (18). After 45 min, animals were sacrificed and the spleens removed and frozen in O.C.T for visualization of dextran binding to cells in tissue sections. Spleen sections were stained with anti-MAdCAM-1 to distinguish the MZ sinus lining cells as a landmark. To confirm that dextran$^{+}$ macrophages were MZM, tissue sections were stained with anti-MARCO antibody for the expression of MARCO, found on the surface of MZM. (Fig. 26A). As reported by Ato and colleagues for young mice (43), after 45 min dextran binds to MZM, appearing as a continuous ring on the outer edge of the MZ sinus. Confocal microscopy revealed a clear "ring" of bound dextran-FITC adjacent to the MAdCAM-1$^{+}$ cells in the MZ of young spleens (Fig. 26B). In contrast,

the tissue sections from old spleens had less bound dextran-FITC in the MZ when compared to the young tissue and showed a patchy deposition similar to immunocytochemistry staining for MARCO (Chapter IV, Fig. 9A). This patchy distribution could be a reflection of fewer MZM present in the spleens of old mice and less indicative of an alteration in cell function.

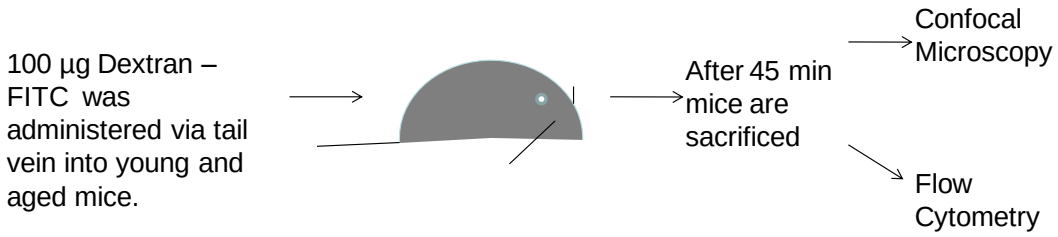


**Figure 25. Intravenous injections of dextran-FITC into young and old mice.** Dextran-FITC was administered i.v. into young and old mice. After 45 min, mice were sacrificed and spleens were removed. One half of the spleen was frozen in O.C.T for sectioning to evaluate the localization of dextran-FITC in the MZ via confocal microscopy. The second half of the spleen was dispersed and single cell suspensions were stained with anti-CD11b and anti-SIGN-R1 antibodies for flow cytometry analysis of the percent of dextran positive MZM.

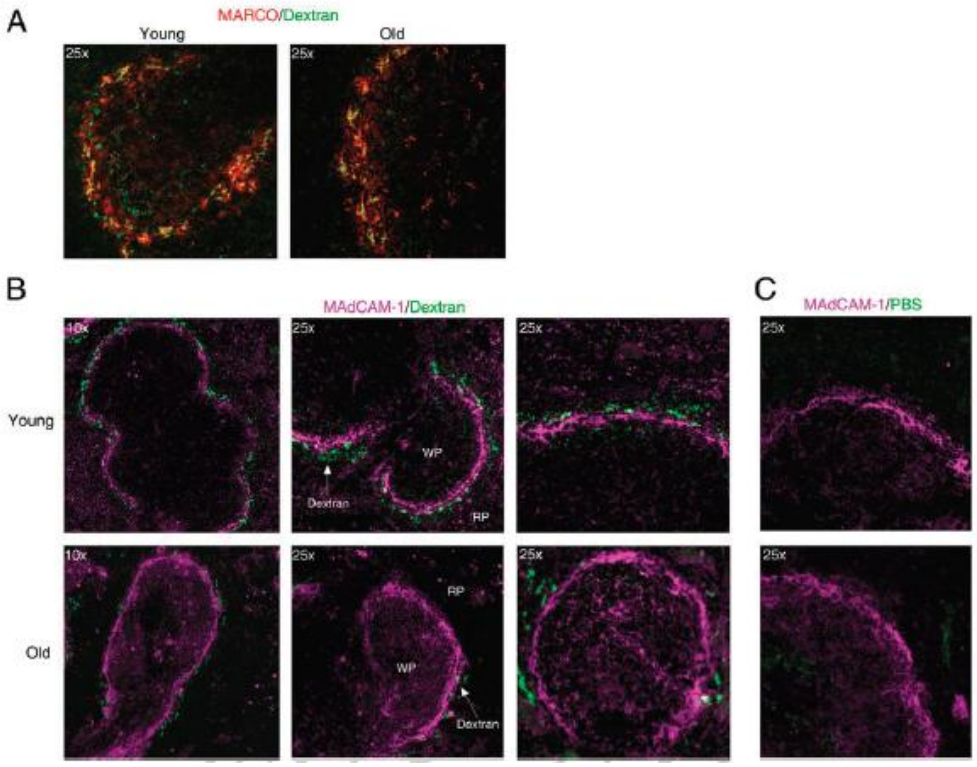


**Figure 26. Binding of dextran by MZM of old versus young mice.** Confocal images of frozen splenic sections harvested 45 min after dextran-FITC (green) was given intravenously to female BALB/c mice. **(A)** Co-localization of dextran (green) with MARCO$^+$ MZM (red) is observed as yellow after staining dextran positive tissue from a representative young (top) and old (bottom) mouse. **(B)** Photos show typical deposition, representing 2 of 18 young (2-3 mo, top panels) and 2 of 16 old (18-23 mo, bottom panels) mice. In the spleens of most old mice, uptake of dextran appeared in discontinuous patches along the outer edge of the MZ sinus. MAdCAM-1$^+$ MZ sinus lining cells (purple) are stained as a landmark. **(C)** Representative young (top) and old (bottom) splenic sections from PBS injected mice.

**Measuring dextran positive MZM by flow cytometry – pitfalls and potentials**

To determine if MZM of old mice are less efficient at capturing dextran, differences in the percentage of dextran positive MZM of young and old mice was next determined by flow cytometry. As described above, mice were injected i.v. with dextran-FITC in the tail veins and after 45 min, 1/2 of each spleen was dispersed for flow cytometry analysis. The MZM population was identified in the CD11b low and SIGN-R1$^+$ fraction and the percentage of MZM that were dextran$^+$ was revealed in the FITC channel. PBS (no fluorophore) was delivered i.v. into the tail veins as a control. From the flow cytometry profiles of PBS injected mice, it was determined that MZM have a high level of autofluorescence in the FITC channel (Fig. 27). Based on this high level of background, the percentage of dextran$^+$ MZM could not be adequately determined in young and old mice.

In order to be able to use flow cytometry to determine binding of dextran-FITC by MZM, this background autofluorescence needs to be corrected. To determine if the experimental design contributed to the high level of background fluorescence, the method of i.v. delivery of dextran-FITC or PBS delivery was first examined. Delivery of dextran-FITC and PBS into the tails veins of mice, which requires warming the mice, was compared to intraocular delivery of dextran-FITC and PBS, a different i.v. route that does not require manipulation. Results were not different between injection routes; therefore, I conclude that the autofluorescence of MZM in the FITC channel prohibited the

determination of differences in the percentage of dextran positive cells in young and old MZM.

To correct for this autofluoresence in the future, either a fluorophore of a higher emission conjugated to dextran needs to implemented or more precise filters need to be used that correct for the observed spectral overlap. MZM from PBS injected mice showed up positive in the dextran-FITC channel; this suggests that the spectral overlap is occurring with the natural autofluoresent properties of MZM with the low emission FITC fluorophore conjugated to the dextran. To reveal dextran-FITC positive MZM populations by flow cytometry, the use of multiple antibodies of which each is conjugated to a unique fluorophore is required. Therefore, a precise bandpass filter, which separates the emission of multiple wavelengths, would be needed to differentiate the emission of the cells autofluoresence from the FITC fluorphore emission.

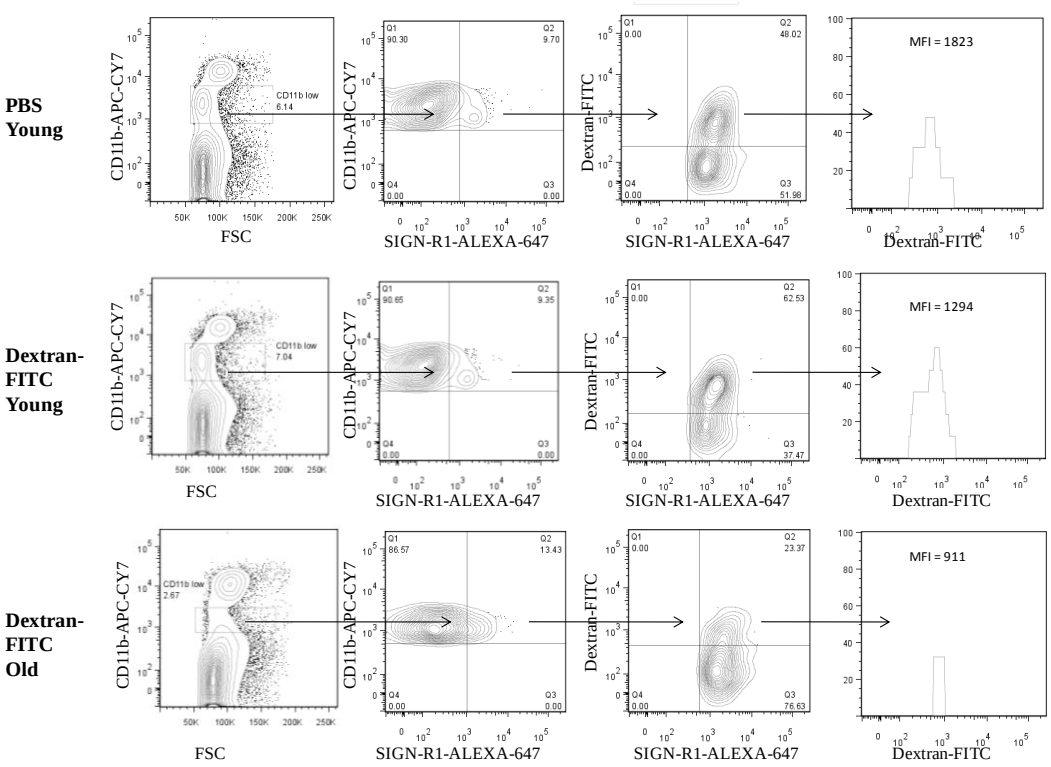


**Figure 27. Flow cytometry of MZM from young and old mice injected with dextran-FITC.** Dextran-FITC was delivered i.v. in the tail vein of young and old mice and analyzed for the percent of dextran-FITC positive MZM. Top panel shows a representative flow cytometry profile of PBS injected control, the middle panel represents a dextran-FITC injected young, and bottom panel represents a dextran-FITC injected old mouse. Far right top panel shows the MFI of PBS injected controls, which are similar to dextran-FITC injected mice (far right middle panel).

**Evaluation of functional differences in the phagocytosis of pHrodo bioparticles by MZM in old and young mice using flow cytometry**

I next aimed to test the phagocytosis of MZM between age groups using a pH sensitive antigen that emits fluorescence in a higher channel (PE) using flow cytometry. Although MZM are known for their highly phagocytic properties (9), it is not known if a decline in the phagocytic function of MZM from old mice, compared to young, contributes to decreased TI immune response in age. Here, pHrodo ™ *S. aureus* bioparticles (pHrodo) were used to specially aim to measure the phagocytosis of MZM. pHrodo consists of killed *S. aureus* conjugated to a fluorescent compound that is pH sensitive and emits fluorescence only under acidic conditions. Binding of antigen by macrophages initiates phagocytosis, which consists of three essential compartments: early endosome, late endosome, and lastly, the lysosome. These separate phagocytic compartments each have a specific pH (56). Progression through early endosome (pH 6), late endosome (pH 5.5), and the lysosome (pH 4) leads to decreases in pH. pHrodo bioparticles start to emit florescence at a pH of 6 and hit peak fluorescence at a pH of 4 (56, 58). The fluorescence of pHrodo can be detected by a microplate reader, flow cytometer, or confocal microscope.

**Phagocytosis of pHrodo bioparticles by a heterogeneous culture of adherent splenocytes measured via a microplate reader**

To measure phagocytosis of pHrodo by the manufacturer's suggested protocol, a microplate reader was first used. The concentration recommended by the manufacturer is 100µg of pHrodo for 100,000 cells (Invitogen). Splenocytes were harvested and 1 x $10^6$ cells/well were cultured onto 96 flat bottom well plates for 1 hr. The adherent cells (macrophages) in the spleen make up approximately 10% of the total splenocyte population. Therefore, non-adherent cells were removed to yield approximately100,000 cells/well. 100µl containing 100µg pHrodo were added per well and allowed to incubate for 2 hrs at 37 C. The 96 well plates were loaded in replicates of three for each animal as follows: cells + pHrodo, cells only, pHrodo only, and media only negative control. After 2 hrs the samples were placed in a microplate reader. Excitation of pHrodo occurred at 550 nm and emission at 600 nm. The ratio of net experimental phagocytosis over net baseline phagocytosis x 100% gives a percentage of the net effect of phagocytosis of pHrodo by the adherent cells (Fig. 28). To calculate the net baseline phagocytosis, the mean of the three replicates of cells only and the mean of the three replicates of pHrodo only were first added. The mean negative control value (media only) was then subtracted from this value. The net experimental phagocytosis was calculated by subtracting the mean negative control value from the mean of cells + pHrodo.

Results showed no differences in the net effect of phagocytosis between old and young total adherent cells (Fig. 28) (n = 3 mice for both young and old, p = 1.0000).

These results did confirm that the pHrodo bioparticles work as the manufacturer suggested, but was not sufficient for specifically targeting MZM.

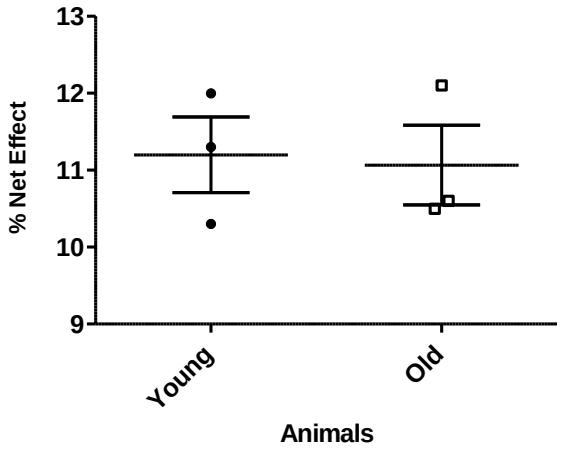


**Table 7. Avg MFI of adherent splenocytes treated with or without pHrodo for 2hrs via microplate**

| Animal | pHrodo & cells | Cells only | pHrodo only | Media only |
|---|---|---|---|---|
| Y-1 | 2685 | 84 | 1657 | 90 |
| Y-2 | 1537 | 90 | 1405 | 90 |
| O-1 | 2045 | 105 | 1795 | 102 |
| O-2 | 1993 | 87 | 1785 | 93 |
| O-3 | 1971 | 86 | 1815 | 90 |

**Figure 28**. **Percent net effect of pHrodo by adherent splenocytes from young versus old Mice.** Results are reported by taking the ratio of net experimental phagocytosis x 100% over net baseline control phagocytosis to give a percentage of the net effect of the adherent cells.

$$\%\,\text{Net Effect} = \frac{\text{Net experimental phagocytosis x 100\%}}{\text{Net baseline control phagocytosis}}$$

The horizontal bars indicate the average and the SEM for each group. p=1.0000 determined by Mann Whitney test (n=3 for each age group; young mice (2-3 mo), filled circles; old mice (18-23 mo), open squares). Bottom table represents raw MFI values obtained from pHrodo + cells, cells only, pHrodo only, and media only of representative young and old animal samples.

**Establishment of concentration, time and inhibitor of pHrodo treatment *in vitro* for flow cytometry analysis**

In order to use flow cytometry to measure phagocytosis of pHrodo the concentration, time, and inhibitor of pHrodo needed to be determined. The manufacturer recommends 100µg of pHrodo for 100,000 cells, which are adhered to a 96 well plate that measures phagocytosis of pHrodo directly in the wells. For flow cytometry, single cell suspensions are run through the flow cytometer in order to detect the amount of fluorescence associated with the cell. The aim of these experiments was to specifically measure the amount of pHrodo phagocytized by MZM; therefore, MZM flow cytometry staining as well as pHrodo treatment was implemented. In order to stain for MZM using cells treated with pHrodo, the cells needed to be adhered to a larger surface than the 96 well plates to allow for collection of the cells. 35 mm culture plates were used and the optimal concentration of pHrodo for flow cytometry detection was determined to be 125µg of pHrodo for approximately 200,000 adherent cells (Fig 29 and 30). The suggested time for pHrodo incubation is 2hrs. Phagocytosis, as measured by the use of latex beads, has been well established to occur in 30 min (55). The 30 min time point for pHrodo, measured by flow cytometry, gave variable MFI when compared to the 2hr time point (Fig. 30). It appears that after 30 min at increasing concentrations (62.5-1000µg), adherent cells are not able to take in additional pHrodo and the MFI decreased to lower values. The use of beads to quantify phagocytosis does not distinguish between beads that bind on the cell surface from beads that are endocytosed. pHrodo reveals

phagocytosis after the phagosome has been endocytosed, which may require additional time to see its fluorescence via flow cytometry. Therefore, it is possible that MZM have a threshold for the amount of pHrodo that can be taken in by the cell before additional bioparticles can be bound and endocytosed.

An effective control for pHrodo would be one that would inhibit its phagocytosis and therefore prove its efficacy. To determine the best control for pHrodo reduced temperatures (-20C) was initially used to inhibit phagocytosis and found to be an ineffective, since a positive fluorescence was still detected (data not shown). Subsequent experiments found that 1.0 % sodium azide, an electron transport chain inhibitor, was found to reduce the phagocytosis of pHrodo. These series of experiments discussed in this section revealed the best concentration, time of pHrodo incubation, and inhibitor to pHrodo *in vitro* for flow cytometry analysis.

**Experimental design of pHrodo treatment for flow cytometry analysis**

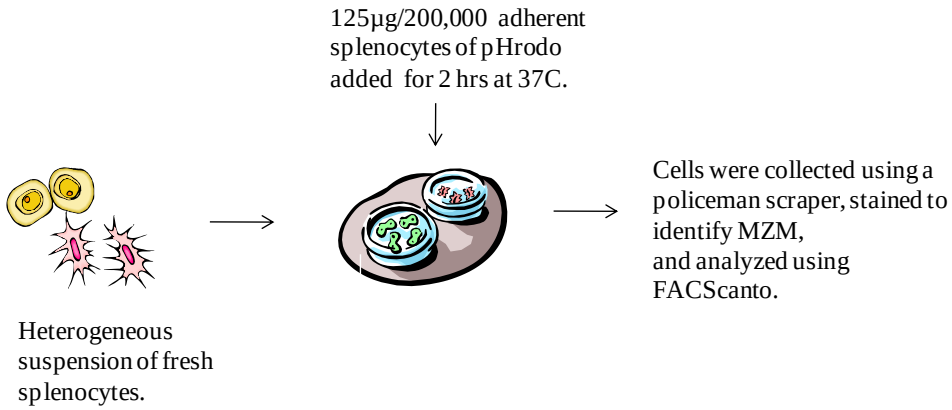


**Figure 29. Experimental paradigm of pHrodo treatment for flow cytometry analysis.** Heterogeneous suspension of fresh splenocytes from young and old mice were allowed to adhere onto 35 mm culture plates for 1hr in RPMI + 10% FBS. Non-adherent cells were removed and 125µg of pHrodo at a volume of 125µl was added to approximately 200,000 adherent splenocytes and allowed to incubate for 2 hrs at 37C. After 2 hrs cells were gently scraped and stained with antibodies for identification of MZM by flow cytometry.

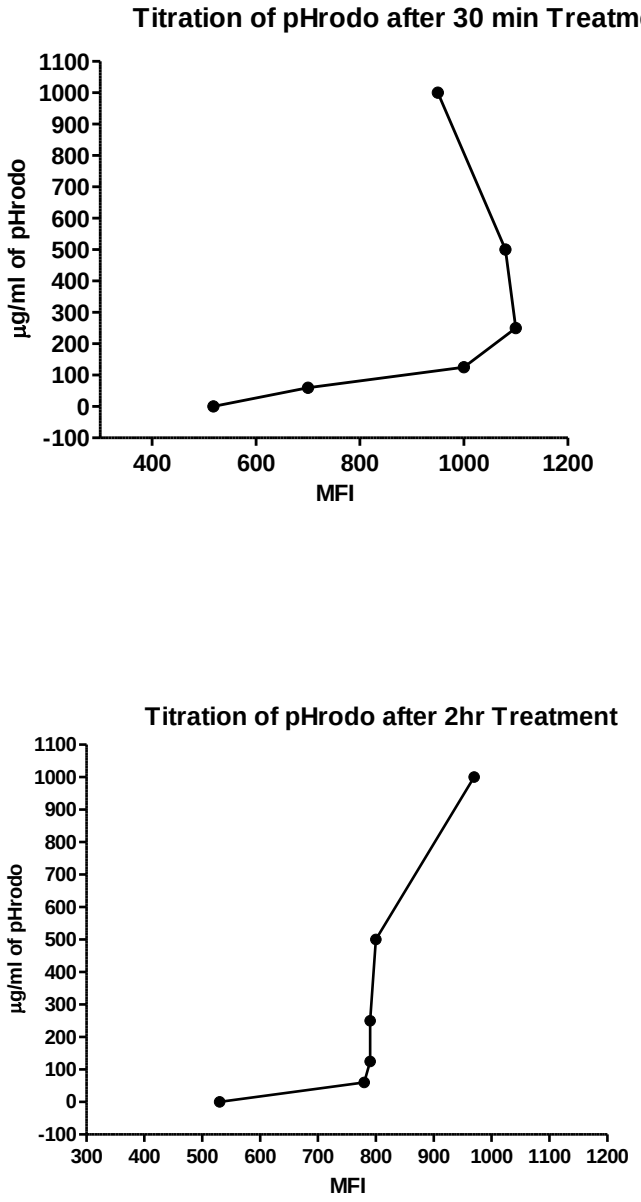


**Figure 30. Titration of pHrodo for use in flow cytometry.** Top panel shows that at increasing concentrations of pHrodo incubated at 37 C for 30 min, there is a gradual increase in the MFI with a threshold at 500 µg/ml/200,000 splenocytes. Bottom panel demonstrates that after 2 hr incubation with pHrodo, fluorescence can be detected starting at 60 µg/ml/200,000 splenocytes and stays steady with increasing concentrations. Media only controls at both 30 min and 2hrs auto-fluoresced at an MFI of near 500.

**Phagocytosis of pHrodo bioparticles revealed by flow cytometry**

To evaluate the differences in phagocytosis of pHrodo by MZM from young and old mice, differences in the percentage of pHrodo positive MZM between age groups were aimed to be determined by flow cytometry. As previously mentioned, pHrodo is killed *Staphylococcus aureus* conjugated to a dye that emits fluorescence under acidic conditions. MZM have been shown to bind *Staphylococcus aureus* via the surface receptor MARCO (15). Adherent splenocytes from young and old mice were cultured and 125 µg of pHrodo was administered for 2 hrs at 37 C. Adherent cells were collected and stained to identify MZM. Initially MZM were stained using the antibodies to CD11b and MARCO. Notably, a 2-3 fold increase in the percentage of CD11b low $MARCO^+$ cells after pHrodo treatment was found compared to media treated controls that exhibited typical $MARCO^+$ MZM phenotypes (Fig. 31). This observation supports prior reports that have shown after LPS treatment, MARCO was upregulated on red pulp macrophages (110, 111). Therefore, I think that the 2 hr incubation with pHrodo induced expression of MARCO on red pulp macrophages and using the antibody to MARCO to identify MZM will not differentiate MZM from the red pulp macrophages. Recent work by Kirby *et al.* examined if non-lymphoid splenocyte populations including red pulp macrophages, neutrophils, and dendritic cells upregulate SIGN-R1 after antigen exposure similar to that which is seen with MARCO (6). Mice were infected with *Leishmania donovani* to specifically deplete MZM and were subsequently infected *S. pneumoniae* to determine if other splenocytes upregulated SIGN-R1 to bind and clear *S. pneumoniae.* Their results showed minimal expression of SIGN-R1 on other splenocyte populations after infection

with *S. pneumoniae* in Leishmania infected mice. As a result of these published findings, I elected to use the antibodies to CD11b and SIGN-R1 to identify pHrodo$^{+}$ MZM. However, an increase in CD11b low SIGN-R1$^{+}$ cells after pHrodo treatment was observed in both young and old mice after incubation with pHrodo for 2hrs *in vitro* from splenocytes obtained from wild type BALB/c mice (Fig. 32). Due to this increase observed in the CD11b low SIGN-R1$^{+}$ cells after pHrodo treatment, it is unclear if MZM are exclusively responsible for the phagocytosis of the pHrodo bioparticles. It is possible that the data obtained via flow cytometry includes other CD11b low splenocytes that have upregulated SIGN-R1 after encounter with antigen.

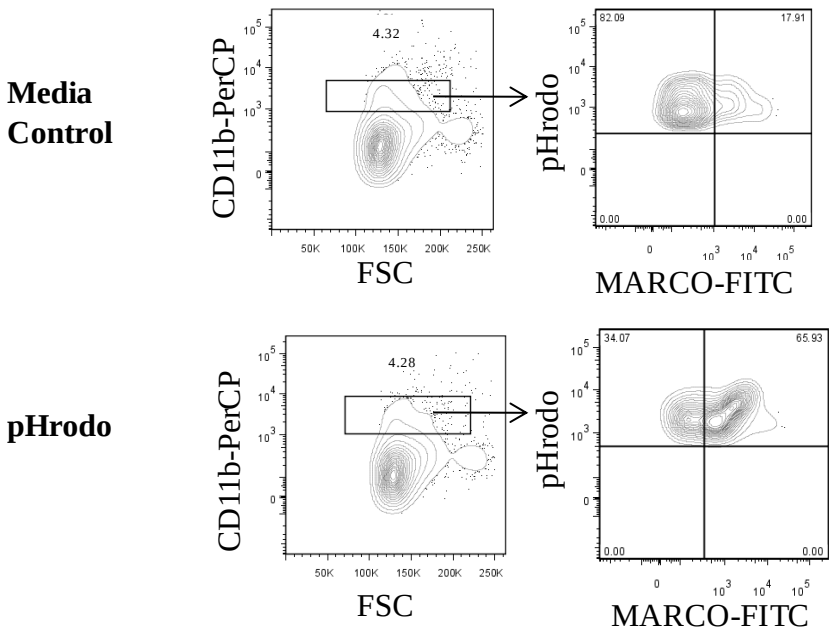


**Figure 31. Representative flow cytometry profile of MARCO upregulation on splenic adherent cells upon treatment with pHrodo.** Flow cytometry was used to distinguish pHrodo$^+$ MZM from cultured adherent splenocytes from young and old mice after 2 hr *in vitro* pHrodo treatment. MARCO$^+$ MZM were defined using the antibodies to CD11b and MARCO. The CD11b low fraction was gated from all viable cells in the spleen and the MZM population revealed in the CD11b low and MARCO$^+$ fraction. The top panel shows media only controls with normal levels of CD11b low MARCO$^+$ MZM (18.0%); the lower panel shows > 3 fold increase in CD11b low MARCO$^+$ after pHrodo treatment and approximately equal decreases in the CD11b low MARCO negative quadrant.

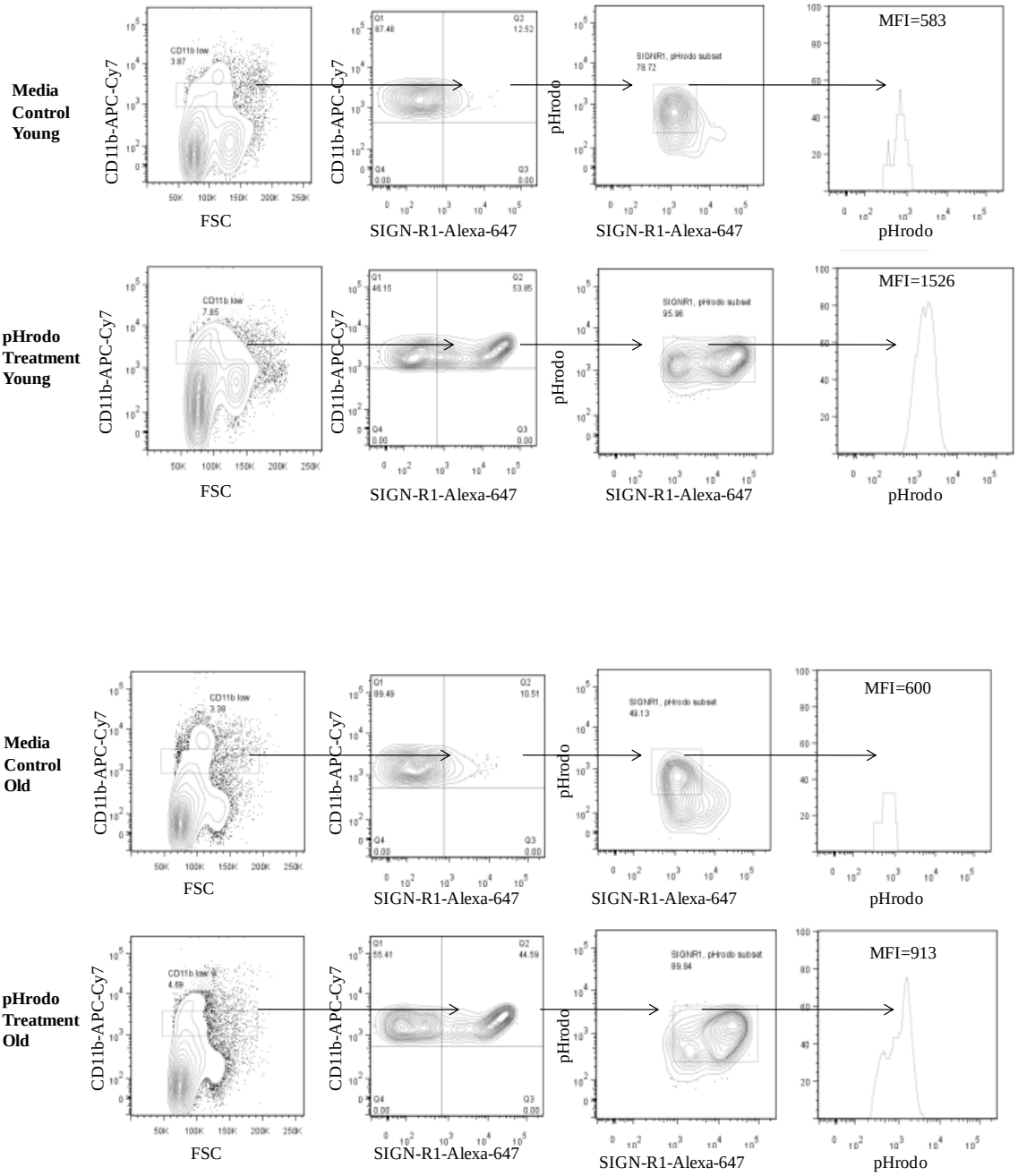
Media Control Young
pHrodo Treatment Young
Media Control Old
pHrodo Treatment Old
CD11b-APC-Cy7
FSC
SIGN-R1-Alexa-647
pHrodo
MFI=583
MFI=1526
MFI=600
MFI=913

**Figure 32. Representative flow cytometry profiles of SIGN-R1$^+$ MZM upon treatment with pHrodo.** Flow cytometry was used to measure phagocytosis of pHrodo by MZM from whole cultured adherent splenocytes isolated from young and old mice after 2hr *in vitro* pHrodo treatment. SIGN-R1$^+$ MZM were targeted using the antibodies CD11b and SIGN-R1. The CD11b low fraction was gated from all viable cells in the spleen and the MZM population revealed in the CD11b low and SIGN-R1$^+$ fraction. Top panels are media treated control and pHrodo treated sample of one representative young mouse and bottom panels are media treated control and pHrodo treated sample of one representative old mouse.

**Summary of the functional studies on MZM (part I)**

From the initial series of experiments, confocal microscopy revealed that less dextran-FITC was bound in the MZM tissue compartments of old mice when compared to young mice. Yet, it remains to be clarified if the presence of less dextran-FITC on MZM is a result of fewer MZM present in the old tissue or the result of an alteration in MZM function with age. Flow cytometry studies attempted to quantify the percentages of dextran$^{+}$ MZM of young and old mice but proved to be limiting with the current instrument filters. Phagocytic differences of young and old MZM using flow cytometry was attempted using pHrodo bioparticles, but this also proved to have limitations. This time, the fluorescence of pHrodo was clearly higher than the control background, but whether the pHrodo$^{+}$ phagocytic cells were exclusively MZM was unclear. The next series of experiments built on the positives gained from these initial experiments to directly determine whether MZM from old mice differ in function when compared to young mice.

**Measuring the phagocytic differences of MZM from young and old mice using live cell confocal microscopy**

To quantify and visualize the phagocytosis of pHrodo by MZM, MZM treated with pHrodo were examined by confocal microscopy. MZM make up 1-2% of total splenocytes and to target this rare population of macrophages for functional analysis can be difficult. Immunocytochemistry showed that MZM bind dextran-FITC *in vivo* in both young and old mice (Fig. 26). Therefore, I next sought to determine if I would be able to

use this experimental approach to mark MZM and distinguish these cells via confocal microcopy in culture. Studies done in the last section also established the *in vitro* culturing and treatment of pHrodo on adherent splenocytes. Once adhered in culture, dextran$^+$ MZM can be co-cultured with pHrodo and the dextran$^+$pHrodo$^+$ MZM can be visually identified by Leica TCS SP5 confocal microscopy (Fig. 33). The Leica TCS SP5 confocal microscope, like the flow cytometer, uses lasers to excite fluorophores; however, the Leica TCS SP5 uses a prism to separate the fluorophore emission. This use of a prism generates a single peak of intensity that is only seen by the flow cytometer through the use of precise optical filters. Therefore, using the Leica TCS SP5 confocal microscope the FITC fluorophore can be differentiated from the natural autofluoresence of the MZM. The phagocytosis of pHrodo (and in turn dextran) can be quantified on a per cell basis using image analysis.

Briefly, results by confocal microscopy revealed fields of dextran$^+$cells, pHrodo$^+$cells, and a small fraction of dextran$^+$pHrodo$^+$ MZM observed by confocal microscopy. Each image taken of these fields targeted the dextran$^+$pHrodo$^+$ MZM (due to the small frequency of MZM present in culture) while including the single positive dextran and pHrodo cells. The pHrodo$^+$ cells showed numerous pHrodo$^+$ phagocytic compartments within each cell – confirming visually that pHrodo was being efficiently phagocytized. A phagocytic compartment is defined as any one compartment of the endocytic pathway: early endosome, late endosome, or the lysosome. Since pHrodo starts

to emit fluorescence at a pH of 6 it is difficult to discern the different compartments of the endocytic pathway.

By image analysis the mean fluorescence intensity (MFI) of the pHrodo$^+$ phagocytic compartments and the dextran-FITC captured by MZM were assessed per cell to determine any differences in phagocytic function between young and old MZM. In addition, the numbers of pHrodo$^+$ phagocytic compartments/cell-image were compared between age groups. Image analysis was also used to determine differences in size of adherent MZM. Finally, the imaged fields were analyzed for the frequency of pHrodo$^+$ cells of the total dextran$^+$ MZM.

**Establishment of the concentration and time of the *in vitro* pHrodo treatment of dextran marked MZM**

In order to view dextran$^+$pHrodo$^+$ MZM live by confocal, the correct concentration and time of pHrodo incubation needed to be determined. Splenocytes obtained from dextran-FITC injected mice were harvested and allowed to adhere onto 4-well chamber slides. The surface area of the chamber slides was significantly smaller than the area of 35 mm culture plates used previously for adherence in the flow cytometry analysis. Therefore, a series of titrations were performed and plating 4 x $10^6$ splenocytes/well (non-adherent cells were removed to yield approximately 400,000 adherent splenocytes) with 100 µg of pHrodo was determined to be optimal for visualizing individual pHrodo$^+$ cells by confocal microscopy. Low numbers

(approximately 100,000/well) of adherent splenocytes took longer to identify dextran$^{+}$pHrodo$^{+}$ MZM and high numbers (approximately 600,000/well) of adherent splenocytes over saturated the chamber. In addition, pHrodo was examined after incubation at 1hr, 1.5 hr, 2 hr, and 3 hr. The 1.5 hr time point was sufficient to observe phagocytic compartments in individual MZM by confocal microscopy and still detect dextran associated with the MZM. It was found that if tissue processing took more than 6 hr, dextran was no longer observed within MZM (data not shown). To assure effective dextran injections, half the spleens removed 45 min post dextran injection were saved for sectioning to once again reveal positioning of dextran to the MZ.

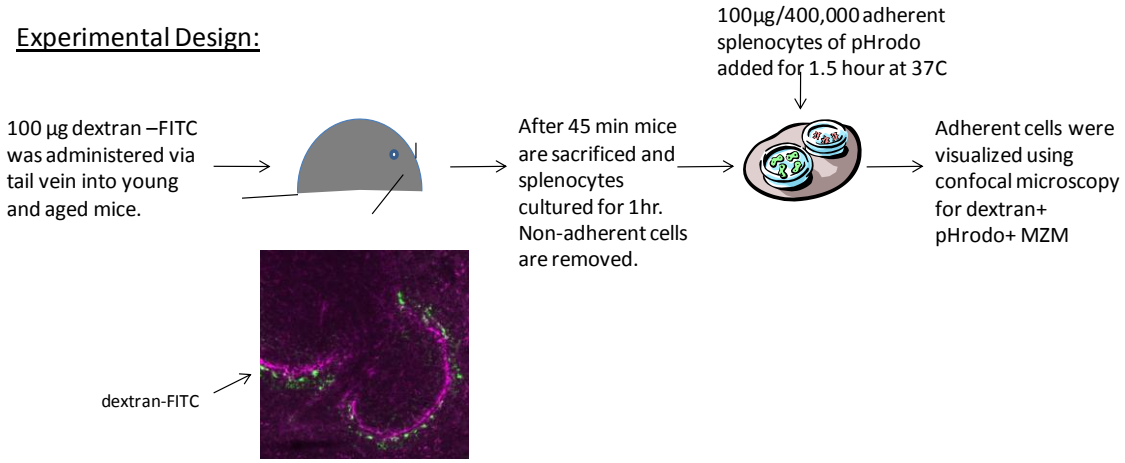


**Figure 33. Experimental paradigm of pHrodo treatment of dextran-FITC marked MZM.** Young and old BALB/c mice were injected with 100 µg of dextran-FITC and sacrificed after 45 min. The spleens were removed and splenocytes dispersed and adhered onto 2 ml chamber wells for 1 hr. Non-adherent cells were removed and 100 µg of pHrodo was administered to approximately 400,000 adherent splenocytes for 1.5 hr. After 1.5 hr incubation with pHrodo, cells were visualized live via a Lecia TC5 SP5 confocal microscopy.

**Imaging pHrodo$^+$ dextran$^+$ MZM**

Once pHrodo$^+$ dextran$^+$ MZM were identified by confocal microscopy, a standardized regimen of imaging was captured for analysis using the Lecia TC5 SP5 confocal microscope. For each animal, approximately15 different pHrodo$^+$ dextran$^+$ MZM were identified and imaged. Images taken targeted the pHrodo$^+$ dextran$^+$ MZM, but also captured single dextran$^+$ and pHrodo$^+$ cells. The images captured of these cells were taken near the middle of the cell at a thickness of 1 micron. The MFI of dextran and pHrodo within each MZM was determined using ImageJ software. Gates were drawn around the perimeter of the MZM and the MFI measured and recorded.

To confirm that images taken near the middle of the cell at 1 micron in thickness give an accurate representation of pHrodo within the MZM, a series of z-stack measurements were done. Z-stack measurements are taken by going through a cell slice by slice from top to bottom. Approximately 34 slices are imaged at 1 micron in thickness (an adherent macrophage is approximately 8 microns in thickness; therefore there is some overlap within the corresponding z-stack sections imaged). For each animal, 2 separate z-stack measurements were done and the MFI of each of the 34 slices was obtained. The average value of the 34 slices imaged was compared to the MFI obtained by taking an image near the middle of the cell. Results show that the values were nearly identical (Table VII); therefore, imaging MZM near the middle of the cell at 1 micron in thickness gave an accurate representation of the live cell. In addition, images of MZM were captured at 1, 2, 3, 4, and 5 microns in thickness by opening up the pinhole of the

microscope. Opening the pinhole of the microscope draws in more light allowing greater depth of capture of the image. However, imaging the MZM at increasing thicknesses resulted in decreased resolution and contrast of the cell; therefore, a thickness of 1 micron was optimal for imaging live MZM.

**Table 8. Avg Z-stack vs standard image of MFI of pHrodo$^{+}$ phagocytic compartments/MZM**

| Animal | Z-Stack Avg | Standard Image |
|---|---|---|
| Y-419 | 268 | 230 |
| Y-420 | 104 | 109 |
| Y-422 | 560 | 592 |
| O-421 | 135 | 158 |
| O-423 | 522 | 592 |

**Table 8.** Values represent the MFI obtained from either the average of 34 images (Z-stack) or the MFI obtained when the image is taken near the middle of the cell. Shown are values obtained from 2 separate experiments.

**pHrodo phagocytic compartments over time**

Each MZM imaged contained numerous pHrodo phagocytic compartments at various stages in the endocytic pathway. To determine if there were drastic changes in the quantity of phagocytic compartments and the MFI over time, two separate time lapse experiments for 60 and 120 minute time points (time 0 = pHrodo administration) were conducted (Fig. 34). Images were taken once every minute for a total of 60 images (for the 60 minute time lapse) and once every 2 minutes for a total of 60 images (for the 120 minute time lapse). Results show for both the 60 and 120 minute time lapse experiments there is an initial peak 10 min post pHrodo administration in pHrodo fluorescence within the MZM before the MFI starts to gradually decline with time.

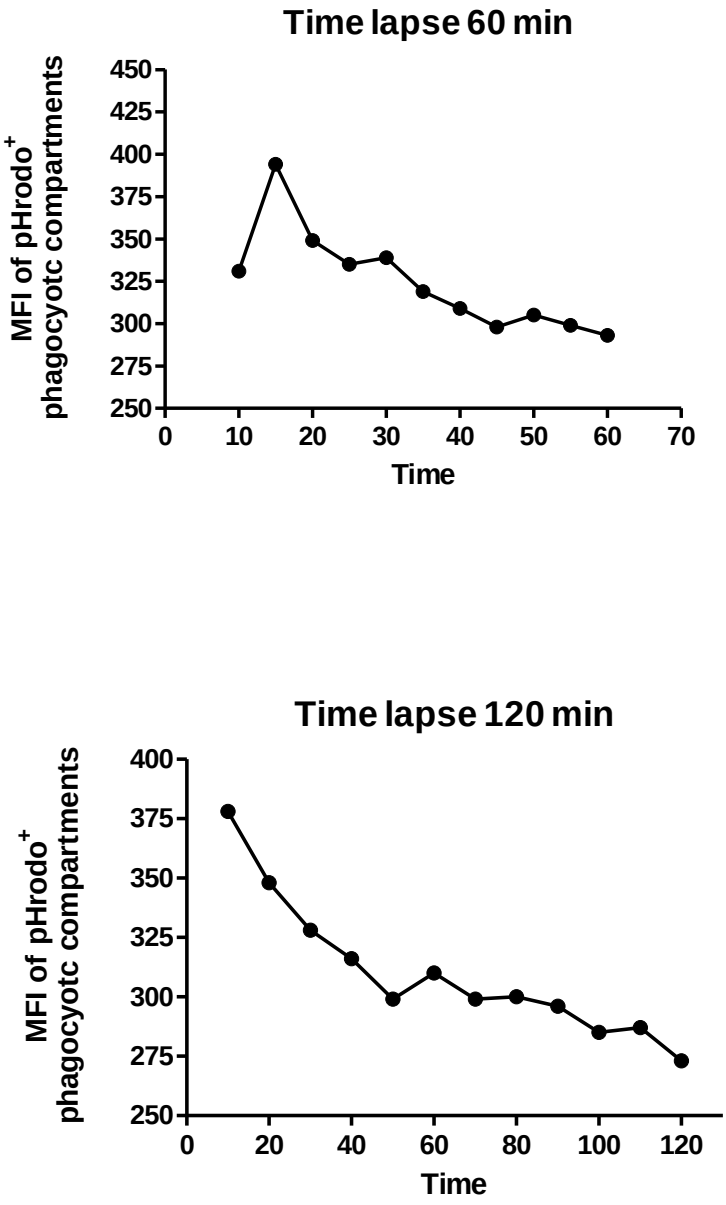


**Figure 34. The MFI of pHrodo$^+$ phagocytic compartments over time.** Top graph shows the range in MFI of pHrodo$^+$ phagocytic compartments in a MZM over 60 minutes. Bottom graph shows the range in MFI in a MZM over 120 minutes. Each symbol represents an image taken every 5 minutes for the 60 minute time lapse experiment and every 10 minutes for the 120 minute time lapse experiment.

**Quantification of pHrodo in dextran$^+$ MZM**

Results obtained from confocal microscopy revealed numerous pHrodo$^+$ phagocytic compartments within MZM (Fig. 35). To determine differences in the phagocytosis of pHrodo between MZM from young and old mice, dextran$^+$ pHrodo$^+$ MZM were first distinguished from dextran only and pHrodo only single positive cells. The MFI of pHrodo from the double positive MZM was then determined. The MFI was taken to reflect the amount of pHrodo phagocytized. Results showed that the MZM from old mice had no differences in the amount of pHrodo phagocytized when compared to MZM from young mice (Fig. 36B) ($n = 10$ young and $n = 9$ old, $p = 0.2689$). To rule out differences in size of adherent MZM in young versus old affecting the data obtained for MFI, the area of the MZM from young and old were also determined and found not to be significantly different between age groups (Fig. 36C) ($n = 10$ young and $n = 9$ old, $p = 0.1317$). Individual phagocytic compartments were also counted in young and old MZM. Data show that there were also no differences in the number of phagocytic compartments between age groups (Fig. 36E) ($n = 8$ young and $n = 7$ old, $p = 0.5989$).

Notably, after imaging numerous pHrodo$^+$dextran$^+$ MZM (15/animal) from both young and old adherent splenocytes that only a fraction of the imaged adherent cells from old mice met the criteria for evaluation of phagocytosis by MZM (macrophage in morphology, dextran$^+$ and pHrodo$^+$) when compared to adherent MZM from young mice. The young mice had roughly 40% more pHrodo$^+$ dextran$^+$ MZM present in culture

compared to old mice. These results are consistent previous findings that the frequency/number of MZM decline with age (Fig. 10; Table III).

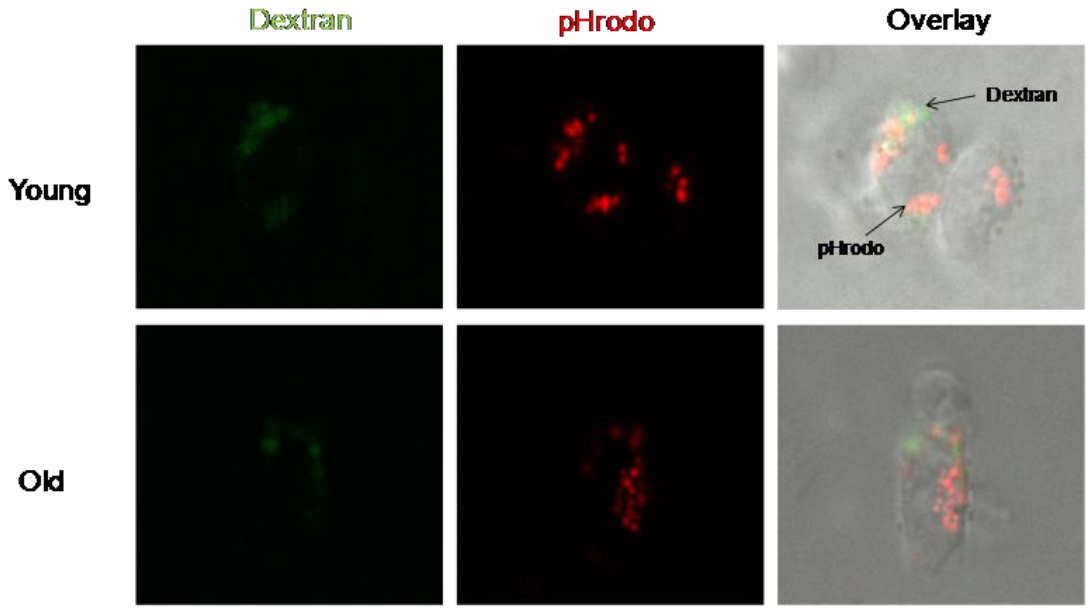


**Figure 35. Comparison of the phagocytosis of MZM isolated from old and young mice.** Confocal images of live adherent MZM administered pHrodo for 1.5 hr after harvested from young and old mice administered dextran-FITC (green) intravenously. Photos show typical dextran$^+$ pHrodo$^+$ MZM taken live at 5000x magnification at cell thickness of 1 micron. Photos are representative of MZM isolated from 1 young of 10 (top panels) and 1 of 9 old (bottom panels). Dextran (green) only uptake can be visualized in the left panels, pHrodo only visualized in the middle panels, and an overlay of the dextran$^+$ pHrodo$^+$ MZM in the right panels.

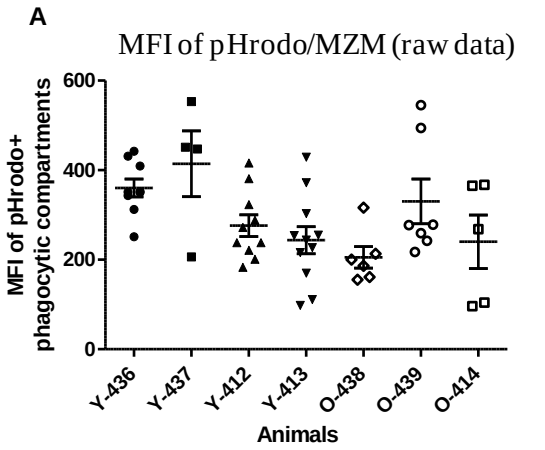
A
MFI of pHrodo/MZM (raw data)
MFI of pHrodo+ phagocytic compartments
600
400
200
0
Y-436
Y-437
Y-412
Y-413
O-438
O-439
O-414
Animals

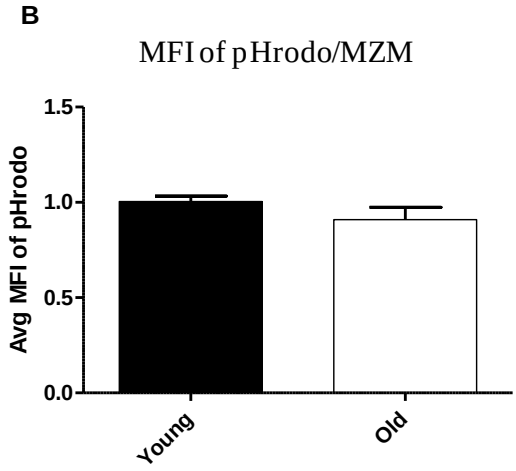
B
MFI of pHrodo/MZM
Avg MFI of pHrodo
1.5
1.0
0.5
0.0
Young
Old

C

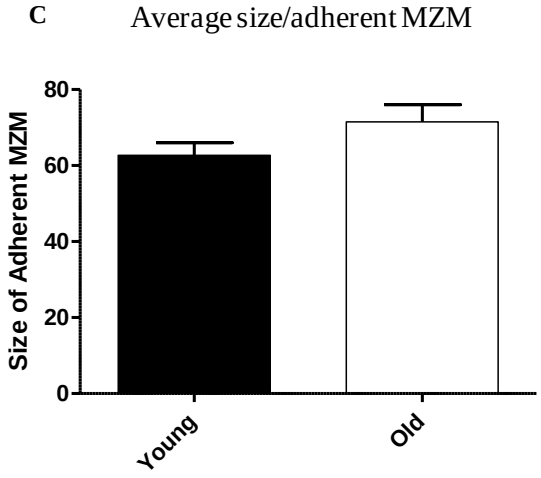
Average size/adherent MZM
Size of Adherent MZM
80
60
40
20
0
Young
Old

D

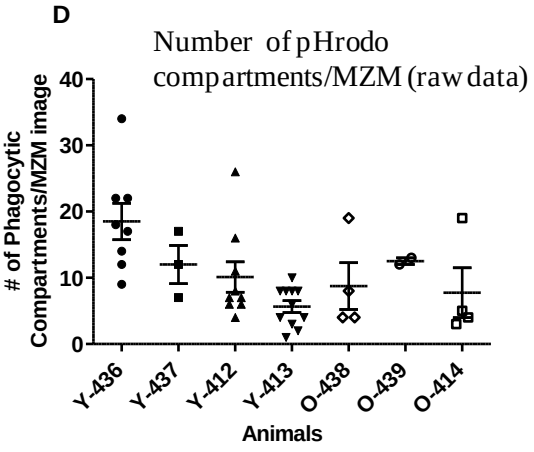
Number of pHrodo compartments/MZM (raw data)
# of Phagocytic Compartments/MZM image
40
30
20
10
0
Y-436
Y-437
Y-412
Y-413
O-438
O-439
O-414
Animals

E

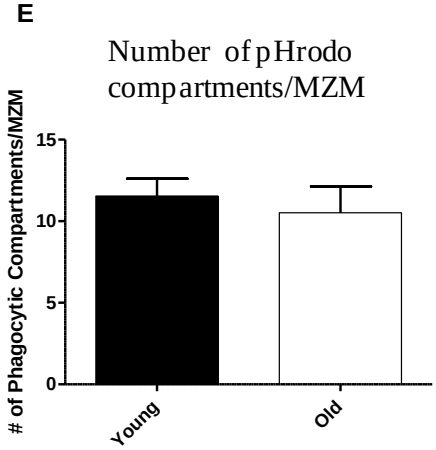
Number of pHrodo compartments/MZM
# of Phagocytic Compartments/MZM
15
10
5
0
Young
Old

**Figure 36. Quantification of pHrodo in dextran$^+$ MZM. (A) and (B)** Comparison of the MFI of pHrodo$^+$ phagocytized compartments by MZM from young and old mice. Using ImageJ software a perimeter was drawn around the area of each MZM analyzed and the MFI was determined for pHrodo (top graph depicts the raw data from 2 separate experiments). p = 0.2689, Mann Whitney test; n = 10 young mice (2-3 mo); n = 9 old mice (19-23 mo). **(C)** Comparison of the area of adherent MZM from young and old mice. p = 0.1317, Unpaired t-test; n = 10 young mice (2-3 mo); n = 9 old mice (19-23 mo). **(D) and (E)** Comparison of the number of phagocytic compartments in MZM from young and old mice (top graph depicts the raw data from 2 separate experiments). p = 0.5989, Unpaired t-test; n = 8 young mice (2-3 mo); n = 7 old mice (19-23 mo). All data in figures (B), (C), and (E) are expressed as mean ± SEM and are representative of six separate experiments.

**Percent pHrodo$^+$ of the dextran$^+$ MZM**

It is possible that the pHrodo$^+$ dextran$^+$ MZM of old mice that were evaluated were from a pool of functional MZM and that non-functional MZM were not imaged because of their inability to phagocytize pHrodo. To test this hypothesis, I determined the proportion of pHrodo$^+$ cells of the dextran$^+$ adherent MZM. As previously mentioned, 15 separate images of pHrodo$^+$dextran$^+$ MZM /animal were captured. Each of these images contained multiple cells that were both single positive for dextran and pHrodo or double positive for dextran and pHrodo (Fig. 37A). The ratios of pHrodo$^+$ cells: dextran$^+$ cells per image were determined and an average of all the images analyzed/animal was reported as a percentage. Results show that there were no differences in the percentage of pHrodo$^+$ cells within the dextran$^+$ MZM population in young and old (Fig. 37B) ($n = 9$ young and $n = 9$ old, $p = 0.9456$). From these results, I conclude that the pHrodo$^+$dextran$^+$ MZM evaluated for phagocytosis in old were from a pool of functional MZM and were a true representation of the old MZM population.

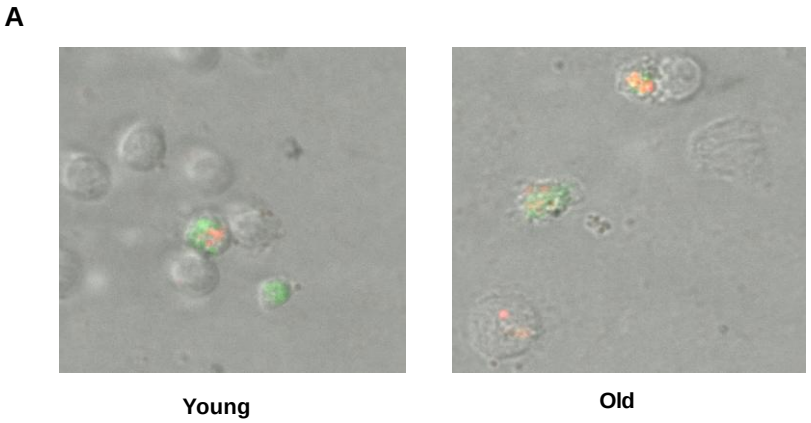


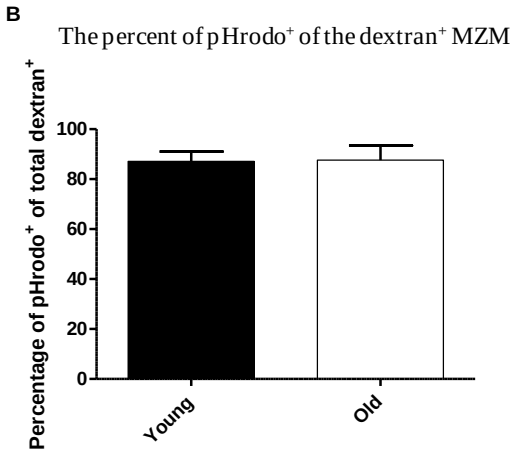


**Figure 37. The percentage of pHrodo$^+$ cells of the dextran$^+$ MZM. (A)** Confocal images taken live of young (left) and old (right) adherent splenocytes isolated from mice given i.v. delivery of dextran-FITC. Splenocytes were harvested and given100 µg pHrodo for 1.5 hr incubated at 37 C. Cells were imaged live at 5000x magnification at cell thickness of 1 micron. The total number of pHrodo$^+$ cells in a single image was quantified over the total number of dextran$^+$ MZM. **(B)** The ratio of pHrodo$^+$ cells: dextran$^+$ MZM/field determined and presented as a percentage. Results are expressed as mean ± SEM and are representative of six separate experiments n = 9 young mice (2-3 mo); n = 9 old mice (19-23 mo). No significant differences present between young and old mice. p = 0.9456, Unpaired t-test.

**Comparison of dextran-FITC phagocytized by MZM from young and old mice *in vivo* as revealed by confocal microscopy**

Tissue sections of spleens revealed that there was reduced dextran-FITC localized on the MZM of old mice when compared to young mice (Fig. 26) and prior data also revealed that there are decreases in the MZM pool with age. Perhaps the reason for reduced MZM capture of dextran-FITC in old mice is a result of less MZM present in old tissue and not a predictor of decreases in the phagocytic function of MZM with age. Initially, the percentage of dextran$^+$ MZM from young and old mice was quantified using flow cytometry techniques (Fig. 27). Results showed a high level of background in the control groups suggesting that the use of flow cytometry is limiting to determine differences in MZM function.

Although cellular fluorescence prevented an accurate assessment of the quantity of dextran bound by MZM by flow cytometry, dextran$^+$ MZM could be visualized live/cell at 5000x magnification under confocal microscopy without interference of background fluorescence. The MFI of dextran-FITC in young and old MZM was measured using confocal microscopy and image analysis. Images of pHrodo$^+$ dextran$^+$ MZM previously captured for measurement of pHrodo phagocytosis were again used to determine the differences in phagocytosis of dextran between young and old MZM. Prior data by Geijtenbeek *et al.* have reported that after initial dextran capture (observed in 45 min), MZM will phagocytosis dextran (17). Results showed that there were no differences in the phagocytosis of dextran by MZM between age groups (Fig. 38). This

data again shows that there are no functional differences between MZM from young and old mice.

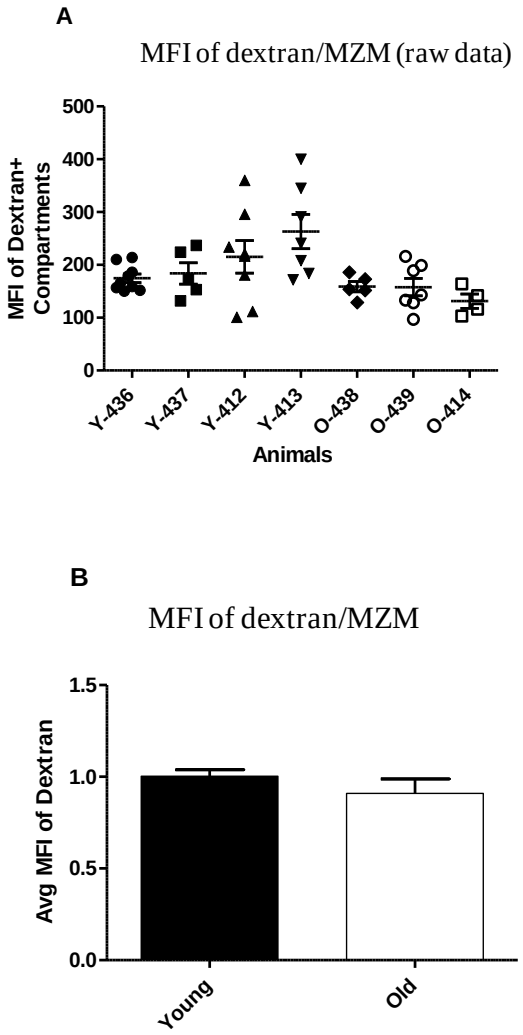


**Figure 38. Quantification of dextran-FITC in MZM from young and old mice as revealed by confocal microscopy.** Comparison of the MFI of dextran captured by MZM from young and old mice. Using ImageJ software areas was drawn around the perimeter of MZM and the MFI of dextran-FITC was determined. **(A)** Raw data gathered from two separate experiments. Each point corresponds to the MFI of dextran captured by MZM **(B)** Data are presented as a ratio of the sample MFI over the average MFI of young per experimental group. $p = 0.4256$, Mann Whitney test. Data are expressed as mean ± SEM and are representative of six separate experiments n = 9 young mice (2-3 mo); n = 9 old mice (19-23 mo).

**Summary of the functional studies on MZM**

In order to determine the functional differences of MZM of young and old mice these rare macrophages needed to be targeted. Currently there are no studies that have reported the ability to isolate MZM without severe manipulation to the cell. Here I have shown that MZM can be marked and its functional properties can be assessed. Initial studies presented aimed to determine functional differences by the capture of dextran-FITC upon i.v. injection. Results showed reduced dextran-FITC localized in MZM of tissue sections of old mice when compared to young mice. However, I was not able to quantify the amount of dextran-FITC capture. Using this experimental paradigm to mark MZM I was able to target MZM while preserving cell viability. Once MZM were targeted pHrodo was administered in order to determine differences in phagocytosis of MZM from young and old mice. Results revealed that there were no differences in phagocytosis between age groups. Therefore, the reduced dextran-FITC observed in tissue sections of old mice are a result of fewer MZM present in old mice and not a result of reduced cellular function.

# CHAPTER VII

# DISCUSSION

The MZ of the spleen is known to be the site where blood-borne antigens first enter the spleen at the porous MZ sinus. In this dissertation, the age-related changes in the overall architecture of the MZ compartment were described. Specific reductions in MZM and MZ B cells were observed. The MZ of young adult mice have a characteristic uniform dense appearance around the white pulp and follicles; in contrast, the MZ of old mice have a statistically significant cellular disruption when compared to young mice. Alterations to the MZ included 1) reduction in abundance of MZM with no differences in the phagocytic function of MZM, 2) a reduction in the frequency of MZ B cells that correlated with the reductions observed with MZM, and 3) unusual staining patterns for MAdCAM-1 sinus lining cells and MMM that may indicate positional changes. Collectively, work from this dissertation showed that with advanced age there is a gross anatomical breakdown of the MZ with decreases particularly striking in the MZM and MZ B cell populations. Therefore, if the spleen architecture in humans suffers a similar decline with advanced age, one consequence may be less efficient clearing and response to bacteria, as has been reported in splenectomized and asplenic patients (112).

In humans, the MZ of the spleen is a clearly defined zone that is divided into outer and inner parts by fibroblasts that are MAdCAM-$1^{+}$ (112, 113). The MZ sinus is

not present as a component of the human MZ and lymphocytes and antigens enter the spleen via the splenic open circulation into the outer MZ area. This outer MZ area is referred to as the perifollicular zone. The perifollicular zone of the human spleen contains MZ B cells and sialoadhesin-positive macrophages, postulated to be the "human equivalent" of MMM and MZM (113). Although differences in microanatomy are present within the rodent and human splenic MZ areas, the human spleen is also important in the immune response to infection with *S. pneumoniae* and its importance can best be seen in epidemiological reports of splenectomized patients. A study showed a 5% lifetime risk of "overwhelming infection syndrome" in these patients, which is lethal in almost 50% (114). Studies have shown that when sepsis occurred in postsplenectomized patients, in 80-90% of reported cases it resulted due to infection with *S. pneumoniae* (115). *S. pneumoniae* are gram-positive bacteria that have a cell wall whose degradation is achieved through phagocytosis (116). Antibody and complement coated *S. pneumoniae* are believed to filter to the human spleen for removal. The phagocytes present in the human splenic MZ are the sialoadhesin-positive macrophages; therefore, future studies can examine these cells to determine if they are the primary phagocytes involved in the removal of *S. pneumoniae*.

Functional abnormalities of the human spleen have been reported in the elderly population. A condition termed hyposplenism in which the spleen has reduced function has been reported in the elderly and in newborn infants (117). Patients with hyposplenism have a reported increased mortality rate as a result of pneumococcal sepsis

(118). Studies have also shown that vaccines that utilize T cell dependent mechanisms are more effective in the prevention of pneumococcal disease in hyposplenic and asplenic patients. Therefore, I believe that the elderly population would too benefit from T cell dependent vaccines.

**Alteration in the structure of the splenic marginal zone**

At the MZ region of the spleen there is continuous migration of lymphocytes, self antigens, and blood borne pathogens (7, 30, 82). The MZ can be seen as a major intersection for the homing of lymphocytes to their respective zones and the sorting station for TI and TD pathogens. Therefore, the positioning of the cellular components that make up this MZ region can be seen as critical in its maintenance. The structure of the MZ is highly ordered in young mice, with definitive boundaries at the white pulp and red pulp regions. Examination of H&E tissue sections of young spleens revealed MZ regions with minimal interface distortion and percent radius involvement. However, the MZ regions of old mice were significantly more disrupted with a high degree of variability. In many old mice, the interface distortion and percent radius involvement was severe; however, in ~20 % of old mice the MZ regions appeared young-like in morphology. What factors could contribute to this young-like morphology, given that these old mice are inbred? An environmental stimulus is one answer. The mice in my studies were housed 4 to a cage, and it is possible that natural dominance leads to chronic stress contributing to the rapid aging of the submissive mice. Studies have shown that chronic social defeat as a result of exposure to an aggressor mouse each day for 10 min

for a total of 10 days leads to chronic stress (119). Chronic stress has been shown to be accompanied by chromatin remodeling of the brain-derived neurotrophic factor gene (BDNF), which has been shown to be important for the hippocampus to deal with stress (120, 121). It may be possible that chronic social defeat may also contribute to damage of immune system cells. The alteration in the morphology of the MZ in old mice appeared to be due to an alteration of the cellular components that make up this zone. The next sections will go through the cells that exhibited an alteration in age.

**Decreases in marginal zone macrophages in old mice**

Decreases in MZM in old mice were seen both semi-qualitatively (in tissue sections) and quantitatively (via flow cytometry). An age related decrease in MZM may have consequences on the immunity of aged individuals. For example, pneumonia caused by *S. pneumoniae* is one of the leading causes of mortality in advanced age (2, 3). SIGN-R1 [the murine homologue of human DC-SIGN (16)] on MZM binds the capsular polysaccharide of *S. pneumoniae* (19, 20). It is possible that a decrease in the SIGN-R1$^{+}$ MZM pool may allow for increased susceptibility to *S. pneumoniae* reported in the elderly. Very little is known about the homeostasis of the MZM compartment. Three possible mechanisms may contribute to the reductions in MZM with advanced age include: decreased MZ B cells, decreased chemotactic factors important for MZM homing to the MZ, or decreased MZM turnover.

Evidence supports the first mechanism since decreases in MZ B cells in old mice, when present, correlate with decreases in MZM (Fig. 14). In addition, a report by Kraal *et al.* observed that recovery of MZM correlated with full restoration of the B cell population in the MZ of mice after *in vivo* liposome treatment that led to depletion of all splenic macrophages and most MZ B cells (39). Furthermore, it is important to point out that although there was a significant decrease in MZM in old mice when compared to young mice, there were approximately ~20% of old mice that had young like MZM distributions in tissue and as revealed by flow cytometry. Data that revealed a correlation between MZM and MZ B cells also showed that there are three separate groups of MZM and MZ B correlates: one group having poor amounts of both cells, a second group having moderate amounts of both cells, and a third group having good/young-like amounts of MZM and MZ B cells. This separation is particularly meaningfully because perhaps it reflects a gradual loss of the "young-like" phenotype in old mice. It is possible that at some point all mice will have a loss of both cell populations. Nolte *et al.* reported that overexpression of CD70 (a TNF family member) specifically in B cells led to a gradual loss of the splenic B cell pool with a subsequent gradual loss of MZM (40). In advanced age, this same phenomenon of a gradual loss may occur and is represented by the moderate group seen here.

It is reasonable to propose that decreases in MZM with age can be influenced by chemotactic factors important for MZM homing to the MZ. The chemokine CCL21 (protein) (Fig. 19A) was found in lesser amounts in the PALS region of old mice when

compared to young mice. In addition, I determined that there was no co-localization of CCL21 with MZM, rather CCL21 when present was localized outside the MZ, as revealed by confocal microscopy (Fig. 20B). Preliminary observations also showed that in some mice that have poor levels of $MARCO^{+}$ MZM also have an abundance of CCL21 proteins in splenic tissue (Fig. 20C). It may be possible that in these mice there is an over production of CCL21 in order to attract precursor MZM (if present) to the MZ to refill the reduced MZM population. Whether this loss is due to the inability of newly made MZM to home to the MZ or a result of loss of the resident MZM remains to be clear. It has yet to be established if MZM are continuously made throughout the lifetime of the animal or if the MZM observed 10 days post birth are maintained throughout a lifetime. If the former is true, then MZM are continuously made every few days, weeks, or months. It is possible in this scenario that the MZM of old mice may have a slower turnover. Kraal *et al.* showed that new MZM will replenish a macrophage-depleted young spleen by 30 days, implying that MZM precursors exist in young animals (39). Therefore, it is possible that with advancement in age there is a decrease in MZM replenishment and/or precursors that is responsible for the age related decrease in MZM.

**Decreases in marginal zone B cells in old mice**

The decrease in MZ B cell frequency in old mice is puzzling because an age-related increase toward maintenance of existing MZ B cells has been predicted by Allman and Miller (67). Moreover, certain conditions in old mice are more aligned with MZ B cell development than follicular (FO) B cell development, such as low levels of

E2A and IL-7 [reviewed in (11, 67, 68, 122) (69, 70, 75-77)]. A shift towards expanded MZ B cell differentiation at the expense of FO B cell production was age is an attractive hypothesis, and as previously mentioned in the background section of this dissertation, increases in MZ B cell numbers were reported by one group using aged B10.D2 mice (78). Furthermore, it may be possible that MZ B cells are being produced at expanded levels in age; however, because of the collapse in the MZ micro-architecture in age, the newly formed MZ B cells may not home effectively to the aged MZ compartment. Adoptive transfer experiments presented in this dissertation (Chapter five) showed that donor MZ B cells from young mice had a decreased ability to home to spleens of old mice when compared to young mice. Moreover, when other lymphoid organs were examined a MZ B cell phenotype was observed in both the lymph nodes and bone marrow of a very few old mice (Table V). Experiments by Cariappa *et al.* have shown a subset of recirculating mature B cells in the bone marrow able to respond to TI antigens (123). It may be possible that these recirculating B cells that were identified were in fact MZ B cells that were displaced to the bone marrow. Data from adoptive transfer experiment suggests that the microenvironment of old mice is altered preventing homing of MZ B cells. Another consideration is suggested by recent studies that have shown that MZ B cells are lost during chronic inflammation (124, 125). Traggiai *et al.* report changes in B-lineage subpopulations that appear similar to those reported in old mice (88, 89, 124). Chronic inflammation has been viewed by many investigators as part of immunosenescence [reviewed in (98, 101)], raising the possibility that increased

inflammation with age promotes gradual loss of MZ B cells, and perhaps, subsequent decline of MZM. Lastly, it may also be that donor MZ B cells were not able to home to the spleens of old mice because of the decreases in the MZM pool with age.

Yet, there are other factors important for the maintenance of MZ B cells to the MZ. Reports by Cinamon *et al.* have demonstrated that $S1P_1$ is needed for MZ B cells to maintain localization in the MZ (64, 65), and reduction in receptor expression causes MZ B cells to leave the MZ and move into the follicle in a CXCL13-dependent manner. If decreases in S1P or its receptors are present in spleens of old mice, a displacement of MZ B cells would be expected, perhaps not only to the follicular area, since CXCL13 expression has been shown to be disrupted with age (27), but near the $MAdCAM1^+$ sinus lining cells at the boundary of the MZ and white pulp interface where CXCL13 is localized with age. Furthermore, recent work has shown that B cells from SHEP1-deficient mice have a reduction in mature MZ B cells and fail to migrate towards CXCL13 and S1P (126). Therefore, it may also be possible that there is an alteration in the SHEP1 with age. SHEP1 is an adaptor molecule shown to partner with the scaffolding protein CasL (important for integrin activation), which leads to the phosphorylation of the serine/threonine of CasL allowing for MZ B cell retainment to the MZ.

**The marginal zone sinus and metallophilic macrophages in old mice**

The marginal zones in old mice also showed alterations in the MAdCAM-$1^+$ MZ sinus lining cells, which are part of the reticular family of cells (127, 128). Moreover, these cells act as a "polarized" barrier to overt penetration of antigen from the MZ sinus into the follicles; whereas, antigen readily moves from the sinus outward toward the MZM and MZ B cell layer (64, 129). Results showed that the expression of MAdCAM-1 was diffused into the white pulp and less organized in old mice when compared to young mice, and MMM were found to be similarly disrupted in old when compared to young spleens. Changes in the morphology of MAdCAM-$1^+$ and MMM compartments appeared consistently disrupted in the majority of spleens from old mice. Strikingly similar morphological disruptions in the MAdCAM-$1^+$ sinus lining cells and MMM were observed by Girkontaite *et al.* in sphingosine-1-phosphate receptor 3 ($S1P_3$) deficient mice (84). $S1P_3$ is necessary for the positioning of MAdCAM-$1^+$ sinus lining cells and MMM along the continuity of the MZ sinus (84). It is possible that in old mice there is a downregulation of $S1P_3$, which is responsible for the morphological disruptions of the MZ sinus and MMM. Furthermore, in the MZ compartment, $S1P_1$ and $S1P_3$ are highly expressed on MZ B cells and FO B cells (65). Therefore, it is possible that S1P and/or its receptors provide a link between reduced MZM/MZ B cells and dispositioning of MAdCAM-$1^+$ cells/MMM (Fig. 8). S1P has also been implicated in the induction of proteins found in junctional complexes, and at least one receptor ($S1P_1$) was found on the surface of reticular stromal cells, as well as endothelial cells, in lymph nodes (130).

Recently, Katakai *et al.* provided evidence that the MAdCAM-1$^+$ sinus lining cells derive from a type of reticular stromal cell that requires constant LTβR stimulation for survival and production of CXCL13 (128). These observations, along with the previous finding that MZ sinus lining cells of aged spleens had less CXCL13 (27) could indicate a problem in LTβR stimulation. It is also possible that either S1P and its receptors or LT/LTβR provide a link between reduced MZM/MZ B cells and dispositioning of MAdCAM-1$^+$ cells.

**No difference in marginal zone macrophage function in old mice**

To determine whether reduced MZM affected antigen clearance in the MZ, fluorescently labeled polysaccharide dextran that is known to bind SIGN-R1 (17, 18), was administered via tail vein into both young and old mice. Less bound dextran in the MZ of old mice was found when compared to young mice as revealed by confocal microscopy (Chapter VI). Less bound dextran in old tissue sections could be a result of fewer MZM available to bind blood-borne dextran. To answer this question, an approach was needed to specifically identify MZM in order to measure functional differences in age. MZM comprise 1-2% of the total splenic population and prior studies have had limited success in isolating these cells for functional analysis *ex vivo*. Using a novel approach, I was able to target MZM of young and old mice and administer pHrodo to measure differences in phagocytosis of live cells using a Leica TCS SP5 confocal microscope. Results showed that the phagocytic function of individual MZM was not different between young and old mice, suggesting that it is this loss in the MZM

population with age that contributes to the reduction in pathogen clearance reported in the elderly.

**Chronic inflammation in age**

It is believed that in aging there is a low level of chronic inflammation as a result of underlying disease a phenomenon termed “Inflam-aging” (101). It is believed that chronic inflammation produces a heightened proinflammatory state. “Inflam-aging” is characterized by a decrease in adaptive immunity and an increase in innate immunity. It has been suggested that cells of the mononuclear phagocyte cell lineage are responsible for the increase production of proinflammatory cytokines in age. Recently, Di Paolo *et al.* showed that macrophages in the MZ trapped blood-borne adenovirus and rapidly produced an IL-1α dependent pro-inflammatory response (131). It is conceivable that a lifetime of repeated exposure and uptake of viruses and bacteria causes repeated production of pro-inflammatory cytokines and chemokines, leading to overall damage to the microenvironment and decrease in immune cells (Fig. 39). Yet, whether a hyper-proinflammatory state or repeated exposure to viruses and bacteria can lead to a hindrance in normal cell frequencies and function still remains to be elucidated for immune cells.

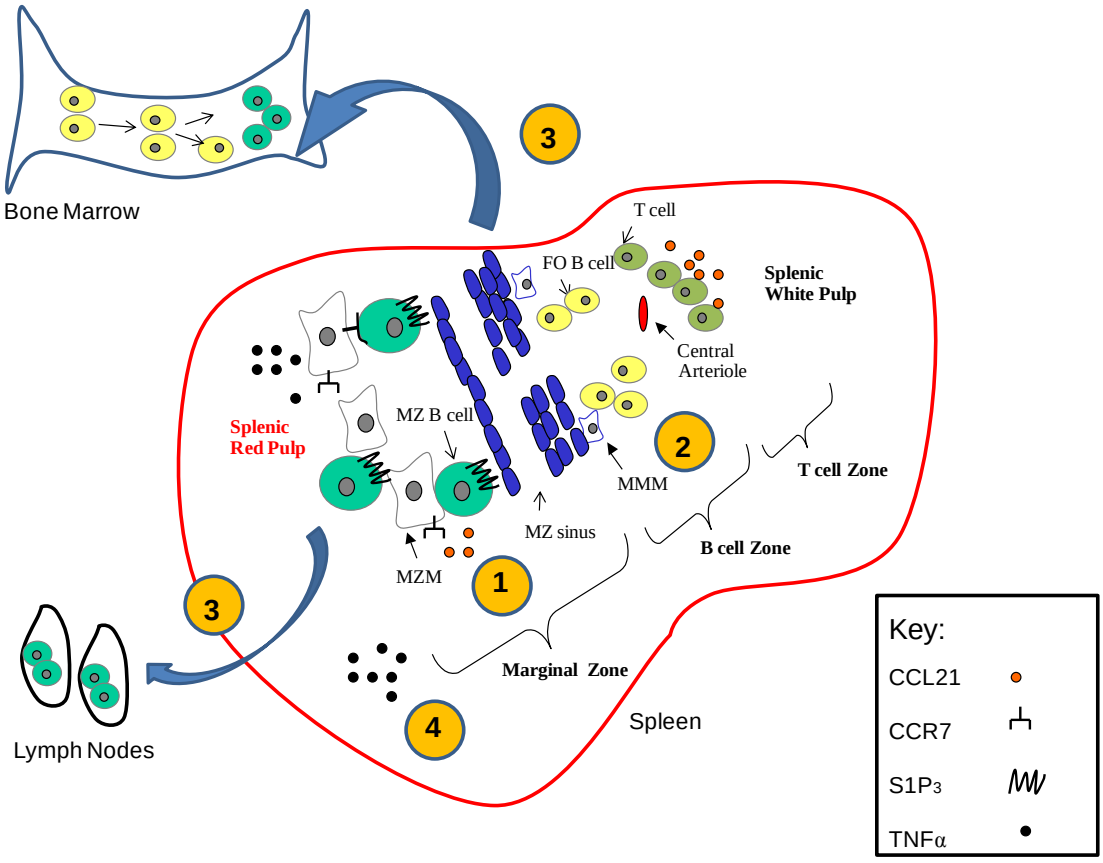


**Figure 39. Model of the Microenvironmental alterations of the Splenic Marginal Zone.** Factors that may contribute to decreases in the cellular components of the MZ. **(1)** There is a correlation between decreases in MZM and MZ B cells in old mice. Decreases in MZM can be a result of decreases in MZ B cells. Furthermore, it may be possible that the chemokine CCL21 is over produced in the spleens of old mice to home precursor MZM to MZ that have a reduction in MZM. On the contrary, decreases in MZ B cells may be due to decreases in MZM or downregulation of $S1P_3$. **(2)** $MAdCAM1^+$ MZ sinus lining cells are observed in multiple cell layers and MMM are not continuous with the MZ sinus. This alteration may also be due to a reduction in $S1P_3$. **(3)** MZ B cells may also exit the spleen and home to the bone marrow or the lymph nodes. **(4)** It is also possible that as a result of "Inflam-aging" there is an over production of proinflammatory cytokines such as TNFα leading to damage and loss of the MZ cells.

**Significance**

Understanding the alterations that occur with age in lymphoid tissues such as the spleen is important for developing more efficient therapies for the prevention of diseases such as bacterial pneumonia that have shown to be highly detrimental in the elderly (2). The cells that contribute to framework of the MZ of the spleen are largely responsible for initiating an effective immune response to the vaccine components for the prevention of *S. pneumoniae* and other TI antigens. The goal of this study was to determine if there were age-related changes in the cellular components of the MZ in old versus young mice. Results show changes throughout the components of the MZ, including the: MZ sinus lining cells, MMM, MZM, and MZ B cells. Furthermore, reductions in MZM in individual old mice correlated with reductions in MZ B cell populations with some of the old mice exhibiting young-like MZM and MZ B cell phenotypes. Future studies can examine old mice in order to determine what attributes to these young-like phenotypes, and perhaps insights gained from these studies can pave the way for a modern day fountain-of-youth. In terms of vaccine efficacy, vaccines can target the deficient MZM and MZ B cell populations in aging individuals to heighten the immune response against the TI components that constitute current vaccines.

## REFERENCES


1. Bureau, U. S. C. 2010. USA Quickfacts. In

2. Artz, A. S., W. B. Ershler, and D. L. Longo. 2003. Pneumococcal vaccination and revaccination of older adults. *Clin Microbiol Rev* 16:308-318.

3. van der Poll, T., and S. M. Opal. 2009. Pathogenesis, treatment, and prevention of pneumococcal pneumonia. *Lancet* 374:1543-1556.

4. Bondada, S., H. Wu, D. A. Robertson, and R. L. Chelvarajan. 2000. Accessory cell defect in unresponsiveness of neonates and aged to polysaccharide vaccines. *Vaccine* 19:557-565.

5. Butler, J. C., E. D. Shapiro, and G. M. Carlone. 1999. Pneumococcal vaccines: history, current status, and future directions. *Am J Med* 107:69S-76S.

6. Kirby, A. C., L. Beattie, A. Maroof, N. van Rooijen, and P. M. Kaye. 2009. SIGNR1-negative red pulp macrophages protect against acute streptococcal sepsis after Leishmania donovani-induced loss of marginal zone macrophages. *Am J Pathol* 175:1107-1115.

7. Kraal, G., and R. Mebius. 2006. New insights into the cell biology of the marginal zone of the spleen. *Int Rev Cytol* 250:175-215.

8. Mebius, R. E., M. A. Nolte, and G. Kraal. 2004. Development and function of the splenic marginal zone. *Crit Rev Immunol* 24:449-464.

9 Dijkstra, C. D., E. Van Vliet, E. A. Dopp, A. A. van der Lelij, and G. Kraal. 1985. Marginal zone macrophages identified by a monoclonal antibody: characterization of immuno- and enzyme-histochemical properties and functional capacities. *Immunology* 55:23-30.

10. Gunn, K. E., and J. W. Brewer. 2006. Evidence that marginal zone B cells possess an enhanced secretory apparatus and exhibit superior secretory activity. *J Immunol* 177:3791-3798.

11. Allman, D., and S. Pillai. 2008. Peripheral B cell subsets. *Curr Opin Immunol* 20:149-157.

12. Vos, Q., A. Lees, Z. Q. Wu, C. M. Snapper, and J. J. Mond. 2000. B-cell activation by T-cell-independent type 2 antigens as an integral part of the humoral immune response to pathogenic microorganisms. *Immunol Rev* 176:154-170.

13. Chelvarajan, R. L., S. M. Collins, J. M. Van Willigen, and S. Bondada. 2005. The unresponsiveness of aged mice to polysaccharide antigens is a result of a defect in macrophage function. *J Leukoc Biol* 77:503-512.

14. Elomaa, O., M. Kangas, C. Sahlberg, J. Tuukkanen, R. Sormunen, A. Liakka, I. Thesleff, G. Kraal, and K. Tryggvason. 1995. Cloning of a novel bacteria-binding receptor structurally related to scavenger receptors and expressed in a subset of macrophages. *Cell* 80:603-609.

15. Karlsson, M. C., R. Guinamard, S. Bolland, M. Sankala, R. M. Steinman, and J. V. Ravetch. 2003. Macrophages control the retention and trafficking of B lymphocytes in the splenic marginal zone. *J Exp Med* 198:333-340.

16. Koppel, E. A., E. Saeland, D. J. de Cooker, Y. van Kooyk, and T. B. Geijtenbeek. 2005. DC-SIGN specifically recognizes Streptococcus pneumoniae serotypes 3 and 14. *Immunobiology* 210:203-210.

17. Geijtenbeek, T. B., P. C. Groot, M. A. Nolte, S. J. van Vliet, S. T. Gangaram-Panday, G. C. van Duijnhoven, G. Kraal, A. J. van Oosterhout, and Y. van Kooyk. 2002. Marginal zone macrophages express a murine homologue of DC-SIGN that captures blood-borne antigens in vivo. *Blood* 100:2908-2916.

18. Kang, Y. S., S. Yamazaki, T. Iyoda, M. Pack, S. A. Bruening, J. Y. Kim, K. Takahara, K. Inaba, R. M. Steinman, and C. G. Park. 2003. SIGN-R1, a novel C-type lectin expressed by marginal zone macrophages in spleen, mediates uptake of the polysaccharide dextran. *Int Immunol* 15:177-186.

19. Kang, Y. S., J. Y. Kim, S. A. Bruening, M. Pack, A. Charalambous, A. Pritsker, T. M. Moran, J. M. Loeffler, R. M. Steinman, and C. G. Park. 2004. The C-type lectin SIGN-R1 mediates uptake of the capsular polysaccharide of Streptococcus pneumoniae in the marginal zone of mouse spleen. *Proc Natl Acad Sci U S A* 101:215-220.

20. Koppel, E. A., C. W. Wieland, V. C. van den Berg, M. Litjens, S. Florquin, Y. van Kooyk, T. van der Poll, and T. B. Geijtenbeek. 2005. Specific ICAM-3 grabbing nonintegrin-related 1 (SIGNR1) expressed by marginal zone macrophages is

essential for defense against pulmonary Streptococcus pneumoniae infection. *Eur J Immunol* 35:2962-2969.

21. Koppel, E. A., M. Litjens, V. C. van den Berg, Y. van Kooyk, and T. B. Geijtenbeek. 2008. Interaction of SIGNR1 expressed by marginal zone macrophages with marginal zone B cells is essential to early IgM responses against Streptococcus pneumoniae. *Mol Immunol* 45:2881-2887.

22. Chen, Y., T. Pikkarainen, O. Elomaa, R. Soininen, T. Kodama, G. Kraal, and K. Tryggvason. 2005. Defective microarchitecture of the spleen marginal zone and impaired response to a thymus-independent type 2 antigen in mice lacking scavenger receptors MARCO and SR-A. *J Immunol* 175:8173-8180.

23. Gebe, J. A., M. Llewellyn, H. Hoggatt, and A. Aruffo. 2000. Molecular cloning, genomic organization and cell-binding characteristics of mouse Spalpha. *Immunology* 99:78-86.

24. Yokota, T., B. Ehlin-Henriksson, and G. K. Hansson. 1998. Scavenger receptors mediate adhesion of activated B lymphocytes. *Exp Cell Res* 239:16-22.

25. Szakal, A. K., Y. Aydar, P. Balogh, and J. G. Tew. 2002. Molecular interactions of FDCs with B cells in aging. *Semin Immunol* 14:267-274.

26. Eaton-Bassiri, A. S., L. Mandik-Nayak, S. J. Seo, M. P. Madaio, M. P. Cancro, and J. Erikson. 2000. Alterations in splenic architecture and the localization of anti-double-stranded DNA B cells in aged mice. *Int Immunol* 12:915-926.

27. Minges Wols, H. A., K. M. Johnson, J. A. Ippolito, S. Z. Birjandi, Y. Su, P. T. Le, and P. L. Witte. 2009. Migration of immature and mature B cells in the aged microenvironment. *Immunology*.

28. Cheung, H. T., and M. J. Nadakavukaren. 1983. Age-dependent changes in the cellularity and ultrastructure of the spleen of Fischer F344 rats. *Mech Ageing Dev* 22:23-33.

29. Zheng, B., S. Han, Y. Takahashi, and G. Kelsoe. 1997. Immunosenescence and germinal center reaction. *Immunol Rev* 160:63-77.

30. Mebius, R. E., and G. Kraal. 2005. Structure and function of the spleen. *Nat Rev Immunol* 5:606-616.

31. Allen, C. D., and J. G. Cyster. 2008. Follicular dendritic cell networks of primary follicles and germinal centers: phenotype and function. *Semin Immunol* 20:14-25.

32. Allman, D., B. Srivastava, and R. C. Lindsley. 2004. Alternative routes to maturity: branch points and pathways for generating follicular and marginal zone B cells. *Immunol Rev* 197:147-160.

33. Johnston, B., and E. C. Butcher. 2002. Chemokines in rapid leukocyte adhesion triggering and migration. *Semin Immunol* 14:83-92.

34. Campbell, D. J., C. H. Kim, and E. C. Butcher. 2003. Chemokines in the systemic organization of immunity. *Immunol Rev* 195:58-71.

35. Lu, T. T., and J. G. Cyster. 2002. Integrin-mediated long-term B cell retention in the splenic marginal zone. *Science* 297:409-412.

36. Sasou, S., R. Satodate, and S. Katsura. 1976. The marginal sinus in the perifollicular region of the rat spleen. *Cell Tissue Res* 172:195-203.

37. Richard A. Goldsby, T. J. K., Barbara A. Osborne, and Janis Kuby. 2003. *Immunology*. Freeman, W.H., Publishers.

38. Mond, J. J., A. Lees, and C. M. Snapper. 1995. T cell-independent antigens type 2. *Annu Rev Immunol* 13:655-692.

39. van Rooijen, N., N. Kors, and G. Kraal. 1989. Macrophage subset repopulation in the spleen: differential kinetics after liposome-mediated elimination. *J Leukoc Biol* 45:97-104.

40. Nolte, M. A., R. Arens, M. Kraus, M. H. van Oers, G. Kraal, R. A. van Lier, and R. E. Mebius. 2004. B cells are crucial for both development and maintenance of the splenic marginal zone. *J Immunol* 172:3620-3627.

41. You, Y., H. Zhao, Y. Wang, and R. H. Carter. 2009. Cutting edge: Primary and secondary effects of CD19 deficiency on cells of the marginal zone. *J Immunol* 182:7343-7347.

42. Takeya, M., and K. Takahashi. 1992. Ontogenic development of macrophage subpopulations and Ia-positive dendritic cells in fetal and neonatal rat spleen. *J Leukoc Biol* 52:516-523.

43. Ato, M., H. Nakano, T. Kakiuchi, and P. M. Kaye. 2004. Localization of marginal zone macrophages is regulated by C-C chemokine ligands 21/19. *J Immunol* 173:4815-4820.

44. Platt, N., R. P. da Silva, and S. Gordon. 1999. Class A scavenger receptors and the phagocytosis of apoptotic cells. *Immunol Lett* 65:15-19.

45. Elomaa, O., M. Sankala, T. Pikkarainen, U. Bergmann, A. Tuuttila, A. Raatikainen-Ahokas, H. Sariola, and K. Tryggvason. 1998. Structure of the human macrophage MARCO receptor and characterization of its bacteria-binding region. *J Biol Chem* 273:4530-4538.

46. Pikkarainen, T., A. Brannstrom, and K. Tryggvason. 1999. Expression of macrophage MARCO receptor induces formation of dendritic plasma membrane processes. *J Biol Chem* 274:10975-10982.

47. Underhill, D. M., and A. Ozinsky. 2002. Phagocytosis of microbes: complexity in action. *Annu Rev Immunol* 20:825-852.

48. Nagaoka, K., K. Takahara, K. Tanaka, H. Yoshida, R. M. Steinman, S. Saitoh, S. Akashi-Takamura, K. Miyake, Y. S. Kang, C. G. Park, and K. Inaba. 2005. Association of SIGNR1 with TLR4-MD-2 enhances signal transduction by recognition of LPS in gram-negative bacteria. *Int Immunol* 17:827-836.

49. Medzhitov, R., P. Preston-Hurlburt, and C. A. Janeway, Jr. 1997. A human homologue of the Drosophila Toll protein signals activation of adaptive immunity. *Nature* 388:394-397.

50. Netea, M. G., C. van der Graaf, J. W. Van der Meer, and B. J. Kullberg. 2004. Toll-like receptors and the host defense against microbial pathogens: bringing specificity to the innate-immune system. *J Leukoc Biol* 75:749-755.

51. Medzhitov, R., and C. A. Janeway, Jr. 1997. Innate immunity: impact on the adaptive immune response. *Curr Opin Immunol* 9:4-9.

52. Bennett, I. L., Jr., and P. B. Beeson. 1953. Studies on the pathogenesis of fever. II. Characterization of fever-producing substances from polymorphonuclear leukocytes and from the fluid of sterile exudates. *J Exp Med* 98:493-508.

53. Cundell, D. R., N. P. Gerard, C. Gerard, I. Idanpaan-Heikkila, and E. I. Tuomanen. 1995. Streptococcus pneumoniae anchor to activated human cells by the receptor for platelet-activating factor. *Nature* 377:435-438.

54. Prescott, S. M., G. A. Zimmerman, and T. M. McIntyre. 1990. Platelet-activating factor. *J Biol Chem* 265:17381-17384.

55. Aderem, A., and D. M. Underhill. 1999. Mechanisms of phagocytosis in macrophages. *Annu Rev Immunol* 17:593-623.

56. Pillay, C. S., E. Elliott, and C. Dennison. 2002. Endolysosomal proteolysis and its regulation. *Biochem J* 363:417-429.

57. Gruenberg, J. 2001. The endocytic pathway: a mosaic of domains. *Nat Rev Mol Cell Biol* 2:721-730.

58. Clague, M. J. 1998. Molecular aspects of the endocytic pathway. *Biochem J* 336 ( Pt 2):271-282.

59. Tjelle, T. E., A. Brech, L. K. Juvet, G. Griffiths, and T. Berg. 1996. Isolation and characterization of early endosomes, late endosomes and terminal lysosomes: their role in protein degradation. *J Cell Sci* 109 ( Pt 12):2905-2914.

60. Bright, N. A., B. J. Reaves, B. M. Mullock, and J. P. Luzio. 1997. Dense core lysosomes can fuse with late endosomes and are re-formed from the resultant hybrid organelles. *J Cell Sci* 110 ( Pt 17):2027-2040.

61. Herzenberg, L. A. 1989. Toward a layered immune system. *Cell* 59:953-954.

62. Herzenberg, L. A., and A. B. Kantor. 1992. Layered evolution in the immune system. A model for the ontogeny and development of multiple lymphocyte lineages. *Ann N Y Acad Sci* 651:1-9.

63. Ferguson, A. R., M. E. Youd, and R. B. Corley. 2004. Marginal zone B cells transport and deposit IgM-containing immune complexes onto follicular dendritic cells. *Int Immunol* 16:1411-1422.

64. Cinamon, G., M. A. Zachariah, O. M. Lam, F. W. Foss, Jr., and J. G. Cyster. 2008. Follicular shuttling of marginal zone B cells facilitates antigen transport. *Nat Immunol* 9:54-62.

65. Cinamon, G., M. Matloubian, M. J. Lesneski, Y. Xu, C. Low, T. Lu, R. L. Proia, and J. G. Cyster. 2004. Sphingosine 1-phosphate receptor 1 promotes B cell localization in the splenic marginal zone. *Nat Immunol* 5:713-720.

66. Allman, D., and J. P. Miller. 2005. The aging of early B-cell precursors. *Immunol Rev* 205:18-29.

67. Allman, D., and J. P. Miller. 2005. B cell development and receptor diversity during aging. *Curr Opin Immunol* 17:463-467.

68. Lopes-Carvalho, T., and J. F. Kearney. 2004. Development and selection of marginal zone B cells. *Immunol Rev* 197:192-205.

69. Stephan, R. P., C. R. Reilly, and P. L. Witte. 1998. Impaired ability of bone marrow stromal cells to support B-lymphopoiesis with age. *Blood* 91:75-88.

70. Stephan, R. P., D. A. Lill-Elghanian, and P. L. Witte. 1997. Development of B cells in aged mice: decline in the ability of pro-B cells to respond to IL-7 but not to other growth factors. *J Immunol* 158:1598-1609.

71. LeMaoult, J., S. Delassus, R. Dyall, J. Nikolic-Zugic, P. Kourilsky, and M. E. Weksler. 1997. Clonal expansions of B lymphocytes in old mice. *J Immunol* 159:3866-3874.

72. Riley, S. C., B. G. Froscher, P. J. Linton, D. Zharhary, K. Marcu, and N. R. Klinman. 1989. Altered VH gene segment utilization in the response to phosphorylcholine by aged mice. *J Immunol* 143:3798-3805.

73. Nicoletti, C., X. Yang, and J. Cerny. 1993. Repertoire diversity of antibody response to bacterial antigens in aged mice. III. Phosphorylcholine antibody from young and aged mice differ in structure and protective activity against infection with Streptococcus pneumoniae. *J Immunol* 150:543-549.

74. Nicoletti, C., C. Borghesi-Nicoletti, X. H. Yang, D. H. Schulze, and J. Cerny. 1991. Repertoire diversity of antibody response to bacterial antigens in aged mice. II. Phosphorylcholine-antibody in young and aged mice differ in both VH/VL gene repertoire and in specificity. *J Immunol* 147:2750-2755.

75. Frasca, D., D. Nguyen, R. L. Riley, and B. B. Blomberg. 2004. Effects of aging on DNA-binding activity of the E47 transcription factor in splenic B cells. *Mech Ageing Dev* 125:111-112.

76. Frasca, D., D. Nguyen, R. L. Riley, and B. B. Blomberg. 2003. Effects of aging on proliferation and E47 transcription factor activity induced by different stimuli in murine splenic B cells. *Mech Ageing Dev* 124:361-369.

77. Frasca, D., D. Nguyen, E. Van der Put, R. L. Riley, and B. B. Blomberg. 2003. The age-related decrease in E47 DNA-binding does not depend on increased Id

inhibitory proteins in bone marrow-derived B cell precursors. *Front Biosci* 8:a110-116.

78. Johnson, S. A., S. J. Rozzo, and J. C. Cambier. 2002. Aging-dependent exclusion of antigen-inexperienced cells from the peripheral B cell repertoire. *J Immunol* 168:5014-5023.

79. Frasca, D., A. M. Landin, S. C. Lechner, J. G. Ryan, R. Schwartz, R. L. Riley, and B. B. Blomberg. 2008. Aging down-regulates the transcription factor E2A, activation-induced cytidine deaminase, and Ig class switch in human B cells. *J Immunol* 180:5283-5290.

80. Streeter, P. R., E. L. Berg, B. T. Rouse, R. F. Bargatze, and E. C. Butcher. 1988. A tissue-specific endothelial cell molecule involved in lymphocyte homing. *Nature* 331:41-46.

81. Nakache, M., E. L. Berg, P. R. Streeter, and E. C. Butcher. 1989. The mucosal vascular addressin is a tissue-specific endothelial cell adhesion molecule for circulating lymphocytes. *Nature* 337:179-181.

82. Kraal, G., K. Schornagel, P. R. Streeter, B. Holzmann, and E. C. Butcher. 1995. Expression of the mucosal vascular addressin, MAdCAM-1, on sinus-lining cells in the spleen. *Am J Pathol* 147:763-771.

83. Tada, T., N. Inoue, D. T. Widayati, and K. Fukuta. 2008. Role of MAdCAM-1 and its ligand on the homing of transplanted hematopoietic cells in irradiated mice. *Exp Anim* 57:347-356.

84. Girkontaite, I., V. Sakk, M. Wagner, T. Borggrefe, K. Tedford, J. Chun, and K. D. Fischer. 2004. The sphingosine-1-phosphate (S1P) lysophospholipid receptor S1P3 regulates MAdCAM-1+ endothelial cells in splenic marginal sinus organization. *J Exp Med* 200:1491-1501.

85. Eikelenboom, P., C. D. Dijkstra, D. M. Boorsma, and N. van Rooijen. 1985. Characterization of lymphoid and nonlymphoid cells in the white pulp of the spleen using immunohistoperoxidase techniques and enzyme-histochemistry. *Experientia* 41:209-215.

86. Yan, J., J. M. Greer, R. Hull, J. D. O'Sullivan, R. D. Henderson, S. J. Read, and P. A. McCombe. The effect of ageing on human lymphocyte subsets: comparison of males and females. *Immun Ageing* 7:4.

87. Lerner, A., T. Yamada, and R. A. Miller. 1989. Pgp-1hi T lymphocytes accumulate with age in mice and respond poorly to concanavalin A. *Eur J Immunol* 19:977-982.

88. Stephan, R. P., V. M. Sanders, and P. L. Witte. 1996. Stage-specific alterations in murine B lymphopoiesis with age. *Int Immunol* 8:509-518.

89. Johnson, K. M., K. Owen, and P. L. Witte. 2002. Aging and developmental transitions in the B cell lineage. *Int Immunol* 14:1313-1323.

90. Kline, G. H., T. A. Hayden, and N. R. Klinman. 1999. B cell maintenance in aged mice reflects both increased B cell longevity and decreased B cell generation. *J Immunol* 162:3342-3349.

91. Kishimoto, S., S. Tomino, H. Mitsuya, H. Fujiwara, and H. Tsuda. 1980. Age-related decline in the in vitro and in vivo syntheses of anti-tetanus toxoid antibody in humans. *J Immunol* 125:2347-2352.

92. Burns, E. A., L. G. Lum, M. C. Seigneuret, B. R. Giddings, and J. S. Goodwin. 1990. Decreased specific antibody synthesis in old adults: decreased potency of antigen-specific B cells with aging. *Mech Ageing Dev* 53:229-241.

93. Weksler, M. E., and T. H. Hutteroth. 1974. Impaired lymphocyte function in aged humans. *J Clin Invest* 53:99-104.

94. Kishimoto, S., T. Takahama, and H. Mizumachi. 1976. In vitro immune response to the 2,4,6-trinitrophenyl determinant in aged C57BL/6J mice:changes in the humoral immune response to, avidity for the TNP determinant and responsiveness to LPS effect with aging. *J Immunol* 116:294-300.

95. Doria, G., G. D'Agostaro, and A. Poretti. 1978. Age-dependent variations of antibody avidity. *Immunology* 35:601-611.

96. Zharhary, D., Y. Segev, and H. Gershon. 1977. The affinity and spectrum of cross reactivity of antibody production in senescent mice: the IgM response. *Mech Ageing Dev* 6:385-392.

97. Shi, Y., T. Yamazaki, Y. Okubo, Y. Uehara, K. Sugane, and K. Agematsu. 2005. Regulation of aged humoral immune defense against pneumococcal bacteria by IgM memory B cell. *J Immunol* 175:3262-3267.

98. Boehmer, E. D., J. Goral, D. E. Faunce, and E. J. Kovacs. 2004. Age-dependent decrease in Toll-like receptor 4-mediated proinflammatory cytokine production and mitogen-activated protein kinase expression. *J Leukoc Biol* 75:342-349.

99. Swift, M. E., A. L. Burns, K. L. Gray, and L. A. DiPietro. 2001. Age-related alterations in the inflammatory response to dermal injury. *J Invest Dermatol* 117:1027-1035.

100. Tasat, D. R., R. Mancuso, S. O'Connor, and B. Molinari. 2003. Age-dependent change in reactive oxygen species and nitric oxide generation by rat alveolar macrophages. *Aging Cell* 2:159-164.

101. Franceschi, C., M. Bonafe, S. Valensin, F. Olivieri, M. De Luca, E. Ottaviani, and G. De Benedictis. 2000. Inflamm-aging. An evolutionary perspective on immunosenescence. *Ann N Y Acad Sci* 908:244-254.

102. Bruunsgaard, H., and B. K. Pedersen. 2003. Age-related inflammatory cytokines and disease. *Immunol Allergy Clin North Am* 23:15-39.

103. Ormerod, M. G. 2000. *Flow Cytometry*. Oxford University Press, U.K.

104. Herzenberg, L. A., J. Tung, W. A. Moore, and D. R. Parks. 2006. Interpreting flow cytometry data: a guide for the perplexed. *Nat Immunol* 7:681-685.

105. Won, W. J., J. B. Foote, M. R. Odom, J. Pan, J. F. Kearney, and R. S. Davis. 2006. Fc receptor homolog 3 is a novel immunoregulatory marker of marginal zone and B1 B cells. *J Immunol* 177:6815-6823.

106. Pillai, S., A. Cariappa, and S. T. Moran. 2005. Marginal zone B cells. *Annu Rev Immunol* 23:161-196.

107. Jablonska, J., K. E. Dittmar, T. Kleinke, J. Buer, and S. Weiss. 2007. Essential role of CCL2 in clustering of splenic ERTR-9+ macrophages during infection of BALB/c mice by Listeria monocytogenes. *Infect Immun* 75:462-470.

108. Lo, C. G., T. T. Lu, and J. G. Cyster. 2003. Integrin-dependence of lymphocyte entry into the splenic white pulp. *J Exp Med* 197:353-361.

109. Manjunath, N., P. Shankar, J. Wan, W. Weninger, M. A. Crowley, K. Hieshima, T. A. Springer, X. Fan, H. Shen, J. Lieberman, and U. H. von Andrian. 2001. Effector differentiation is not prerequisite for generation of memory cytotoxic T lymphocytes. *J Clin Invest* 108:871-878.

110. van der Laan, L. J., E. A. Dopp, R. Haworth, T. Pikkarainen, M. Kangas, O. Elomaa, C. D. Dijkstra, S. Gordon, K. Tryggvason, and G. Kraal. 1999. Regulation and functional involvement of macrophage scavenger receptor MARCO in clearance of bacteria in vivo. *J Immunol* 162:939-947.

111. van der Laan, L. J., M. Kangas, E. A. Dopp, E. Broug-Holub, O. Elomaa, K. Tryggvason, and G. Kraal. 1997. Macrophage scavenger receptor MARCO: in vitro and in vivo regulation and involvement in the anti-bacterial host defense. *Immunol Lett* 57:203-208.

112. Weill, J. C., S. Weller, and C. A. Reynaud. 2009. Human marginal zone B cells. *Annu Rev Immunol* 27:267-285.

113. Steiniger, B., P. Barth, and A. Hellinger. 2001. The perifollicular and marginal zones of the human splenic white pulp : do fibroblasts guide lymphocyte immigration? *Am J Pathol* 159:501-512.

114. Lynch, A. M., and R. Kapila. 1996. Overwhelming postsplenectomy infection. *Infect Dis Clin North Am* 10:693-707.

115. Waghorn, D. J. 2001. Overwhelming infection in asplenic patients: current best practice preventive measures are not being followed. *J Clin Pathol* 54:214-218.

116. Ram, S., L. A. Lewis, and P. A. Rice. Infections of people with complement deficiencies and patients who have undergone splenectomy. *Clin Microbiol Rev* 23:740-780.

117. Zago, M. A. 1989. The evaluation of spleen function in man. *Braz J Med Biol Res* 22:159-169.

118. William, B. M., and G. R. Corazza. 2007. Hyposplenism: a comprehensive review. Part I: basic concepts and causes. *Hematology* 12:1-13.

119. Tsankova, N. M., O. Berton, W. Renthal, A. Kumar, R. L. Neve, and E. J. Nestler. 2006. Sustained hippocampal chromatin regulation in a mouse model of depression and antidepressant action. *Nat Neurosci* 9:519-525.

120. Nestler, E. J., M. Barrot, R. J. DiLeone, A. J. Eisch, S. J. Gold, and L. M. Monteggia. 2002. Neurobiology of depression. *Neuron* 34:13-25.

121. Duman, R. S. 2004. Depression: a case of neuronal life and death? *Biol Psychiatry* 56:140-145.

122. Pillai, S., and A. Cariappa. 2009. The follicular versus marginal zone B lymphocyte cell fate decision. *Nat Rev Immunol* 9:767-777.

123. Cariappa, A., I. B. Mazo, C. Chase, H. N. Shi, H. Liu, Q. Li, H. Rose, H. Leung, B. J. Cherayil, P. Russell, U. von Andrian, and S. Pillai. 2005. Perisinusoidal B cells in the bone marrow participate in T-independent responses to blood-borne microbes. *Immunity* 23:397-407.

124. Traggiai, E., A. Casati, M. Frascoli, S. Porcellini, M. Ponzoni, F. Sanvito, L. Leng, R. Bucala, L. Moretta, and F. Grassi. Selective preservation of bone marrow mature recirculating but not marginal zone B cells in murine models of chronic inflammation. *PLoS One* 5:e11262.

125. Tortola, L., K. Yadava, M. F. Bachmann, C. Muller, J. Kisielow, and M. Kopf. IL-21 induces death of marginal zone B cells during chronic inflammation. *Blood*.

126. Browne, C. D., M. M. Hoefer, S. K. Chintalapati, M. H. Cato, Y. Wallez, D. V. Ostertag, E. B. Pasquale, and R. C. Rickert. SHEP1 partners with CasL to promote marginal zone B-cell maturation. *Proc Natl Acad Sci U S A* 107:18944-18949.

127. Wang, S. L., M. Kutsche, G. DiSciullo, M. Schachner, and S. A. Bogen. 2000. Selective malformation of the splenic white pulp border in L1-deficient mice. *J Immunol* 165:2465-2473.

128. Katakai, T., H. Suto, M. Sugai, H. Gonda, A. Togawa, S. Suematsu, Y. Ebisuno, K. Katagiri, T. Kinashi, and A. Shimizu. 2008. Organizer-like reticular stromal cell layer common to adult secondary lymphoid organs. *J Immunol* 181:6189-6200.

129. Hoek, K. L., L. E. Gordy, P. L. Collins, V. V. Parekh, T. M. Aune, S. Joyce, J. W. Thomas, L. Van Kaer, and E. Sebzda. Follicular B cell trafficking within the spleen actively restricts humoral immune responses. *Immunity* 33:254-265.

130. Singer, II, M. Tian, L. A. Wickham, J. Lin, S. S. Matheravidathu, M. J. Forrest, S.Mandala, and E. J. Quackenbush. 2005. Sphingosine-1-phosphate agonists increase macrophage homing, lymphocyte contacts, and endothelial junctional complex formation in murine lymph nodes. *J Immunol* 175:7151-7161.

131. Di Paolo, N. C., E. A. Miao, Y. Iwakura, K. Murali-Krishna, A. Aderem, R. A. Flavell, T. Papayannopoulou, and D. M. Shayakhmetov. 2009. Virus binding to a plasma membrane receptor triggers interleukin-1 alpha-mediated proinflammatory macrophage response in vivo. *Immunity* 31:110-121.

## VITA

The author, Shirin Birjandi, was born in Chicago, IL on April 30, 1978 to Hossein Birjandi and Nahid Zahedi. She received a Bachelor of Science in Biology from Loyola University Chicago in May 2001 and a Master's of Science in Cell Biology, Neurobiology and Anatomy from Loyola University Chicago Medical Center in May 2005. The focus of her master's thesis work was on neuroplasticity after middle cerebral artery occlusion in rats.

In August 2005, Shirin joined the Ph.D. Program of Cell Biology, Neurobiology and Anatomy at Loyola University Chicago Medical Center. Shortly thereafter, she joined the laboratory of Dr. Pamela L. Witte, where she studied the age related alterations in the splenic marginal zone and function of marginal zone macrophages using a murine model. While at Loyola, Shirin was appointed to a pre-doctoral training grant from the National Institute on Aging, served on the Graduate Student Association Council, and was a Graduate Student department representative. Shirin also was the recipient of travel awards to present her work at the Society for Leukocyte Biology and the American Association of Immunologists national conferences.

Shirin is engaged to be married to Morteza Dehghani, a research assistant professor at University of Southern California. After completing her Ph.D., Shirin will go onto a post-doctoral position at the University of California, Los Angeles.